UNIVERSITÀ DEGLI STUDI DI PADOVA

DIPARTIMENTO DI BIOLOGIA

Master degree in Marine Biology

THESIS

Exploring morphodynamic co-benefits of salt-marsh restoration

Relatore: Professor Alvise Finotello

Correlatore: Professor Davide Tognin

Laureando: Frasson Sebastiano

ANNO ACCADEMICO 2022/2023

Dedicato alla determinazione, che ti permette di raggiungere ogni obbiettivo,
anche se non sei tu a portelo, lasciandoti i limiti alle spalle.

Abstract

The Venice Lagoon possesses one of the planet's most fascinating and distinctive ecosystems, owing to its unique geographical location. Situated in the northern reaches of the Adriatic Sea, this natural lagoon has undergone significant human-induced changes over time to accommodate various activities. Originally characterized by shallow waters, resulting from limited erosion from the sea and significant sediment deposition from major rivers such as the Piave, Sile, Brenta, and Bacchiglione, human intervention in past centuries diverted these primary waterways and excavated channels to deepen the lagoon for navigation purposes. In addition, land reclamation efforts were initiated to convert salt marshes (i.e., low-lying vegetated wetlands periodically flooded by tides) into agricultural, residential, or aquacultural land.

Salt marshes are a defining feature not only of the Venice Lagoon but also of many low-lying temperate and subtropical coastal regions. Currently, extensive loss of salt marshes is occurring worldwide, and significant efforts are underway to conserve and restore these valuable ecosystems, along with the services they provide to the environment and society, such as blue-carbon sequestration, environmental remediation, shoreline protection, and habitat provision. While it is undeniably valuable to restore salt marshes for ecological and economic reasons, most previous studies have not closely examined the co-benefits of marsh restoration on coastal system morphodynamic evolution. In particular, it remains unclear whether marsh restoration can return the system to the conditions observed before marshes were degraded. The Venice Lagoon provides a unique opportunity to study this issue in detail, given its extensive historical data and state-of-the-art numerical modeling techniques that enable the reconstruction of past, present, and future lagoon morphologies. We can investigate the effects of marsh degradation and the potential impacts of future restoration projects at the scale of the entire tidal basin. In this study, I used numerical modeling techniques to examine the hydrodynamic and sediment transport processes in three different configurations of the Venice Lagoon: the present one and

those observed in 1932 and 1901. These two historical configurations serve as references to simulate the effects of marsh restoration projects aimed at restoring the total marsh area that existed at those times. The research I conducted demonstrates that even extensive marsh restoration alone will not suffice in fully returning the Venice Lagoon's hydro-morphodynamics to those observed at the beginning of the last century. This is because not only have salt marshes changed, but the overall lagoon morphology has also evolved, making marsh restoration projects essentially neutral with respect to current hydrodynamic and sediment transport processes within the lagoon.

While not diminishing the intrinsic significance of marsh restoration projects, the findings of this study specifically illustrate that marsh restoration may not provide a practical solution to address the long-standing issue of morphological degradation observed in Venice over the past century, also urging caution in considering the restoration of similar shallow-water back-barrier lagoons that are prevalent along coastlines worldwide.

Figure 1: Aerial photo of salt marshes in the Venice Lagoon

INDEX

List of Figures

1. Introduction

Salt marshes are widespread morphological features in coastal and estuarine tidal landscapes (Cronk, J.K., Fennessy, 2001; Luternauer et al., 1995; Mitsch & Gossilink, 2000; Rogers & Woodrofe, 2015, p. 201). They consist of low-relief wetlands characterized by a predominantly continuous cover of salt-tolerant (halophytic) vascular plants. These areas exist in a transitional zone, mostly covered by water during high tide and largely uncovered during low tide. In the lower transition zones, where mudflats meet the marsh, annual species may dominate the canopy, while the upper salt marsh areas, more landward, are typically dominated by perennial plants. On the adjacent tidal flats, specialized invertebrates often thrive, showcasing a rich diversity of species that are sensitive to localized conditions.

Salt marshes are typically located in the upper intertidal zone, and are ecologically and economically important as they significantly contribute to coastal primary production, support high biodiversity, and provide valuable ecosystem services (Barbier et al., 2011; Costanza et al., 1997; Mitsch & Gossilink, 2000).

Salt marshes serve as vital habitats for breeding, feeding, and roosting for numerous bird species, particularly migratory ones. They are also significant habitats for fish and various aquatic and marine invertebrates. While salt marshes are usually defined ecologically, their presence and functionality fundamentally hinge on the interplay of ecological processes with hydrodynamic and sedimentary processes. These processes take place within an intertidal "accommodation space," an area suitable for marsh development. The vertical boundaries of this space typically extend between mean high-water neap and the highest astronomical tide. The seaward lateral boundary is a junction, either cliffed or ramped, with unvegetated intertidal and subtidal mudflats and sandflats, where seagrasses may be present.

In areas with an ample supply of sediment, salt marsh formation usually follows the development of shallow drainage on tidal flats. Pioneer plant

colonization on higher surfaces subsequently leads to increased sediment deposition through a positive biomorphodynamic feedback. Over time, convex surfaces between tidal creeks develop a concave cross-section due to the preferential deposition of tidally imported sediment near creek banks. This illustrates the transition from a young marsh with a low tidal range to a mature marsh platform. Once established, the salt marsh system retains various elements within its cross-section, extending from the tidal channels or open coast to its landward limit. The coastal zone exhibits a degree of self-organization, where changes in one area affect another, creating a reciprocal relationship.

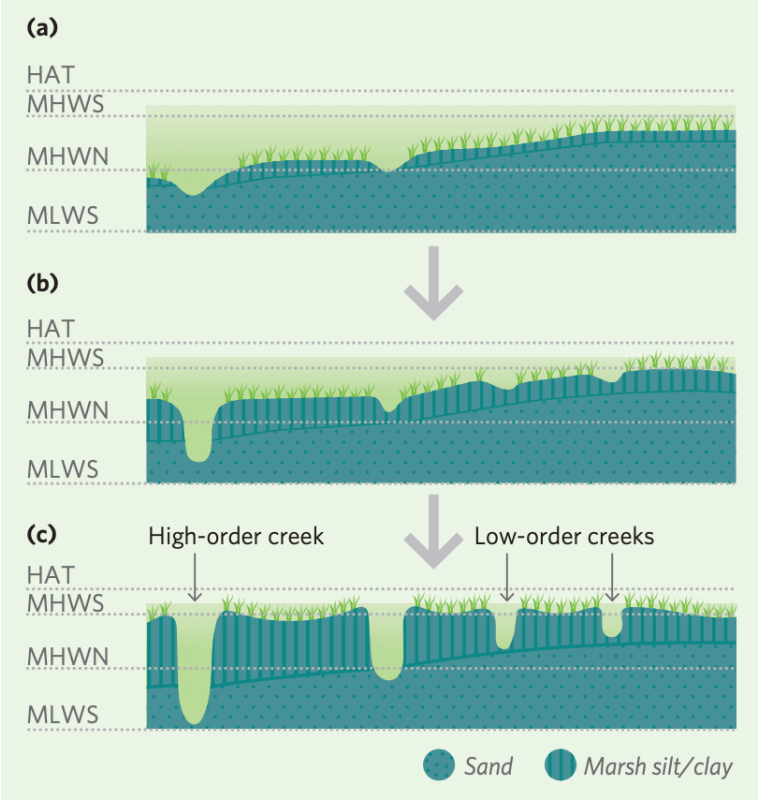

Figure 2: Sketch evolution of salt marsh (Racheal and Hudson et all 2011)

Both the physical and biological components of the salt marsh are influenced by and, in turn, influence the flow of water, nutrients, and sediment within, across, and around them. This interaction occurs alongside external factors like sea level, climate, and sediment supply, which also impact salt marshes. While unvegetated mudflats experience phases of both erosion and accretion, leading to variations in surface elevation, once salt

marsh vegetation becomes established, surfaces become more resistant to erosion. Observations of vegetated salt marsh surfaces following storm surge events, as well as large-scale flume experiments to scale, have demonstrated their remarkable stability even under high hydrodynamic forces. The rate of infilling of the accommodation space is initially rapid but then slows as surface elevation rises, and tidal inundation frequency and sediment supply decrease, eventually reaching a state of equilibrium.

In recent years, there has been a notable shift in the perception of salt marshes, despite their long history of land reclamation and conversion for agricultural and other purposes. Indeed, until the mid-20th century, salt marshes were often considered of little value to society, viewed as land waiting to be reclaimed for agriculture, urban development, or waste disposal. However, more recently, their remarkable biodiversity and the diverse functions they perform have gained increasing recognition. Here's a brief overview of some of the ecosystem services provided by salt marshes:

Coastal Protection by Salt Marshes:

Wave Attenuation: Salt marshes act as natural buffers, where waves break in shallow coastal waters and dissipate energy, reducing erosion and sediment transport. Healthy salt marsh complexes, with wide intertidal flats, divert wave-breaking and erosion away from critical flood defenses and vulnerable areas.

Surge Attenuation: Extensive salt marsh areas can mitigate the impact of storm surges by increasing friction as surges propagate into estuaries, similar to wave attenuation but on a larger scale.

Sediment Trapping: Functioning salt marshes have a natural ability to trap and retain sediment, maintaining an equilibrium elevation relative to the tidal frame. This resilience to erosion allows for natural recovery following erosive events such as storms.

Carbon Uptake and Storage by Salt Marshes: Salt marshes are vital blue carbon ecosystems, storing carbon outside of the tropics. They bury carbon at a higher rate and store more carbon per unit area below ground

than their subtidal (e.g., seagrass) and terrestrial (e.g., forests) counterparts. This contributes to climate regulation by sequestering carbon dioxide (CO2) through carbon burial and long-term storage, owing to the highly productive ecosystem, depositional environments, and low oxygen concentrations in the sediments.

Water Quality Impact: Salt marshes in sheltered water bodies, like estuaries and coastal embayments, play a crucial role in regulating water quality. They can reduce concentrations of fecal organisms and absorb heavy metals from the water, thus improving water quality.

Provisioning Services of Salt Marshes: Salt marshes are highly productive ecosystems, supporting diverse communities of salt-tolerant species. They provide essential resources and habitat structures for bird breeding, wintering, and migratory activities, as well as serving as important fish nursery grounds. Abundant marine invertebrates found in these habitats serve as a food source for various species, including birds, fish, and terrestrial animals like voles and small mammals. Additionally, intertidal marshes are vital nursery and feeding areas for young fish and commercially important shellfish.

Cultural and Touristic Value: Coastal salt marshes contribute to the natural landscape and cultural heritage. Some are even designated as UNESCO World Heritage sites, like "Venice and its lagoon," making them attractive tourist destinations. (Hudson et al., 2021)

Hence, coastal salt marshes, situated at the interface of marine and terrestrial environments, are of paramount ecological, geomorphological, and socio-economic importance. However, the sustainability of salt-marsh ecosystems is severely threatened by climate changes and increasing anthropogenic pressures. (A. D'Alpaos, 2011; A. D'Alpaos & Marani, 2016; Fitzgerald & Hughes, 2019; Mudd, 2011; Ratliff et al., 2015; Silvestri, 2018). As a result, extensive salt-marsh areas are being lost worldwide every year at alarmingly increasing rates (Carniello et al., 2009; Day et al., 2000; DeLaune & Pezeshki, 2003; Gedan et al., 2009; Tommasini et al., 2019)

To counteract this ongoing erosion and restore ecosystem services, several conservation and restoration projects have been and are still being implemented worldwide. While there is no doubt that these efforts are commendable and intrinsically valuable in restoring valuable landscape features and facilitating biotic interactions, there is a lack of studies demonstrating the co-benefits of marsh restoration in terms of ecomorphodynamics. Ecomorphodynamics is a fundamental concept in my research, and it requires some clarification. My thesis aims to investigate coastal dynamics, a topic also covered in the course on 'Coastal Environments Under Climate Change.' Morphodynamics, at its core, refers to the reciprocal adjustment of the landscape and fluid dynamics, particularly involving the movement of sediment. This concept comprises three essential components: morphology (landscape shape), hydrodynamics (the movement of water), and sediment transport. Climate acts as the starting point for morphodynamics, representing the primary driving force on the sea and water bodies. Factors such as sea level and its variations, in combination with external forces like wind, waves, tides, and currents, further shape the coastal environment. Additionally, the geological makeup and sediments on the seabed provide static boundary conditions that influence hydrodynamics, sediment transport, and landscape shape. Ecomorphodynamics, as a concept, merges classical physical morphodynamic processes with biotic influences, which are particularly significant in salt marsh ecosystems. Biotic influences primarily stem from the effects of plant and animal life on hydrodynamic and sediment transport processes.

Figure 3: Salt marshes in the Venice lagoon (©Google immagini)

In this thesis, my objective is to explore how marsh restoration projects can influence the ecomorphodynamics of low-lying, shallow coastal areas, with a specific focus on the impact of extensive restoration projects on hydrodynamic and sediment transport processes. The overarching goal of my research is to determine whether marsh restoration alone is sufficient to restore coastal systems that have suffered significant degradation due to the complex interplay of natural processes and human activities, ultimately returning them to a more natural, pristine state. Hence, I will explore the co-benefit of marsh restoration for coastal morphodynamics, taken here as hydrodynamics and sediment transport processes.

Figure 4: Brushwoow groynes to protect salt marshes against lateral erosion (August

2008; image©Mark Schuerch)

To achieve this, I will concentrate on the microtidal lagoon of Venice, where the interplay between natural processes and human interventions has led to substantial morphological changes over the past approximately 150 years (Luigi D'Alpaos, 2010). Specifically, I will employ well-established numerical methods to model the morphodynamics of shallow coastal landscapes affected by tides and waves. Initially, I will analyze the changes in lagoon morphodynamics from 1901 to the present. Subsequently, I will investigate the potential effects of extensive marsh restoration projects aimed at reverting the total marsh area to its previous state, as observed through historical maps.

Crucially, the importance of this research transcends the particular case of the Venice lagoon. The methodology I've utilized and the results I've garnered can be extrapolated to other shallow water coastal settings that exhibit similarities to the Venice lagoon. Such systems are prevalent worldwide, with notable examples found along the coasts of the United States' East and Gulf of Mexico, Northern Europe, Australia's eastern coast, and the Atlantic coasts of South America. Therefore, this study may establish a foundation for future systematic exploration of the co-benefits of marsh restoration projects on morphodynamics in shallow tidal embayments.

2. Study area

2.1 Geomorphology of the Venice lagoon

Situated in the northern Adriatic Sea, the Venice Lagoon covers an expansive area of 550 square kilometers, making it the largest brackish waterbody in the Mediterranean Basin. This lagoon took shape over a span of 7500 years, formed by the gradual deposition of Late Pleistocene alluvial sediments, locally referred to as Caranto (Zecchin et al., 2008). The contemporary configuration of the lagoon features three main inlets, proceeding from North to South: Lido, Malamocco, and Chioggia (as illustrated in Figure 5).

Tidal patterns within the lagoon adhere to a semidiurnal microtidal regime, with an average spring tidal range of 1 meter and maximum tidal fluctuations of approximately 0.75 meters relative to Mean Sea Level (MSL). This characteristic is illustrated in studies by D'Alpaos et al. (2013) and Valle-Levinson et al. (2021) (A. D'Alpaos et al., 2013; Valle-Levinson et al., 2021).

Meteorological phenomena often coincide with astronomical tides, resulting in notably high or low tides when atmospheric pressure is low or high, respectively. Furthermore, wind-related processes play a pivotal role in influencing the hydrodynamics and morphodynamics of the lagoon. Seasonal wind-storm events have a pronounced impact on morphodynamic changes over timescales ranging from decades to centuries, as elucidated in studies conducted by Carniello et al. in 2009 and 2012 (Carniello et al., 2009, 2012).

Detailed assessments of the wind climate reveal minimal year-to-year fluctuations in wind energy. The wind-storm events that have the most significant morphological and hydrodynamic effects are those associated with Bora and Sirocco winds, as depicted in Figure 1e. The north-easterly Bora winds, which blow nearly parallel to the lagoon's major axis, create substantial water-level changes in the southern region of the lagoon and

generate large waves with significant wave heights exceeding 1 meter. These waves have a considerable impact on resuspending sediments from the tidal mudflats. Conversely, the South-Eastern Sirocco winds induce substantial water-level changes in the northern Adriatic Sea and are often responsible for extensive flooding in Venice and other communities within the lagoon.

Simultaneously, the extraction of groundwater and natural gas for industrial purposes hastened the natural subsidence of the soil (Carbognin et al., 2004; Gatto & Carbognin, 1981; Zanchettin et al., 2021).

To facilitate the passage of increasingly larger vessels within the lagoon, two major waterways, the Vittorio Emanuele and the Malamocco-Marghera channels (fig 5 a, b, c), were excavated in 1925 and 1968, respectively. Significant transformations in the lagoon's hydrodynamics arose from the construction of jetties at the lagoon inlets, designed to ensure adequate water depths for commercial ship traffic. The construction of these jetties, spanning different time periods at various inlets, resulted in several changes.

The construction of these jetties significantly narrowed the inlets, as anticipated during the design phase, deepening the water in the process. However, these structures brought about critical alterations in the hydrodynamic and morphodynamic regimes of the lagoon. The construction of the jetties caused more sustained changes in the lagoon's tidal regime than the typical periodic variations, which are a consequence of the nodal modulation of tides in the Adriatic Sea, typically accounting for about 4% of the characteristic tidal range (Amos et al., 2010; Valle-Levinson et al., 2021). Between 1909 and 1973, the average tidal range within the lagoon surged by up to 25% (Luigi D'Alpaos, 2010; Ferrarin et al., 2015; Tomasin, 1974), with local changes potentially being even more significant (Finotello et al., 2019, 2022; Silvestri, 2018).

The alterations in the lagoon's hydrodynamics due to the construction of jetties, in combination with the rise in eustatic sea level (with an average rate of 1.23±0.13 mm/year between 1872 and 2019; and 2.76±1.75 mm/year between 1993 and 2019, as reported by Zanchettin (Zanchettin et al., 2021),

had a significant impact on the lagoon's morphological evolution. This led to the initiation of positive morphodynamic feedbacks, causing larger sections of the lagoon to become ebb-dominated, particularly in the vicinity of the inlets where the jetties introduced strong flow imbalances. These imbalances in tidal flows facilitated the outward transport of fine sediments and impeded the import of sediment carried in suspension by longshore currents, an effect outlined by L. D'Alpaos in 2010 (Luigi D'Alpaos, 2010).

This situation was aggravated by the anthropogenic-induced reduction of fluvial sediments, leading to a negative sediment budget and the widespread loss of salt marshes (Carniello et al., 2009; Luigi D'Alpaos, 2010; Tommasini et al., 2019) The diminishing marsh coverage resulted in extended wind fetches, promoting the generation of higher, more energetic waves that exacerbated lateral marsh retreat and caused the erosion of tidal mudflats (Carniello et al., 2009; Finotello et al., 2020; Leonardi et al., 2016; Marani et al., 2011; Mariotti & Fagherazzi, 2013; Tommasini et al., 2019). The deepening of the mudflats (Figure 2l), amplified by rising eustatic sea levels and both natural and anthropogenic-induced subsidence, led to the generation of even more substantial wind waves, intensifying the erosion of salt marshes and mudflats through a positive feedback loop.

Further human-made modifications were introduced to the inlet morphologies between 2006 and 2014 to accommodate the mobile floodgates of the Mo.S.E. (short for "Modulo Sperimentale Elettromeccanico," or Electromechanical Experimental Module) system. This system was designed to protect the city of Venice and other lagoon settlements from extensive flooding (Mel et al., 2021). These interventions marginally increased hydraulic resistances at the inlets, resulting in a reduction of tidal amplitudes and an increase in tidal-phase delays within the lagoon (Ghezzo et al., 2010; Matticchio et al., 2017).

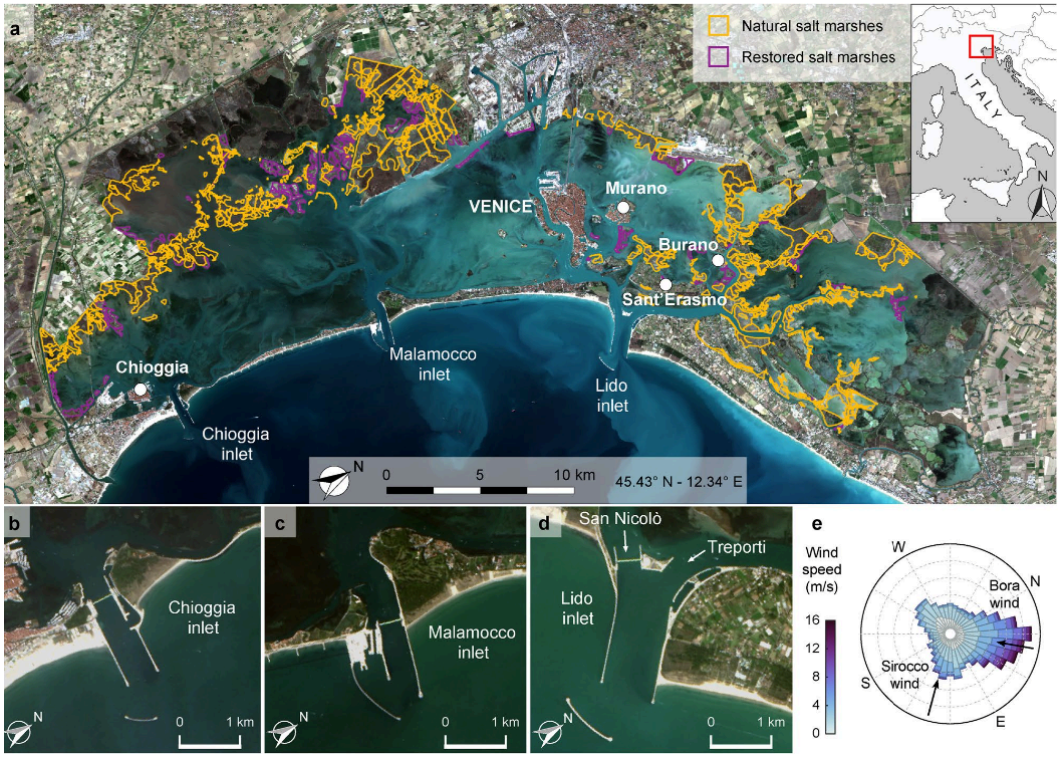

Figure 5: Geomorphological Setting. (a) The Venice Lagoon captured in satellite imagery (Copernicus Sentinel, 2020). Natural salt marshes are outlined in yellow, while restored salt marshes are depicted in purple. (b, c, d) Detailed views of the three primary lagoon inlets. (e) A rose-diagram illustrating the wind climate data recorded at the "Chioggia Diga Sud" anemometric station from 2000 to 2019. Notably, it highlights the two predominant winds: the north-easterly Bora wind and the south-easterly Sirocco wind. (Image © Finotello et al., 2023, WRR).

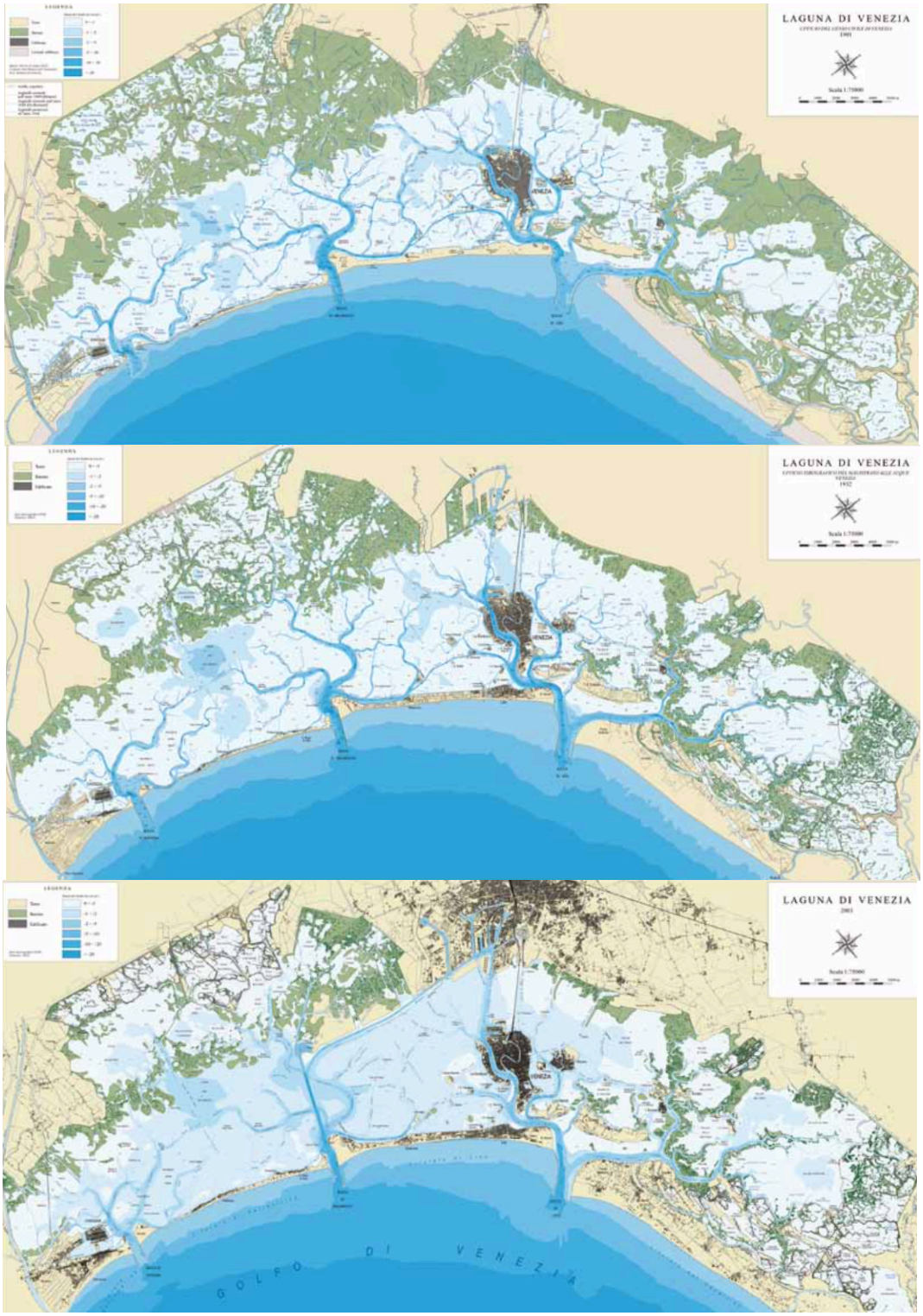

Figure 6: historic reconstruction of a topographic map showing the evolution of Venice Lagoon through years: (from top) 1901, 1932, 2003. (L. D'Alpaos, 2010)

2.2 Salt marshes in the Venice lagoon: current state

Salt marsh erosion persists today, albeit at significantly reduced rates compared to the previous century. This is attributable to a series of critical interventions aimed at safeguarding and restoring salt marshes, initiated by the Venice Water Authority since the early 1990s, with additional contributions from some EU-funded LIFE projects (Barausse et al., 2015; Tagliapietra et al., 2018; Tommasini et al., 2019).

In Venice, the traditional approach to safeguarding salt marshes has involved the use of artificial salt marshes. However, this approach has several notable characteristics: it often leads to a significant environmental impact during construction, faces challenges in replicating what nature has crafted over centuries, and can be challenging to implement on large scale. Frequently, artificial salt marshes are less effective in term of restoration and their artificial nature is easily distinguishable from natural ones.

A more effective and environmentally friendly approach to restoration involves the use of nature-based solutions. Nature-based solutions leverage biodiversity and ecosystem services to complement traditional actions like infrastructure development. These solutions can include biodegradable structures placed in an area for protection, such as Life Vimina Nature-based solutions are favored for several reasons: they are cost-effective, have a longer-lasting impact, and contribute to habitat protection and restoration. Nature-based solutions offer various advantages, including minimal environmental and landscape impact, the use of natural resources from the area, cost-effectiveness as a small number of solutions can cover a large area. Additionally, they often foster a sense of community, with volunteers or workers participating in construction and maintenance efforts. Many projects in the Venice Lagoon have embraced Nature-Based Solutions, Including Life Vimine (https://www.lifevimine.eu), Life Lagoon Refresh (http://www.lifelagoonrefresh.eu), and Life Seresto (http://www.lifeseresto.eu).

One of the projects that I have encountered during my academic career is “Life Vimine” (https://www.lifevimine.eu/), coordinated by the University

of Padova under the guidance of Professor Alberto Barause. This project focuses on the northern Venice lagoon and seeks to explore an innovative approach to protect the innermost salt marshes and mudflats from erosion using an integrated approach. The project relies on nature-based solutions, including the placement of numerous small biodegradable protections, such as fascines made from branches, along the edges of salt marshes. These fascines are manually positioned and subsequently filled with a small amount of sediment to encourage plant colonization and restore the edges and surface. Sediments are sourced from nearby mud flats, either manually or through the use of a small pump, minimizing both environmental impact and transportation costs. The project operates on a smaller scale to ensure that the proper height for vegetation can be restored. Prevention is a key component of salt marsh restoration in this project. By strategically placing small protections in various locations, it indirectly safeguards a larger surface area. The involvement of local workers, who possess intimate knowledge of the Venice Lagoon, enhances the collaborative efforts of volunteers in protecting the salt marshes, creating an integrated approach to restoration.

Currently, approximately 12% of existing salt marshes have been either entirely artificially created or partially restored (as indicated by the purple lines in Figure 1a), with a substantial portion of the remaining natural marshes being protected against lateral erosion through the use of manmade wooden piles or berms (as shown in Figure S2 in the Supporting Information). It is evident that without these restoration and conservation efforts, the total area of salt marshes would be significantly smaller than it is today.

Lastly, it's worth noting that the operation of the Mo.S.E. floodgates will further diminish the resilience of salt marshes against rising relative sea levels, primarily by reducing inorganic deposition during storm-surge events, which, although sporadic, play a crucial role in marsh vertical accretion (Tognin, 2022; Tognin et al., 2021).

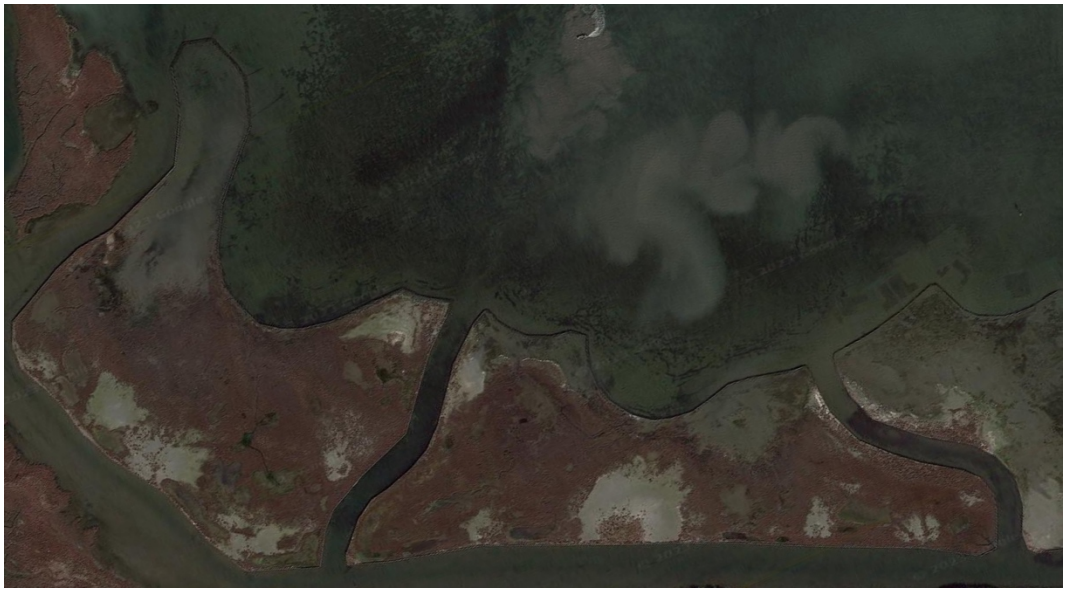

Figure 7: Google Earth photo showing the artificial saltmarshes in the south lagoon near Chioggia. This type of restoration is quite inefficient, is clearly seen that the border of restore operation do not overlap with the actual salt marsh border.

Figure 8: Nature-based solution in life vimine; northern lagoon. (prof Barause marine conservations principles and applications class)

3. Material and Methods

3.1 Numerical model

I employed a two-dimensional (2D) model consisting of three interconnected modules: the hydrodynamic module coupled with the wind-wave module (WWTM) (Carniello et al., 2011) and the sediment transport and bed evolution module (STABEM) (Carniello et al., 2012). This model is well-suited for simulating sediment dynamics that govern the morphodynamic evolution of shallow micro-tidal basins.

The hydrodynamic module solves the two-dimensional depth-integrated shallow water equations (SWEs), which are phase-averaged over a representative elementary area characterized by irregular topography to account for very shallow flows, wetting, and drying (Defina, 2000). In a Cartesian frame (x, y), these SWEs can be expressed as follows:

$$\vartheta(\eta)\frac{\partial \eta}{\partial t} + \nabla \cdot \mathbf{q} = 0 \tag{1}$$

$$\frac{\mathrm{D}}{\mathrm{D}t}\left(\frac{\mathbf{q}}{Y}\right) + \frac{1}{Y}\nabla \cdot \mathbf{Re} + \frac{\boldsymbol{\tau}_t}{Y\rho} - \frac{\boldsymbol{\tau}_s}{Y\rho} + g\nabla h = 0 \tag{2}$$

In the equations, several symbols and terms are defined as follows:

- t represents time.
- η is the free surface elevation measured relative to a datum.
- $q = (q_x, q_y)$ represents the depth-integrated velocity, indicating discharge per unit width.
- ∇ and $\nabla \cdot$ denote the 2D gradient and divergence operators, respectively.
- The symbol ϑ represents the wet fraction of the computational domain, which depends on water depth and local topographic irregularities (Defina, 2000).

In the momentum equation (eq. 2), $D\,/\,Dt$ represents the material (or Lagrangian) time derivative, while Y represents the water volume per unit

area, equivalent to the water depth. τ_t and τ_s are the shear stresses at the bottom (due to tidal currents) and at the free surface (due to wind drag), respectively. Additionally, ρ denotes water density, and g represents gravity.

The Reynolds stresses are computed using a depth-averaged version of Smagorinsky's model (SMAGORINSKY, 1963) and can be expressed in tensor index notation as follows:

$$\mathbf{Re} = R_{ij} = \nu_e Y\left(u_{i,j} + u_{j,i}\right) \tag{3}$$

$$\nu_e = 2C_S^2 A_e \sqrt{2\left(u_{x,x}\right)^2 + \left(u_{x,y} + u_{y,x}\right)^2 + 2\left(u_{y,y}\right)^2} \tag{4}$$

In equation (3), the indices i and j represent either the x or y coordinates, while $u = q/Y$. The eddy viscosity, denoted as ν_e, is proportional to the strain rate and involves parameters such as A_e, which represents the area of the computational element, and C_s, which is the Smagorinsky coefficient with a value of 0.2.

The numerical scheme employs a mixed Eulerian-Lagrangian approach, where the material derivative in equation (2) is computed as a finite difference in time and solved using the method of characteristics. This approach enables solving the continuity equation (1) with a semi-implicit scheme, resulting in a self-adjoint spatial operator. The solution is achieved on a staggered triangular grid using the finite element method of Galerkin, as described by Defina (2000), and flow rates are obtained through back-substitution.

The wind-wave module, as presented by Carniello et al. (2011), resolves the wave action conservation equation on the same computational grid as the hydrodynamic module. The wind-wave module utilizes water depths and depth-averaged flow velocities from the hydrodynamic module to propagate the wind-wave field. The evolution of the wave action density (N_0) in the frequency domain is governed by the equation presented in Carniello et al. (2011).

$$\frac{\partial N_0}{\partial t} + \frac{\partial}{\partial x} c'_{gx} N_0 + \frac{\partial}{\partial y} c'_{gy} N_0 = S_0 \tag{5}$$

The wind-wave module, as explained by Carniello et al. (2011), calculates the group celerity components, c'_{gx} and c'_{gy}, to approximate the propagation speed of N_0. The source terms related to wind-wave effects, collectively represented as S_0, encompass both positive (wind energy input) and negative (bottom friction, whitecapping, and depth-induced breaking) contributions to wave energy. Wave period distribution is determined based on the relationship between peak-wave period, local wind speed, and water depth, following Young and Verhagen (1996) (Young & Verhagen, 1996). Given the nearly vertical and jagged margins of the lagoon, refraction effects are disregarded, and waves are assumed to propagate in the direction of the wind.

The horizontal orbital velocity at the bottom, derived from significant wave height using linear wave theory, contributes to the bottom shear stress, τ_w, induced by the wind-wave field. Nonlinear interactions between τ_w and current-induced bottom shear stress (τ_t) are considered through the empirical formulation developed by Soulsby (1995), which increases the total bottom shear stress, τ_b, beyond the simple sum of τ_t and τ_w.

Incorporating the same computational grid, the STABEM module, detailed by Carniello et al. (2012), addresses the advection-diffusion equation for suspended sediment with a conservative, second-order spatial scheme. Additionally, it tackles Exner's equation, which describes sediment bed evolution and interactions with the suspended sediment.

$$\frac{\partial C_i Y}{\partial t} + \nabla \cdot (\boldsymbol{q} C_i) - \nabla \cdot (\mathbf{D}_h \nabla C_i) = E_i - D_i \qquad i = s, m \tag{6}$$

$$(1 - n) \frac{\partial z_b}{\partial t} = \sum_i (D_i - E_i) \tag{7}$$

In the equations, C represents the depth-averaged sediment concentration, and $D_h(x, y, t)$ is a two-dimensional diffusivity tensor that varies in space and time. This diffusivity tensor is assumed to be equal to

the eddy viscosity computed by the hydrodynamic module, as explained by Viero and Defina (2016) (Viero & Defina, 2016). The terms E and D are associated with the entrainment and deposition of bed sediment, while z_b denotes the bed elevation, and n is the bed porosity, which is assumed to have a constant value of 0.4.

The subscript "i" is used to distinguish between non-cohesive (sand, denoted as "s") and cohesive (mud, denoted as "m") sediment classes that are typically found in the bed of tidal lagoons. The relative content of mud (p_m), representing the sum of clay and silt, is assumed to vary both in time and space. This variation determines whether the sediment behaves in a cohesive or non-cohesive manner and sets the critical value of the bottom shear stress.

A threshold value of mud content (p_{mc} = 10%) is used to distinguish between non-cohesive and cohesive behavior, following Van Ledden et al. (2004). The median diameters D_{50} adopted in the simulations to describe cohesive and non-cohesive sediments are 20 μm and 200 μm, respectively, based on measurements conducted in the Venice Lagoon, as described by Carniello et al. (2012).

The deposition rate of sand D_s is computed as

$$D_s = w_s r_0 C_s \tag{8}$$

Where w_s represents the absolute value of the sand settling velocity, and r_0 is the ratio of near-bed to depth-averaged concentration. In this context, r_0 is considered constant and is assumed to be equal to 1.4, as reported in Parker et al. (1987).

The deposition rate of pure cohesive mud, D_m, is determined by Krone's formula, which can be expressed as:

$$D_m = w_m C_m \max\{0; 1 - \tau_b/\tau_d\} \tag{9}$$

where:

- w_m represents the absolute value of the mud settling velocity.

- τ_b is the bottom shear stress, computed by the hydrodynamic module.

- τ_d is the critical shear stress for deposition, and it is set to a value of 1.0 Pa.

The settling velocities, w_s and w_m, are calculated using the Van Rijn formulation (van Rijn, 1984) for solitary particles in clear and still water. This formulation does not incorporate flocculation effects, which are considered negligible for particle diameters larger than 20 μm (Mehta et al., 1989).

The erosion rate is highly dependent on the degree of cohesion of the sediment mixture. For non-cohesive mixtures (where the mud content p_m is less than the critical value p_{mc}), the erosion rate of sand, E_s is described by the Van Rijn formulation (van Rijn, 1984). Meanwhile, the erosion rate of mud, E_m, can be computed using the formulation proposed by Van Ledden (Van Ledden et al., 2004).

$$\begin{aligned} E_s &= (1-p_m) w_s \cdot 1.5 \left(\frac{D_{50}/Y}{D_*^{0.3}}\right) T^{1.5} \\ E_m &= \frac{p_m}{1-p_m} M_{nc} T \end{aligned} \qquad for\ p_m < p_{mc} \qquad (10)$$

For cohesive mixtures ($p_m > p_{mc}$), both sand and mud erosion rates can be computed using the Partheniades's formula

$$\begin{aligned} E_s &= (1-p_m) \cdot M_c\, T \\ E_m &= p_m \cdot M_c\, T \end{aligned} \qquad for\ p_m > p_{mc} \qquad (11)$$

In equations (10) and (11), the various parameters are defined as follows:

- D_* is the dimensionless grain size and is calculated as $D_{50}\,[(s-1)g\,/\,\nu^2\,]^{1/3}$, where D_{50} is the median sediment diameter, s is the sediment's specific density, ν is the water's kinematic viscosity, g represents the gravitational acceleration.

- T is the transport parameter.

- M_{nc} and M_c are specific entrainment values for non-cohesive and cohesive mixtures, respectively. These entrainment values are based on formulations provided by Van Ledden et al. in 2004 and van Rijn in 1984.

$$M_{nc} = \alpha \frac{\sqrt{(s-1)gD_{50}}}{D_*^{0.9}}, \quad M_c = \left(\frac{M_{nc}}{M_m} \cdot \frac{1}{1-p_{mc}}\right)^{\frac{1-p_m}{1-p_{mc}}} \cdot M_m \qquad (12)$$

where M_m is the specific entrainment for pure mud ($M_m = 5 \cdot 10^{-2} g\ m/s$) and α is set equal to $1 \cdot 10^{-5}$.

The transport parameter is usually defined as $T = \max\{0; \tau_b/\tau_c - 1\}$, where τ_b represents the local bottom shear stress, and τ_c is the critical shear stress for erosion. This definition results in a sharp transition between T = 0 and $T = \tau_b/\tau_c - 1$.

However, in real tidal systems, both τ_b and τ_c vary in space. Therefore, it is assumed that they are both random variables and follow a log-normal distribution, as described in Carniello et al. (2012). This stochastic approach leads to a smoother transition between T = 0 and $T = \tau_b/\tau_c - 1$.

All the model parameters fall within the range of variability of similar deposition and erosion formulations (Breda et al., 2021; Temmerman et al., 2005). Notably, erosion is set to zero on salt marshes because the presence of vegetation reduces velocity and wave energy, protecting the sediment from erosion (Möller et al., 1999; Temmerman et al., 2005).

The combined effect of erosion and deposition fluxes of sand and mud results in a variation in bed level over time, which is calculated based on equation (8).

The model has been extensively tested and validated against hydrodynamic, wind-wave, turbidity, and satellite data from various locations, including the Venice Lagoon (Italy), Virginia Coast Reserve lagoons (USA), and Cadiz Bay (Spain), as documented in previous studies (Carniello et al., 2011, 2014; Mariotti & Fagherazzi, 2010; Zarzuelo et al., 2018).

3.2 Numerical simulations

3.2.1 Computational grids

Numerical simulations were performed considering five different morphological configurations of the Venice Lagoon. Three of these configurations represent past-lagoon morphologies reconstructed from available topographic and bathymetric data (Fig 9), whereas the additional two configurations consist of hypothetical scenarios characterized by widespread marhs restoration project that produces significant expansion of marsh area compared to the present-day lagoon morphology.

a) Existing Computational grid

To investigate the historical impact of marsh loss on the morphodynamics of the Venice Lagoon, three existing WWTM computational grids were used, representing the lagoon's morphological configurations in 1901, 1932, and 2014 (the present day). Each grid accurately reflects the lagoon's features as of the selected topobathymetric surveys. The 1901 grid was constructed based on the "Topographic/hydrographic map of the Venice Lagoon" created by the Genio Civile of Venezia in 1901, including jetties at the Lido inlet that were already in place at that time. In contrast, different topographic surveys conducted in 1932 and 2003 by the Venice Water Authority (Magistrato alle Acque di Venezia) were utilized to create the computational grids for the years 1932 and 2014, respectively. The 2014 grid incorporates anthropogenic modifications at the three inlets related to the Mo.S.E. system, which were completed in 2014.

For more detailed information regarding the calibration of both the hydrodynamic and wind-wave models, along with applications specific to the Venice Lagoon, readers are referred to Carniello et al. (2005, 2011) and Tognin et al. (2022) (Carniello et al., 2005, 2011; Tognin et al., 2022). Calibration and testing of the model primarily pertain to the most recent lagoon configurations for which field data are available. Conversely, local

bed-friction coefficient values for the older lagoon configurations (1901, 1932) were assumed based on those selected for the calibrated grids, taking into account factors such as local sediment grain size, bed elevation, and the potential presence of vegetation, such as in salt marshes.

To summarize the model's performance, we use the standard Nash-Sutcliffe Model Efficiency (NSE) parameter. The model performs as follows:

- Tidal Levels: Excellent (NSEmean=0.970, NSEmedian=0.984, NSEstd=0.040)

- Significant Wave Heights: Very good to excellent (NSEmean=0.627, NSEmedian=0.756, NSEstd=0.357)

- Flow Rates at the Inlets: Excellent (NSEmean=0.853, NSEmedian=0.184, NSEstd=0.931)

These statistics were derived from data reported in Tognin et al. (2022, Table S2) (Tognin et al., 2022) and Carniello et al. (2011, Tables 1, 2, and 3) (Carniello et al., 2011). The categorization of model performance follows Allen et al. (2007) (Allen et al., 2007), with four categories ranging from excellent to poor, based on NSE values.

b) Computational grids for simulating marsh restoration projects

In addition to the previous investigations, I also explored the hydrodynamic effects of marsh restoration projects under two distinct scenarios characterized by different degrees of marsh area creation (Barausse et al., 2015; Tagliapietra et al., 2018). Specifically, I used the 2014 computational grid as a reference and reconstructed marshes based on their observed spatial distribution in 1901 and 1932. This allowed me to recreate the marsh distribution observed in those respective years while leaving the rest of the computational grid unaltered.

The computational grids for these two scenarios were built upon the 2014 baseline grid, with marsh areas gradually added. Elements located along the marsh margins were moved to their corresponding locations in 1901 and 1932, respectively. Their characteristics in terms of topographic elevation and bed roughness were adjusted to match those of the surrounding tidal flats.

This is a general introduction to the mathematical model, and now I will explain my practical approach. My task was to recreate a scenario of the salt marsh from 1901 and 1932 in the year 2014, effectively restoring the marsh. This procedure was not straightforward and required some time.

Here's how I proceeded:

- I began by defining the marsh perimeter, creating a contour file (.CNT) file for both 1901 and 1932 based on the original .geo file (see Fig. 13).
- I incorporated this CNT data into the 2014 .geo file and observed all the differences in salt marsh configuration (see Fig. 14).
- The initial step involved adjusting the characteristics, in terms of bed roughness (k_s) of the land polygons that were not part of the marsh in the 2014 file but fell within the new perimeter. To make this adjustment more understandable, I used color coding to distinguish these areas on the map and highlight the differences (see Fig. 15).
- Subsequently, I had to standardize the elevations of these land polygons to align with those of the existing salt marsh. I calculated the mean using the existing heights and then redistributed the values within the new salt marsh boundaries (see Fig. 15).
- Finally, I obtained a new .geo file featuring the 'restored' salt marsh.

- To complete the process, I initiated a simulation using specialized software that provided the necessary data (see Fig. 16 and Fig. 17)."

This approach allowed me to explore two restoration scenarios, referred to as "Restored 1932" and "Restored 1901" hereinafter. These scenarios provide insight into the potential effects of restoring salt marshes to their historical presence and serve as a baseline for assessing whether expanding marsh restoration efforts to larger spatial scales would yield observed morphodynamic benefits, such as changes in hydrodynamic and sediment transport processes within the lagoon.

Although salt-marsh creation could theoretically alter the water volume exchanged between the sea and the lagoon (i.e., tidal prism), leading to adjustments in inlet cross-sectional areas according to the O'Brien-Jarrett-Marchi law (A. D'Alpaos et al., 2009; Jarrett, 1976) the geometry of the lagoon inlets was kept unchanged in the hypothetical scenarios involving marsh restoration. This is because the current inlet geometry is fixed both horizontally and vertically due to the presence of jetties and concrete housing structures built to accommodate the Mo.S.E. floodgates. Additionally, scour processes induced by the jetties over the last century have already deepened the inlets down to the overconsolidated Caranto layer, which would have prevented further deepening, even if the Mo.S.E. barriers had not been constructed.

```
C:\Users\Utente\Desktop\tesi frasson sebastiano\elementi per simulazioni  copia\geo_add_salt_marshes\VE1901-2014\VE2014_2D.geo
2.0 creato con Incidenze    14/08/2023     11:54:50
 55637         0             105735       0            0            0               nodi,nodS,maglie,magS,ncan,ntroS
 ***************** CARATTERISTICHE DI SCABREZZA ****************
 6                numero tipologie scabrezza
   35.00   15.00   20.00   30.00   40.01   15.01
 ***************** CARATTERISTICHE DEI NODI ****************
  2307704.6895  5012156.1842      0.0000
  2307702.0922  5012179.2272      0.0000
  2307702.8973  5012203.1432      0.0000
  2307690.5206  5012253.6014      0.0000
  2307686.0173  5012222.3144      0.0000
  2307677.0119  5012159.7413      0.0000
  2307681.5152  5012191.0283      0.0000
  2307695.0238  5012284.8872      0.0000
  2307665.1911  5012273.2604      0.0000
  2307660.8789  5012241.8924      0.0000
  2307656.6098  5012210.8363      0.0000
  2307652.5945  5012181.6294      0.0000
  2307650.0625  5012163.2113      0.0000
  2307699.5259  5012316.1742      0.0000
  2307704.0291  5012347.4602      0.0000
  2307711.6754  5012403.9682      0.0000
  2307707.8522  5012375.7142      0.0000
  2307715.4996  5012432.2233      0.0000
  2307719.3227  5012460.4772      0.0000
  2307669.5053  5012304.6423      0.0000
  2307635.5395  5012261.4703      0.0000
  2307639.6806  5012293.0664      0.0000
  2307631.3972  5012229.8745      0.0000
  2307627.2551  5012198.2775      0.0000
  2307623.1129  5012166.6812      0.0000
  2307673.7855  5012335.8013      0.0000
  2307677.8636  5012365.6103      0.0000
  2307685.6048  5012422.2622      0.0000
  2307681.7427  5012394.0643      0.0000
  2307694.1052  5012477.5213      0.0000
  2307702.0806  5012500.1882      0.0000
  2307698.9984  5012520.9312      0.0000
  2307689.5611  5012450.2872      0.0000
  2307643.8228  5012324.6633      0.0000
  2307608.0458  5012276.7405      0.0000
  2307614.9394  5012248.8075      0.0000
  2307611.0659  5012315.2225      0.0000
  2307606.8699  5012225.7635      0.0000
  2307595.0153  5012201.1065      0.0000
  2307607.1100  5012184.4244      0.0000
  2307583.0547  5012171.6345      0.0000
  2307647.9649  5012356.2594      0.0000
```

Figure 9: Example of a .geo file where each computational element (i.e., 'maglie') is described along with its characteristics.

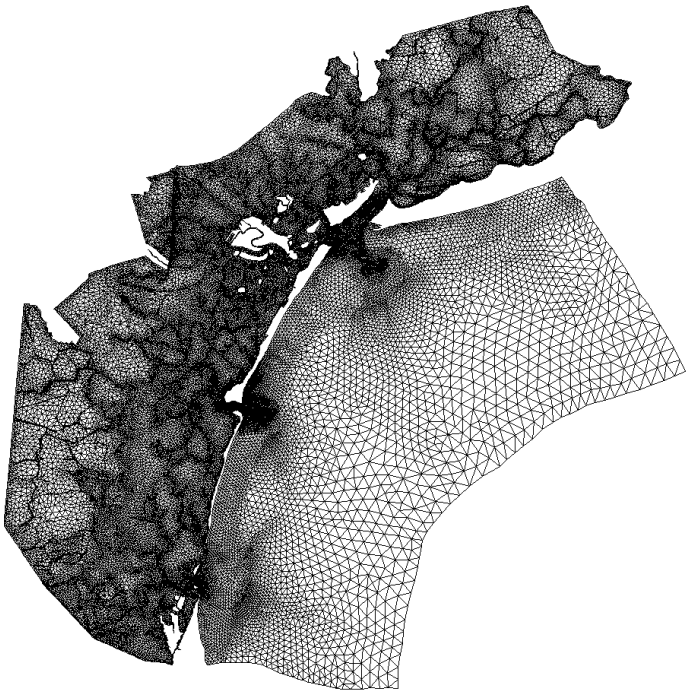

Figure 10: Visualization of a .geo file through the graphical user interface (GUI) software ("Incidenze")

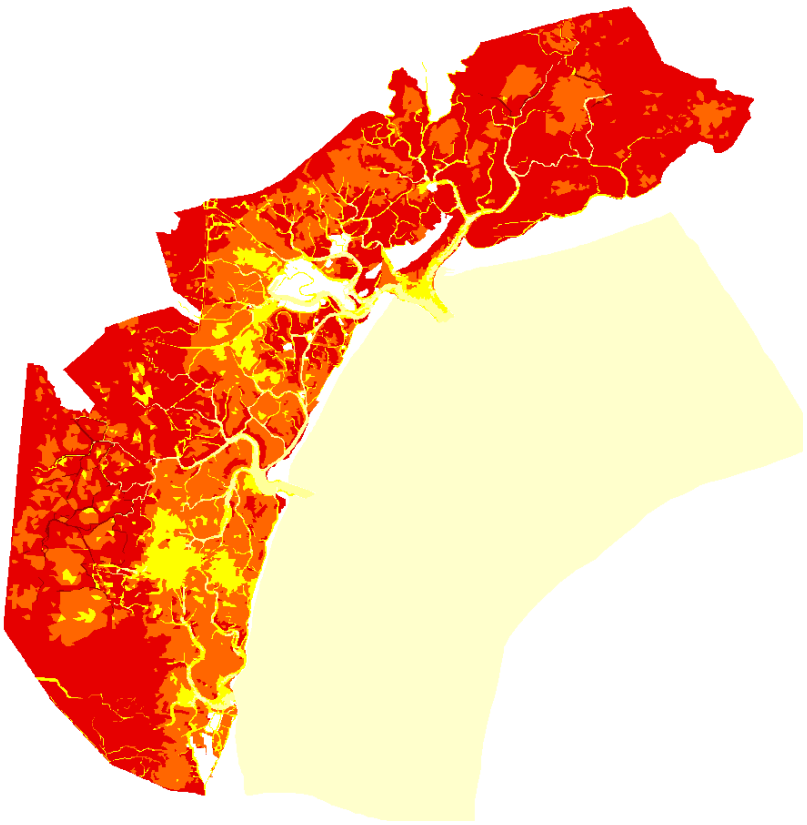

Figure 11: Color-coded map of a .geo file illustrating the morphological configuration of the Venice Lagoon in 1901. Various colors are used to highlight distinct bed roughness coefficients (K_s) across different areas.

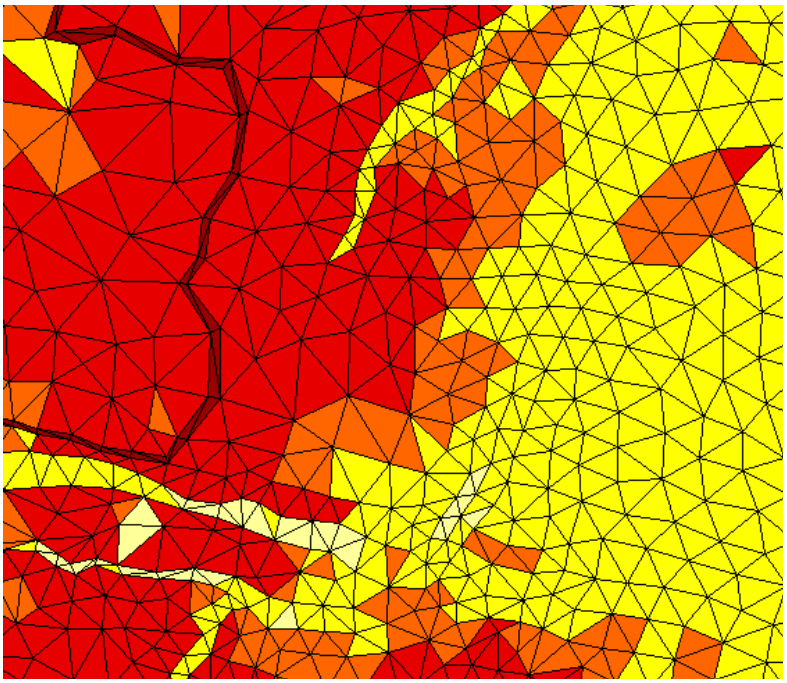

Figure 12: Detail from Figure 11 in the Central South Lagoon, highlighting the "maglie" (triangles) and distinguishing between salt marsh (red), tidal flat (orange), and deeper water (yellow) as a function of K_s

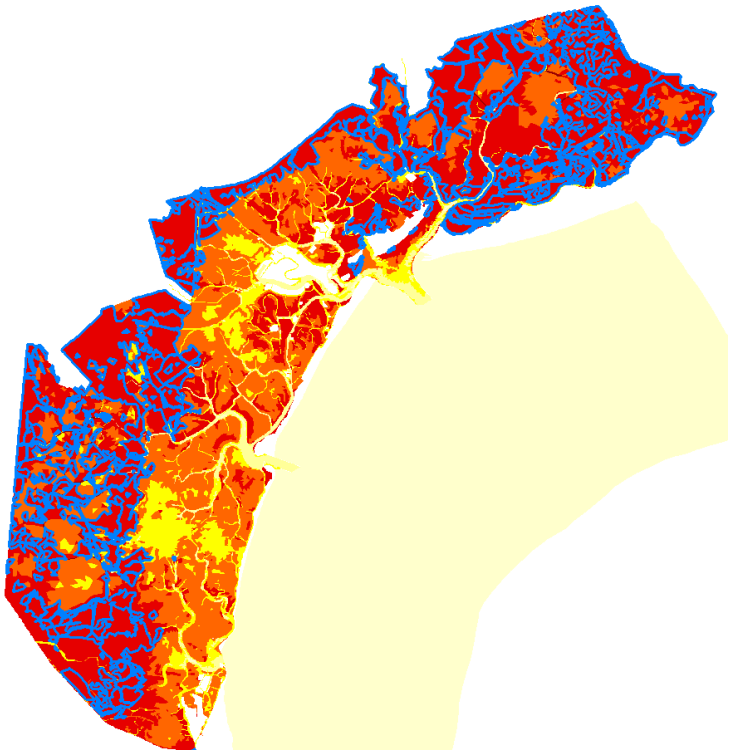

Figure 13: Utilizing the generated geo file, a blue line is employed to form a Contour Line (CNT) marking the boundary of the salt marsh in the Venice Lagoon in 1901.

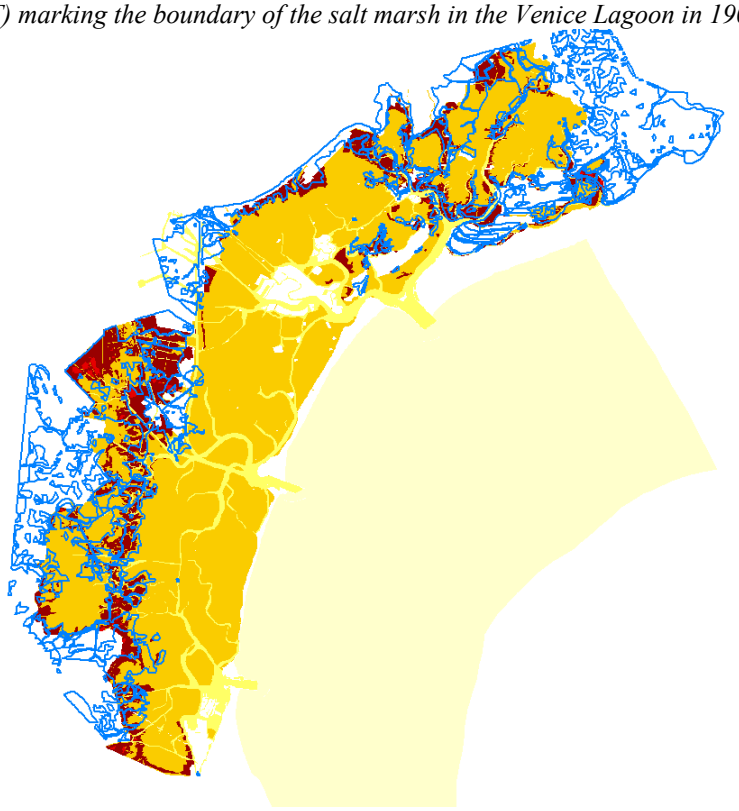

Figure 14: The CNT is uploaded onto the geo file of 2014 to observe distinctions between the current marsh and the marsh designated for restoration.

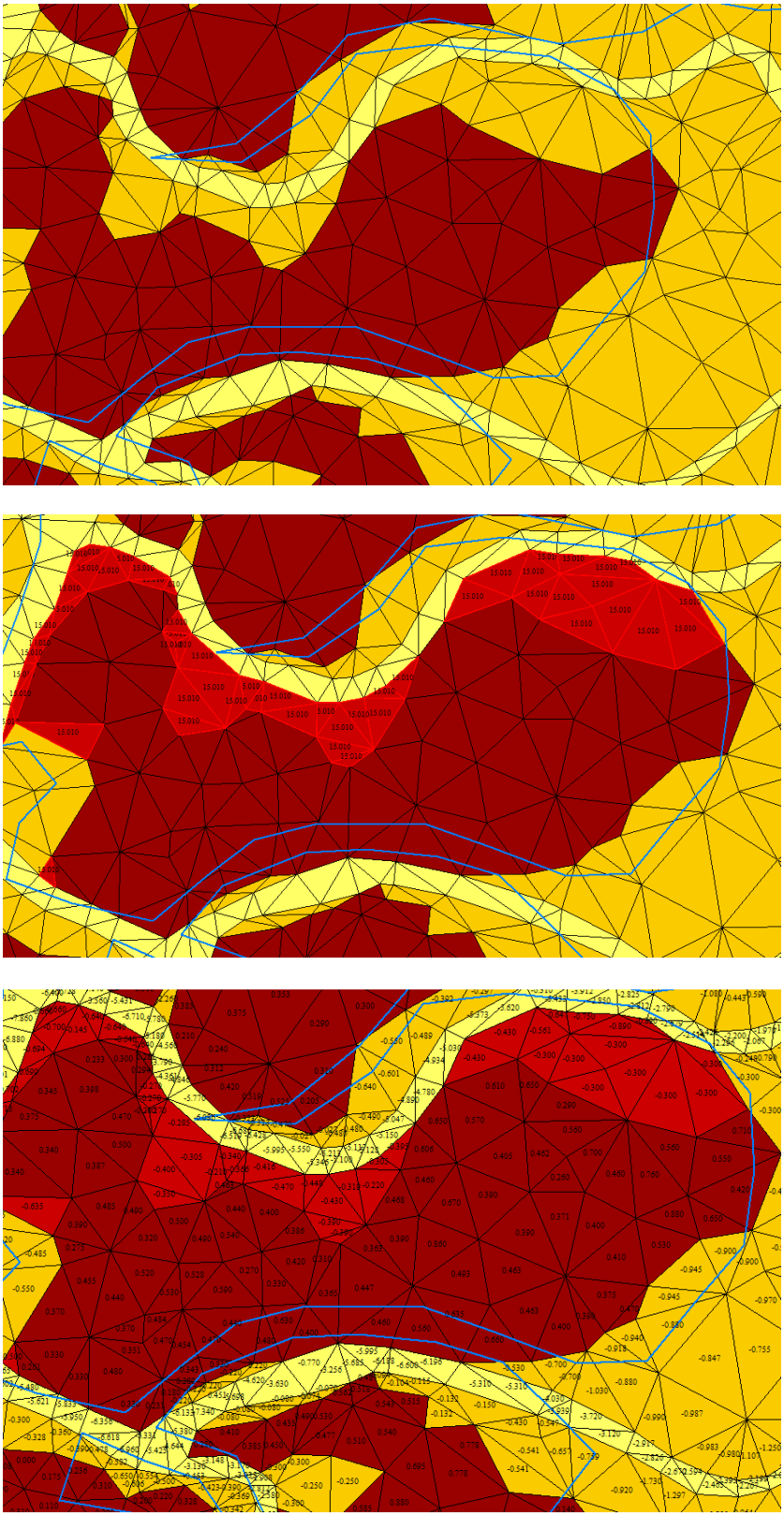

Figure 15: Sketch of the adopted workflow: In the initial image, the existing salt marshes are depicted alongside the border of the 1901 marsh. The restoration process commences by assigning a K_s value of 15.00 (indicated in light red), effectively covering the area within the specified border. Subsequently, adjustments are made to the bed elevation of each computational element to ensure alignment with the existing marsh in terms of topographic elevation.

```
dt stampa,stampa video(1/0),term convettivi(1/0),ritardo Convettivi,term Reynolds(1/0),ritardo Reynolds,Coriolis Par (2wsinLAT)
3600.   1    1   1800.  1   1800.  0.00010363  (coriolis a VENEZIA)
VE1901_2014_2D.geo     nome file geo
30gg_Lincei_2014-IDRO.out      nome file out IDRODINAMICO
30gg_Lincei_2014-MO.out        nome file out MOTO ONDOSO
simulazione Laguna 2014, 30 giorni dal 17-11-2005 al 16-12-2005
2512800.00  4.0  durata,timestep
 0             condizioni iniziali IDRODINAMICA (0=livello_costante; 1=file_restart)
 0.30          valore iniziale delle quote nodali
 xxxIDRO.rts   file di restart
   4 , numero tabelle
   3600         699       tabella 1 livelli in mare (DTtab,Valori)
0.30    0.39    0.40    0.40    0.35    0.24    0.13    0.05    0.04    0.10    0.23    0.35
0.51    0.56    0.56    0.43    0.25    0.01   -0.19   -0.31   -0.36   -0.34   -0.24   -0.08
0.07    0.20    0.29    0.31    0.26    0.20    0.12    0.04    0.03    0.10    0.21    0.34
0.47    0.52    0.50    0.40    0.24    0.05   -0.17   -0.32   -0.43   -0.46   -0.42   -0.31
-0.16   -0.01    0.13    0.18    0.20    0.16    0.09    0.05    0.03    0.06    0.11    0.20
0.28    0.32    0.33    0.26    0.12   -0.03   -0.19   -0.32   -0.40   -0.45   -0.43   -0.35
-0.24   -0.11    0.01    0.12    0.17    0.20    0.21    0.17    0.13    0.13    0.14    0.16
0.18    0.23    0.23    0.17    0.15    0.05   -0.08   -0.15   -0.24   -0.28   -0.27   -0.22
-0.11    0.01    0.16    0.26    0.34    0.41    0.42    0.37    0.31    0.28    0.21    0.14
0.14    0.13    0.10    0.11    0.06    0.00   -0.06   -0.11   -0.17   -0.24   -0.25   -0.22
-0.18   -0.12    0.04    0.10    0.18    0.28    0.34    0.28    0.23    0.21    0.17    0.07
0.03    0.05    0.05    0.13    0.15    0.19    0.17    0.07    0.05    0.03    0.05    0.08
-0.03   -0.03   -0.04    0.00    0.05    0.12    0.16    0.18    0.20    0.16    0.12    0.10
0.09    0.08    0.08    0.08    0.07    0.08    0.09    0.13    0.15    0.13    0.08   -0.01
-0.10   -0.15   -0.19   -0.15   -0.08    0.00    0.13    0.20    0.29    0.33    0.33    0.32
0.26    0.21    0.16    0.12    0.13    0.20    0.25    0.33    0.40    0.41    0.40    0.35
0.30    0.13    0.03    0.05    0.03    0.12    0.29    0.41    0.55    0.62    0.63    0.57
0.46    0.30    0.19    0.12    0.12    0.18    0.28    0.40    0.51    0.57    0.60    0.58
0.50    0.42    0.29    0.14    0.20    0.24    0.32    0.51    0.61    0.64    0.64    0.56
0.44    0.26    0.10    0.05   -0.04    0.00    0.05    0.17    0.32    0.37    0.43    0.47
0.38    0.29    0.18    0.09    0.05    0.04    0.16    0.25    0.40    0.49    0.57    0.52
0.48    0.32    0.12    0.01   -0.11   -0.14   -0.10   -0.02    0.13    0.23    0.34    0.37
0.31    0.23    0.16    0.07    0.03    0.05    0.12    0.22    0.36    0.52    0.59    0.61
0.60    0.51    0.36    0.16   -0.01   -0.09   -0.16   -0.07    0.07    0.20    0.35    0.49
0.55    0.47    0.39    0.28    0.19    0.11    0.12    0.18    0.27    0.43    0.55    0.63
0.60    0.52    0.33    0.09   -0.16   -0.32   -0.40   -0.37   -0.22   -0.01    0.22    0.40
0.52    0.51    0.46    0.35    0.23    0.15    0.15    0.16    0.28    0.38    0.53    0.62
0.61    0.54    0.37    0.15   -0.11   -0.27   -0.39   -0.44   -0.39   -0.26   -0.06    0.14
0.29    0.36    0.40    0.33    0.24    0.13    0.05    0.05    0.12    0.23    0.37    0.50
0.58    0.57    0.49    0.30    0.10   -0.12   -0.28   -0.33   -0.31   -0.19   -0.03    0.16
0.32    0.44    0.49    0.52    0.48    0.44    0.39    0.39    0.45    0.55    0.72    0.82
0.96    1.02    0.98    0.84    0.61    0.38    0.13   -0.03   -0.10   -0.08   -0.04    0.08
0.20    0.34    0.37    0.38    0.36    0.25    0.18    0.14    0.13    0.16    0.31    0.42
0.57    0.67    0.71    0.63    0.46    0.26    0.02   -0.15   -0.21   -0.23   -0.17   -0.04
0.11    0.25    0.34    0.47    0.52    0.45    0.43    0.39    0.36    0.35    0.44    0.56
0.66    0.72    0.73    0.71    0.59    0.40    0.22    0.05   -0.08   -0.19   -0.20   -0.16
-0.08    0.00    0.13    0.23    0.34    0.41    0.46    0.48    0.46    0.47    0.45    0.50
0.53    0.56    0.59    0.59    0.52    0.40    0.23    0.08   -0.08   -0.21   -0.31   -0.35
-0.31   -0.19    0.02    0.23    0.44    0.60    0.68    0.71    0.70    0.61    0.53    0.42
0.32    0.29    0.30    0.32    0.31    0.27    0.19    0.04   -0.10   -0.22   -0.31   -0.35
-0.32   -0.23   -0.06    0.13    0.31    0.45    0.58    0.60    0.56    0.48    0.37    0.24
```

Figure 16: An illustration of a simulation file (.sim) containing all pertinent parameters for the simulations, encompassing boundary conditions. This file is utilized by the model to furnish the necessary data

```
time:    0.022   ore    3       0.300000       0.299850       0.000373       0.000000
time:    0.023   ore    3       0.300000       0.299832       0.000375       0.000000
time:    0.024   ore    3       0.300000       0.299812       0.000376       0.000000
time:    0.026   ore    3       0.299999       0.299790       0.000377       0.000000
time:    0.027   ore    3       0.299999       0.299765       0.000378       0.000000
time:    0.028   ore    3       0.299999       0.299738       0.000379       0.000000
time:    0.029   ore    3       0.299999       0.299709       0.000380       0.000000
time:    0.030   ore    3       0.299998       0.299679       0.000381       0.000000
time:    0.031   ore    3       0.299998       0.299646       0.000382       0.000000
time:    0.032   ore    3       0.299997       0.299612       0.000383       0.000000
time:    0.033   ore    3       0.299997       0.299578       0.000384       0.000000
time:    0.034   ore    3       0.299997       0.299542       0.000385       0.000000
time:    0.036   ore    3       0.299996       0.299506       0.000386       0.000000
time:    0.037   ore    3       0.299996       0.299469       0.000387       0.000000
time:    0.038   ore    3       0.299996       0.299433       0.000388       0.000000
time:    0.039   ore    3       0.299995       0.299395       0.000389       0.000000
time:    0.040   ore    3       0.299995       0.299358       0.000390       0.000000
time:    0.041   ore    3       0.299995       0.299321       0.000391       0.000000
time:    0.042   ore    3       0.299995       0.299283       0.000392       0.000000
time:    0.043   ore    3       0.299995       0.299245       0.000393       0.000000
time:    0.044   ore    3       0.299995       0.299208       0.000394       0.000000
time:    0.046   ore    3       0.299995       0.299170       0.000395       0.000000
time:    0.047   ore    3       0.299995       0.299133       0.000396       0.000000
time:    0.048   ore    3       0.299996       0.299096       0.000397       0.000000
```

Figure 17: Screenshot of the model during a numerical simulation.

3.2.2 Boundary conditions

In the numerical model, water levels are prescribed at the seaward boundary of the computational domain, representing the portion of the northern Adriatic Sea in front of the Venice Lagoon (as shown in Fig. 16). Water-level data are obtained from measurements taken at the CNR Oceanographic Platform, situated in the Adriatic Sea approximately 15 km from the coastline. As water levels and bed elevations in each computational grid reference mean sea level at the time of each survey, they implicitly account for historical rises in relative sea level.

Wind speeds and directions are measured at the "Chioggia Diga Sud" anemometric station, and are applied to the entire lagoonal basin, as detailed in Carniello et al. (2005) (Carniello et al., 2005).

Consistent boundary conditions were used for all simulations, enabling direct comparisons between different lagoon configurations. The model was driven by hourly water levels and wind velocities and directions recorded from November 16th, 2005, to December 17th, 2005, as illustrated in Fig. 18. This 30-day period serves as a representative snapshot of the hydro-meteorological conditions typically experienced annually in the Venice Lagoon between October 1st and January 30th, a period known for significant storm-surge events. The cumulative frequency of water levels during this study period closely matches the average distribution observed between 2000 and 2020 (Fig.18).

Furthermore, the selected study period encompasses two relatively strong Bora wind events (as shown in Fig 18 D), which are characteristic of the wind climate in Venice (Fig 18). Therefore, this study period allows for a focus on both typical tides and representative storm events.

Notably, a morphological acceleration factor of 12 was employed to accelerate morphological evolution. The use of a morphological acceleration factor is a common practice aimed at reducing the computational time required for extended morphodynamic simulations. This factor is a scalar quantity applied to the Exner's sediment continuity equation, operating under the assumption that morphodynamic changes occur at longer time

scales compared to the hydrodynamic processes (Lesser et al., 2004). The implementation of this morphological acceleration factor allows our month-long simulations to be effectively interpreted as year-long simulations (i.e., one month multiplied by 12) when considering morphological evolution processes, such as salt marsh sedimentation and vertical accretion. It is, however, essential to recognize that, while this approximation is reasonably accurate, the period under analysis is particularly favorable for salt marsh growth. This is due to the significant resuspension of sediment by waves, which is subsequently deposited over salt marshes (Tognin et al., 2021) Consequently, the application of a morphological factor may lead to a somewhat higher general interpretation than the actual conditions in reality.

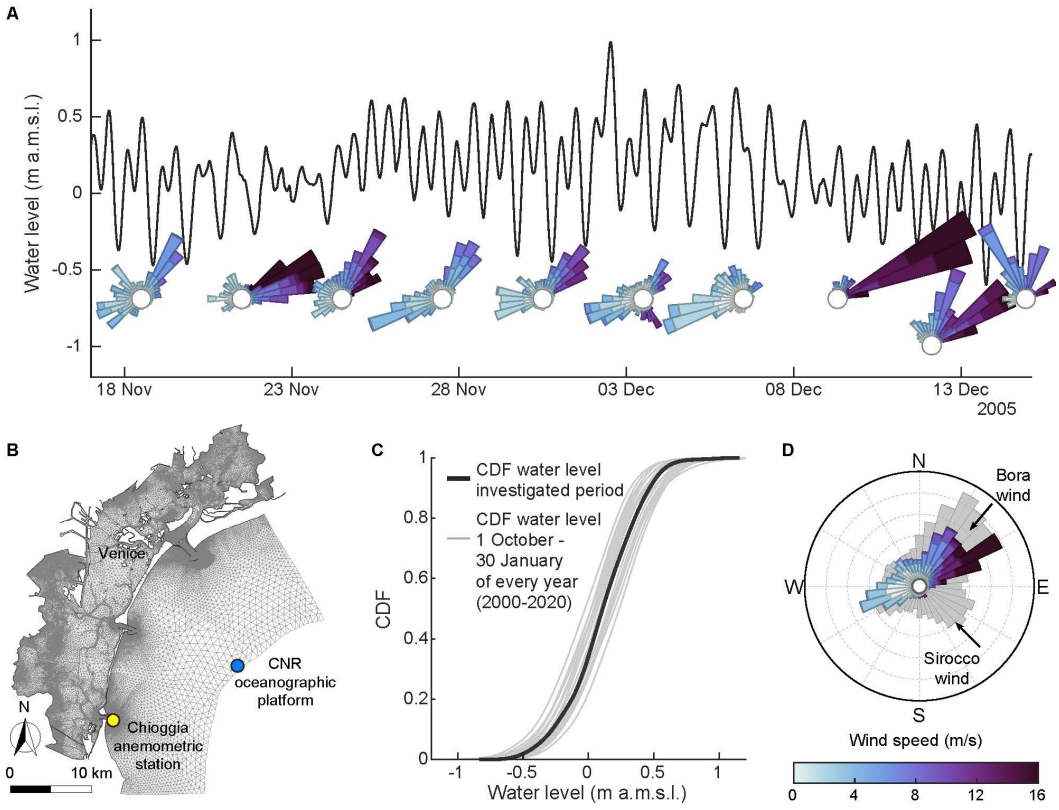

Figure 18: The data used in the numerical simulations pertain to a specific time period from November 17, 2005, to December 17, 2005. Water levels were monitored and recorded at the "CNR Oceanographic Platform," and wind data were collected from the "Chioggia Diga Sud" anemometric station, as depicted in panel (b). The computational grid employed in the numerical model is illustrated in panel (b) and corresponds to the 2014 morphological configuration of the Venice Lagoon. Panels (c) and (d) compare the distributions of water levels (c) and wind climate (d) during the analyzed period to those observed over the period from 2000 to 2019, represented in grey. These comparisons provide valuable context for understanding the conditions simulated in the study. (Image from Finotello et al., 2023)

4. Result and discussion

Several hydrodynamic and sediment transport-related parameters can be examined using the outcomes of the numerical simulations. These attributes encompass water levels, wind wave heights, bed shear stresses, tidal and sediment flux at the Lagoon inlet, and bed evolution, which pertains to marsh vertical accretion. A comprehensive analysis of each of these variables is presented below, encompassing both storm conditions and fair-weather conditions as well as spatiotemporal integrated metrics (i.e., concerning the entire duration of the simulation).

Figure 19: Map of the Venice Lagoon from Google Earth, showing the five points taken into consideration for the analyses: North Lagoon, Central North Lagoon, Central Lagoon, Central South Lagoon, South Lagoon.

4.1 Local Hydrodynamics

Within the 30-day timeframe covered by the numerical simulations, two specific time series were examined. The first one spans from hour 100 to 200 and represents storm conditions, characterized by significant Bora winds blowing from the east-northeast. The second time series covers hours

200 to 300, corresponding to fair weather conditions with calm winds. These two intervals provide valuable insights into the different stages of morphodynamic processes taking place within the lagoon.

For initial evaluation, five representative points within the Venice Lagoon were selected: North Lagoon (NL), Central North Lagoon (CNL), Central Lagoon (CL), Central South Lagoon (CSL), and South Lagoon (SL). (Figure XXX). While these points may not provide an exact assessment of the Venice Lagoon's hydro and morphodynamic behavior (which may vary substantially both in space and time) they are suitable for obtaining a general overview of the primary processes, which suffices for this research.

4.1.1 Water levels

a) Storm Condition

Regarding water levels, a detailed analysis of conditions was conducted. Notably, distinct variations exist from the northern region to the southern region as a function of tidal fluctuations and, more importantly, wind-induced water level setup (which occur due to the semienclosed nature of the Venice lagoon). Specifically, during storm conditions, the highest water levels occur in the southern lagoon due to the predominant wind direction.

In the North Lagoon (NL), two clear trends emerge: 1901 and 1932, which, while not identical, exhibit coherent alignment. In contrast, 2014, “Restore 1901”, and “Restore 1932” practically overlap. A similar pattern is observed in the Central North Lagoon (CNL), where 1901 and 1932 show greater similarity, although not identical levels. In the Central Lagoon (CL), the situation shifts slightly. Here, 1901 and 1932 are quite similar, and 2014 and “Restore 1932” overlap, while “Restore 1901” differs slightly (although not significantly, likely due to the chosen data points). In the Central South Lagoon (CSL), the situation parallels CNL, with 1901 and 1932 showing similarity, and 2014, “Restore 1901”, and “Restore 1932” all overlapping. Conversely, in the South Lagoon (SL), which experiences the highest water levels, the scenario is distinct. Here, all lines are clearly separated but follow a similar trend. 1901 and 1932 are in close proximity, and for the majority

of the graph, so are 2014, “Restore 1901”, and “Restore 1932”. Nonetheless, there are some discrepancies, likely stemming from the chosen data points (spatial variability in water level across the marsh should be always expected due to the highly frictional character of the flow therein).

In conclusion, it can be affirmed that the restoration efforts in terms of hydrodynamics appear to have a negligible impact. The trends indicate that there aren't significant enough differences to validate a positive effect.

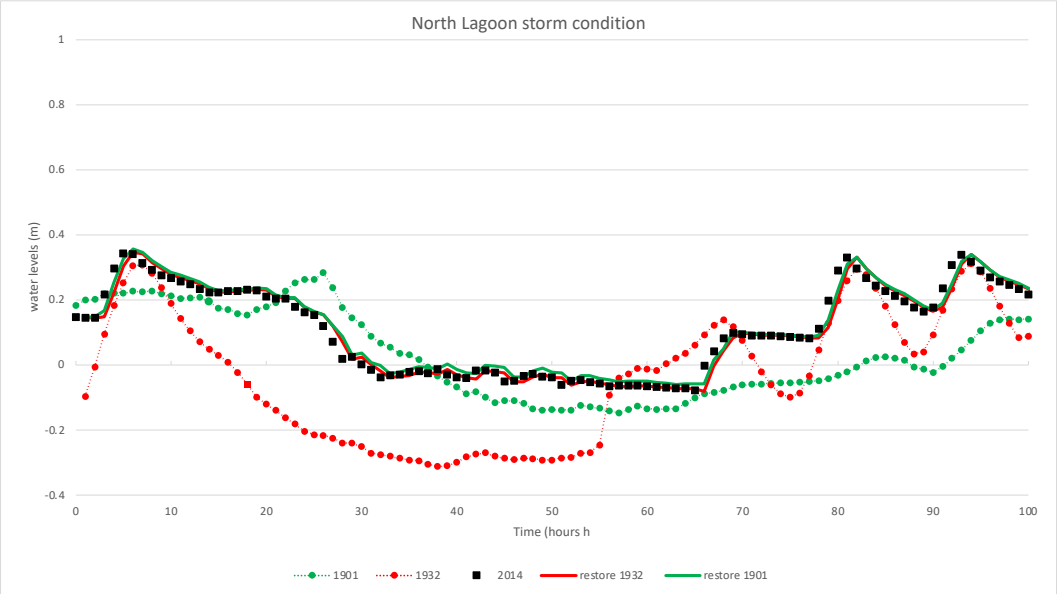

Figure 20: North Lagoon storm condition water levels

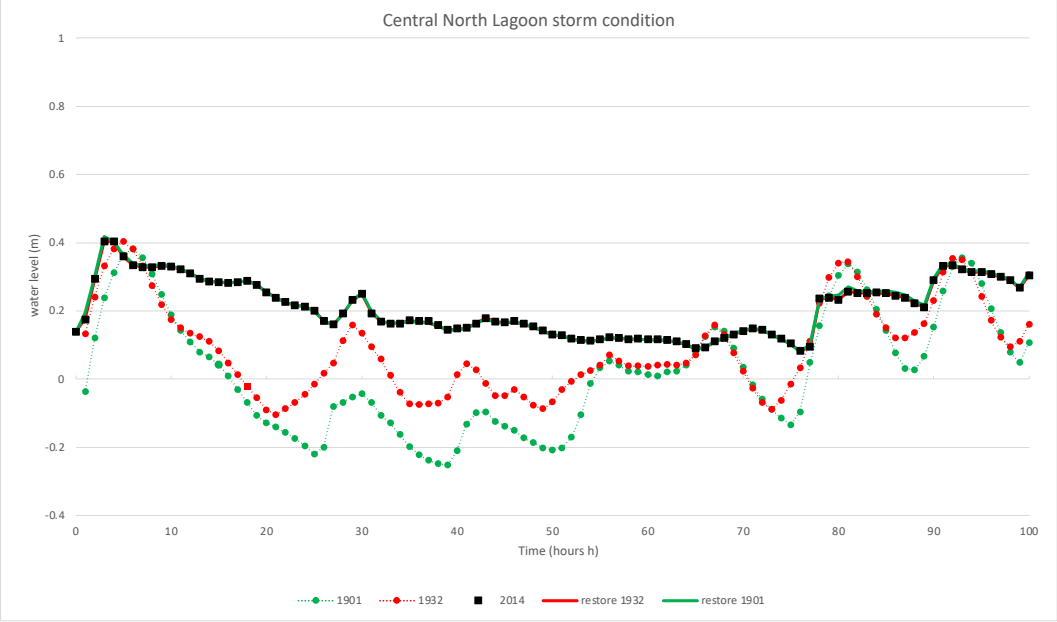

Figure 21: Central North Lagoon storm condition water levels

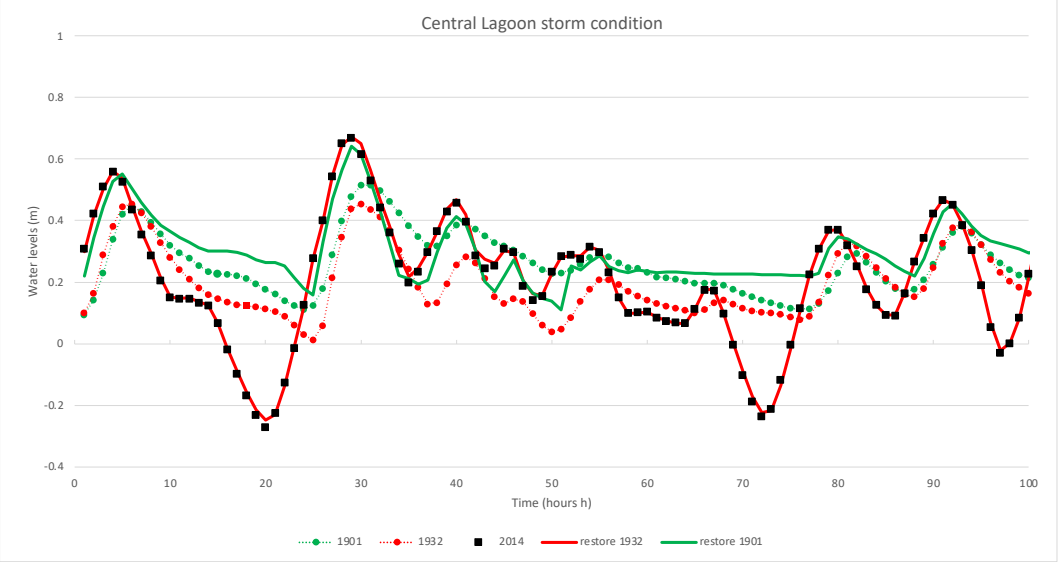

Figure 22: Central Lagoon storm condition water levels

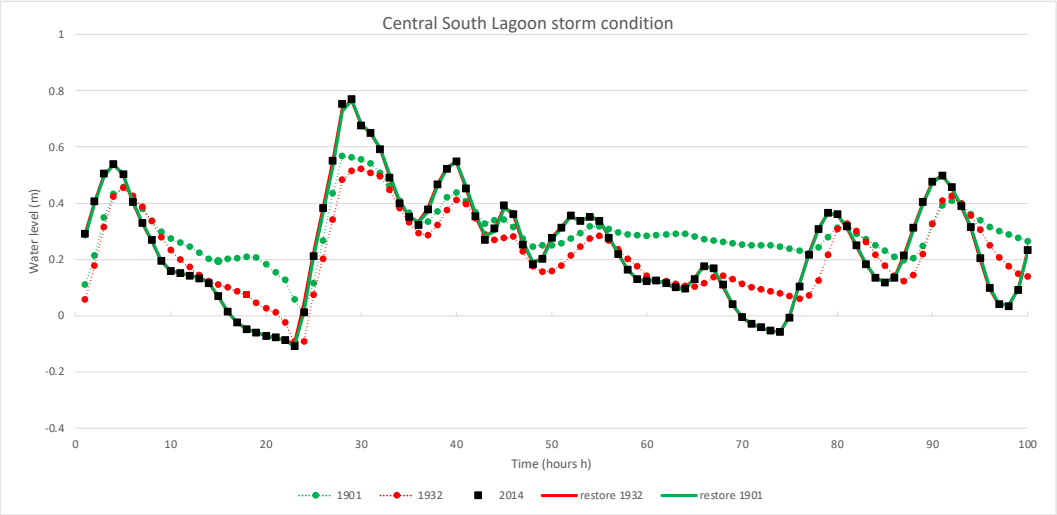

Figure 23: Central South Lagoon storm condition water levels

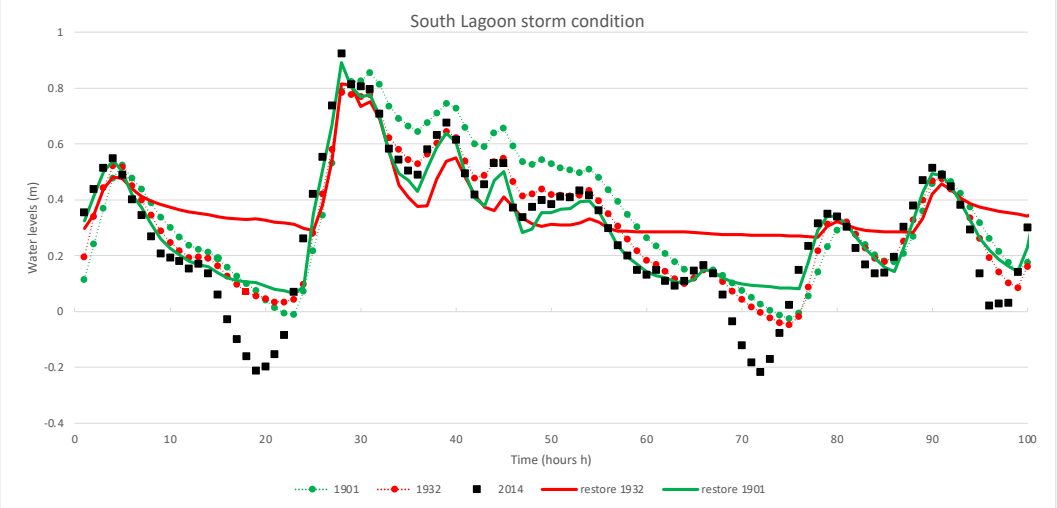

Figure 24: South Lagoon storm condition water levels

b) Fair weather conditions

During fair weather conditions, water levels are notably lower compared to storm conditions, with the highest point reaching about 70 cm, as opposed to the approximately 1 m observed during storms. This highlights the significant influence of the Bora wind on the hydrodynamics of the Lagoon. The situation appears to be somewhat more uniform during fair weather, with fewer disparities between locations.

In the North Lagoon (NL), 1901 and 1932 display similar patterns, while 2014 and the restored configuration overlap perfectly. In the Central North Lagoon (CNL), 1901 and 1932 exhibit nearly identical trends, and the other three lines converge closely. Within the Central Lagoon (CL), there are slight distinctions between configurations; “Restore 1901” tends to align with 1901 at certain points, but the overall graph is closer to 2014 and “Restore 1932”. Meanwhile, 1901 and 1932 show similar patterns. Similar to CNL, the situation in the Central South Lagoon (CSL) mirrors that of CNL.

In the South Lagoon (SL), due to its specific geographical position, there are some variances. While the trend remains consistent for the majority of the graph, there are moments where the situation appears to diverge. This

could likely be attributed to specific events occurring during those times. Under fair conditions, the graph depicts conditions that are more similar, with fewer distinctions between the primary points of analysis.

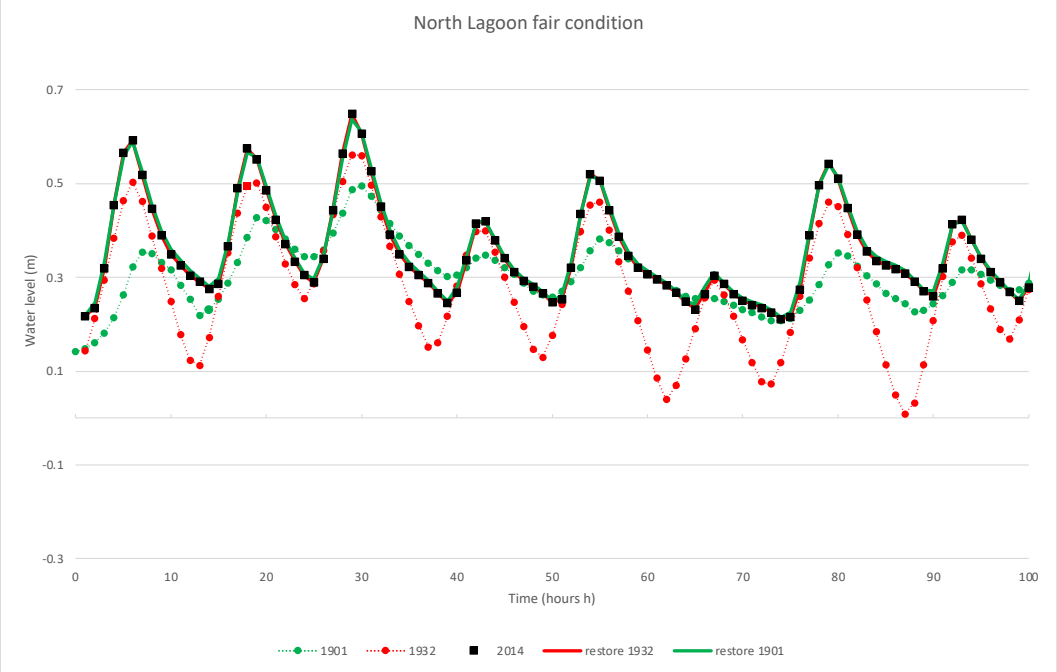

Figure 25: North Lagoon fair weather condition water levels

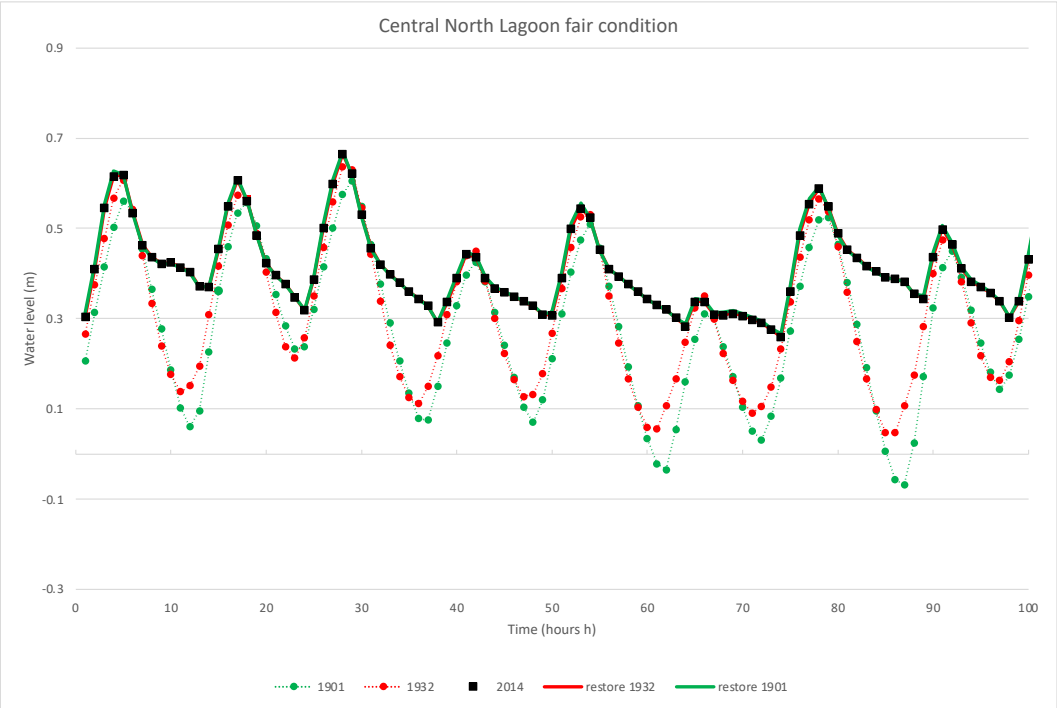

Figure 26: Central North Lagoon fair weather condition water levels

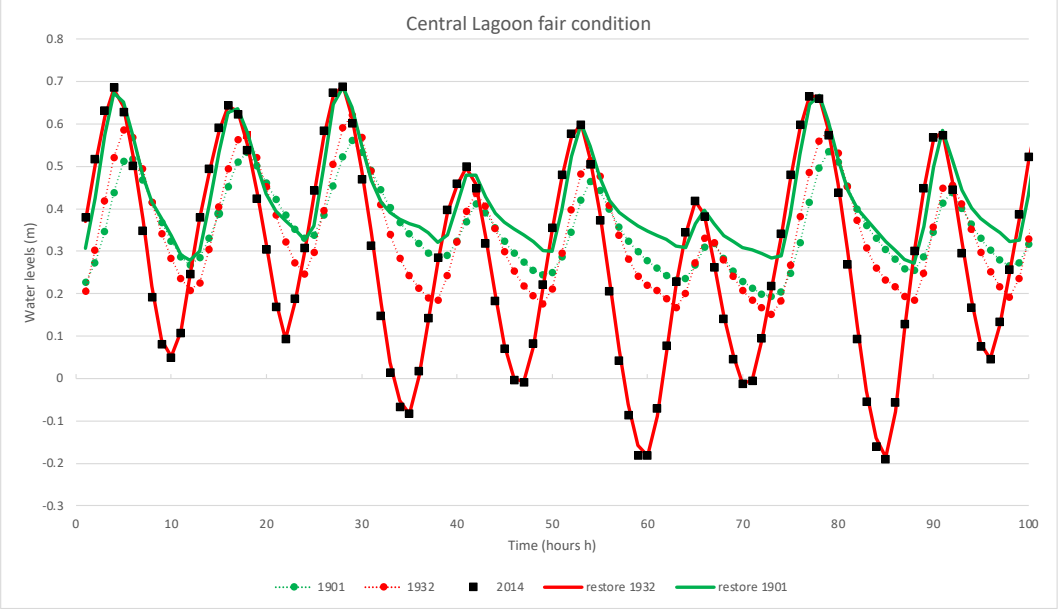

Figure 27: Central Lagoon fair weather condition water levels

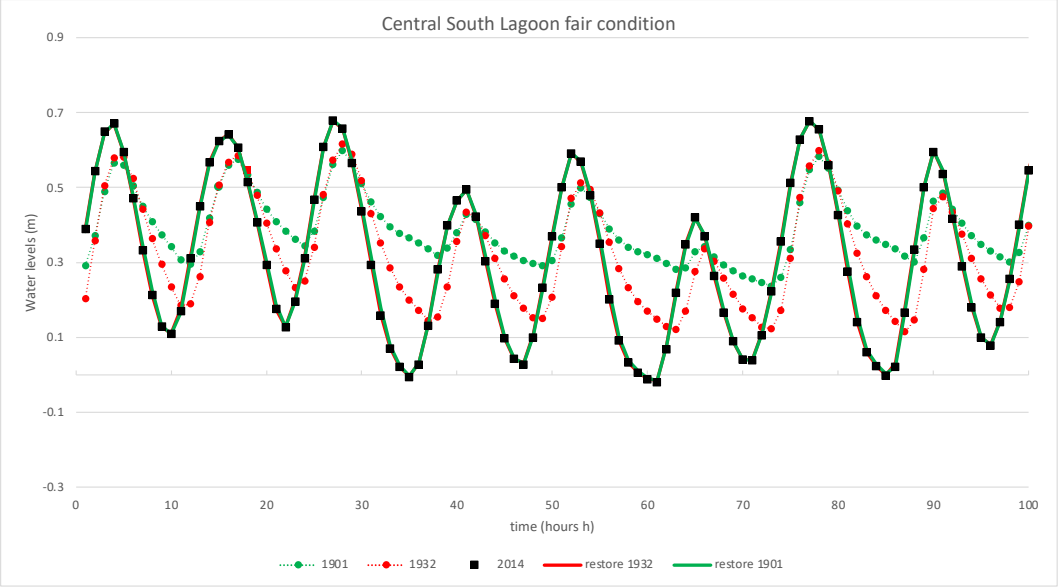

Figure 28: Central South Lagoon fair weather condition water levels

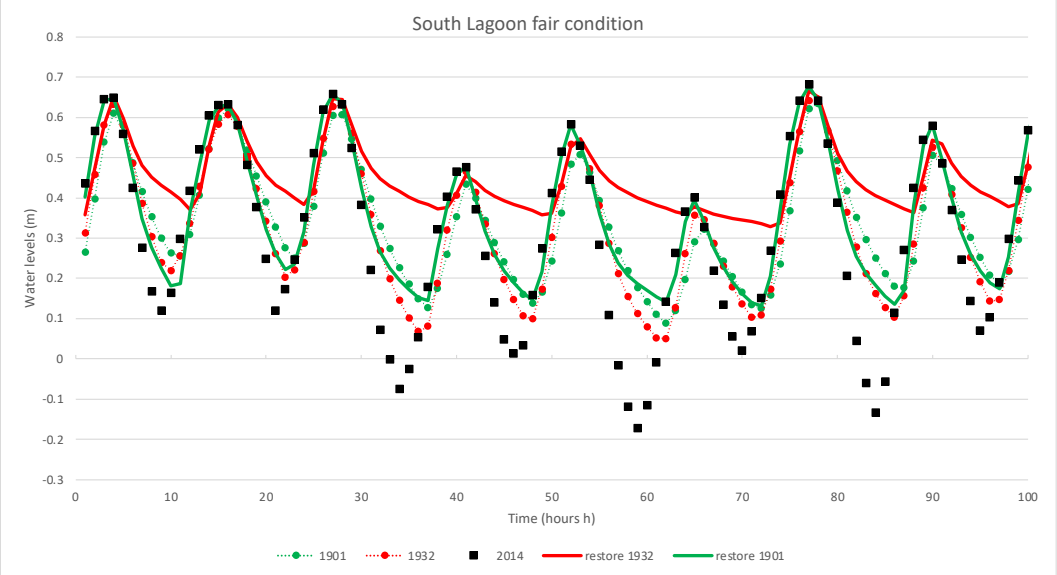

Figure 29: South Lagoon fair weather condition water levels

4.1.2 Wind waves heights

a) Storm Condition

The wind wave heights range from 0m to 0.4m during storm conditions, emphasizing the significant role of wind in the Lagoon. Notably, the northern region experiences relatively minor oscillations compared to more pronounced fluctuations in the south and central areas. In the North Lagoon (NL), a consistent trend is observed across all years and configurations, except for "Restore 1932," which exhibits a slightly deviating trend, likely due to specific data points chosen. The situation in the Central North Lagoon (CNL) closely mirrors that of NL, indicating that the impact of salt marsh restoration on hydrodynamics is negligible.

However, in the Central Lagoon (CL), there is a notable oscillation. The restoration of salt marshes leads to a reduction in wave height, while the 2014 scenario exhibits significantly higher wave heights. While marsh restoration may offer modest benefits, returning to the original condition seems unattainable.

In the Central South Lagoon (CSL), a consistent trend is evident, with three primary trajectories: one for 1901, one for 1932, and another for 2014.

"Restore 1932" and "Restore 1901" align closely. Therefore, the effect of marsh restoration on hydrodynamics in this area is considered negligible.

The South Lagoon (SL) presents a significantly different scenario. Here, a diverse trend is observed, with each year and configuration following a distinct trajectory. This variability is likely influenced by the specific geographical position of the south lagoon and the impact of the Bora wind.

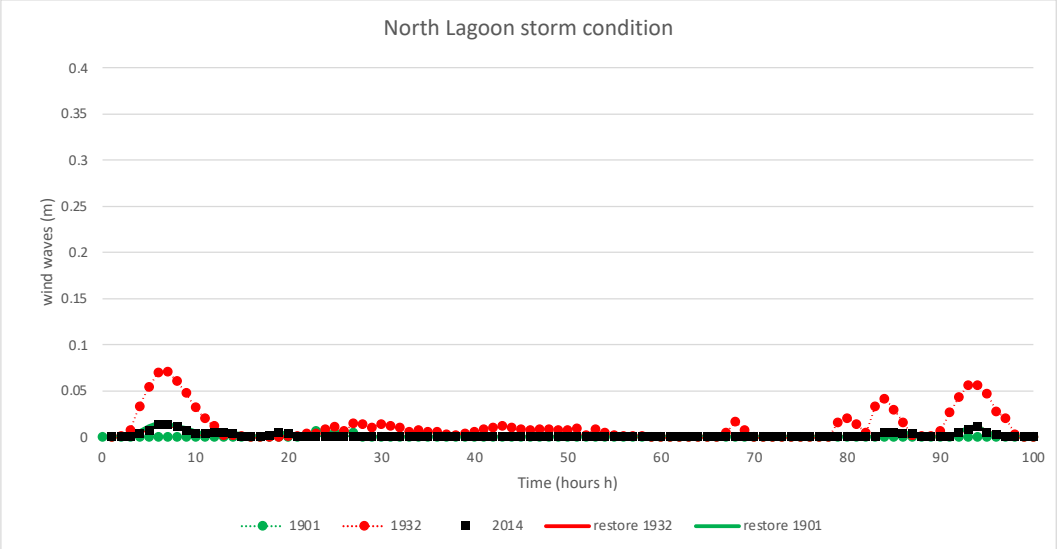

Figure 30: North Lagoon storm condition wind-wave height

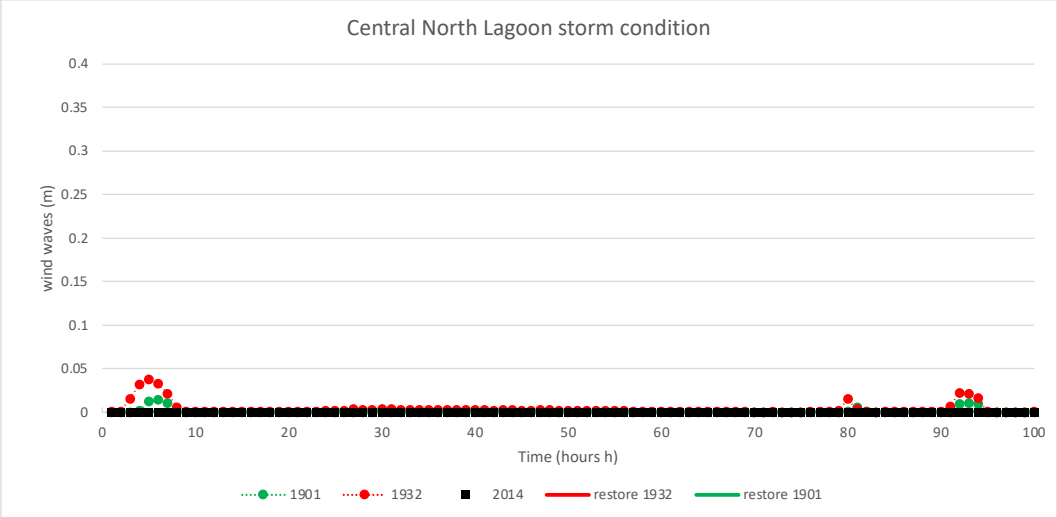

Figure 31: Central North Lagoon storm condition wind-wave height

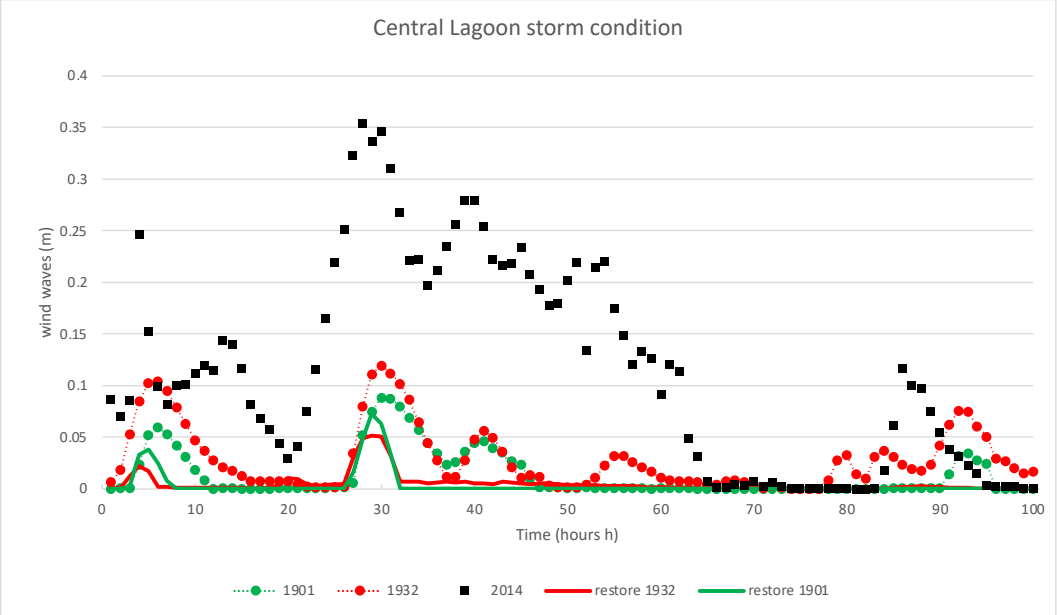

Figure 32: Central Lagoon storm condition wind-wave height

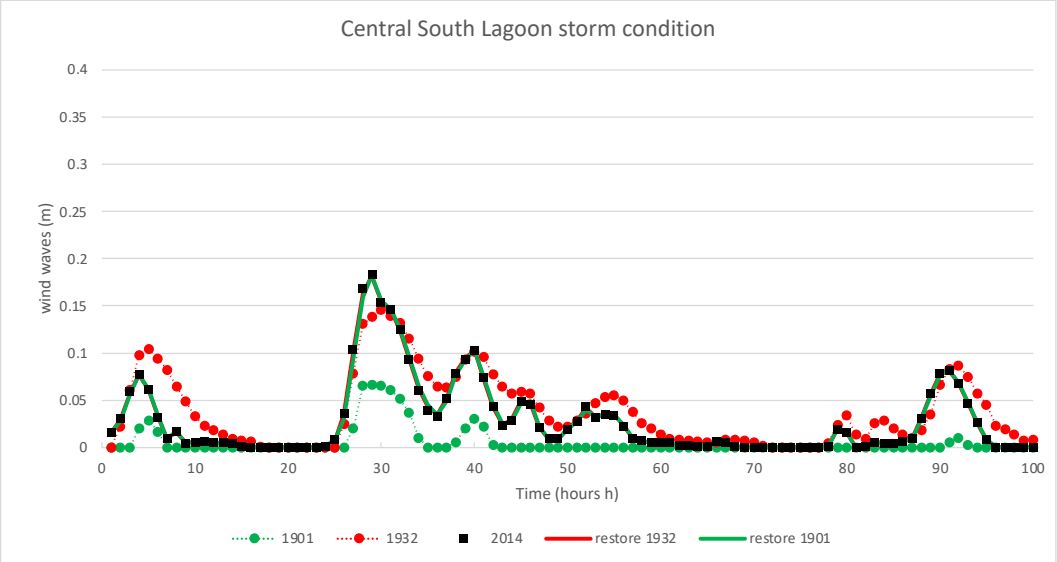

Figure 33: Central South Lagoon storm condition wind-wave height

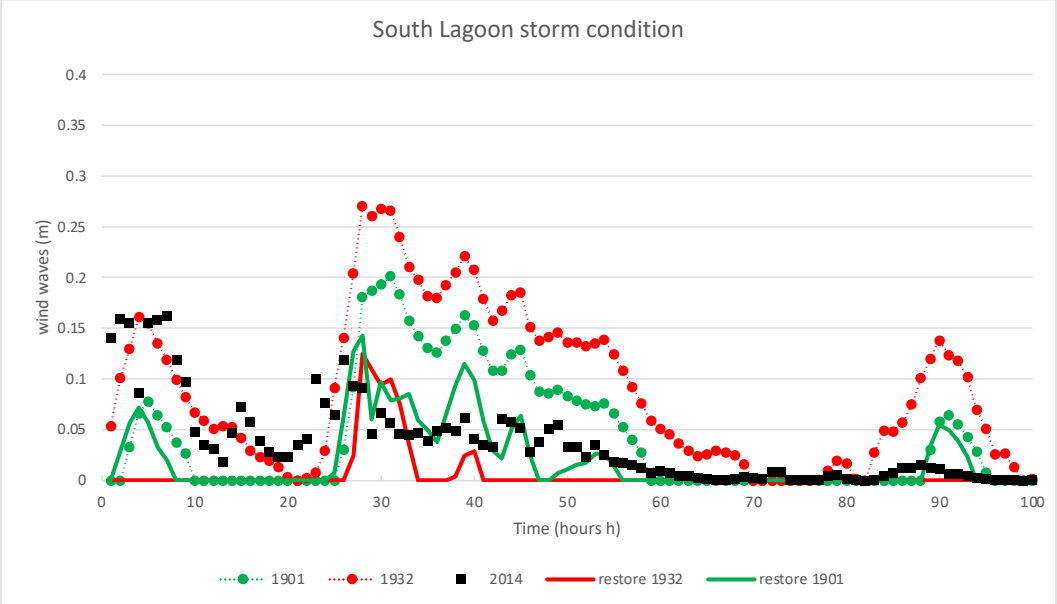

Figure 34: South Lagoon storm condition wind-wave height

b) Fair weather conditions

Under fair weather conditions, the influence of wind diminishes, leading to shifts in wave dynamics across the Venice Lagoon. In the North Lagoon (NL), three primary trends emerge: one for 1932, another for 1901, and an overlapping one for 2014, "Restore 1901", and "Restore 1932". These findings clearly indicate that marsh restoration activities do not induce significant changes in the lagoon's hydrodynamics.

A similar pattern is evident in the Central North Lagoon (CNL), further substantiating the notion of minimal alterations in the lagoon due to restored marshes. However, in the Central Lagoon (CL), distinct changes are observed, with all five trends clearly delineated. It is noteworthy that "Restore 1901" and "Restore 1932" closely align with 2014 in certain sections, but they never mirror the trends observed in 1901 and 1932. This suggests that the specific geographic position of the chosen point in CL influences the observed trend.

In the Central South Lagoon (CSL), the trend mirrors that of NL. However, a significant difference arises: the configuration in 1932 exhibits

higher wave heights than those in 2014, “Restore 1932”, and “Restore 1901”, while 1901 displays lower wave heights.

In the South Lagoon (SL), variations are observed, likely attributed to its southern location. Specifically, 1901 and 1932 show higher wave heights, whereas 2014, “Restore 1901”, and “Restore 1932” exhibit distinct trends. Furthermore, 2014, “Restore 1901”, and “Restore 1932” share overall similar trends but manifest some slight differences at specific points.

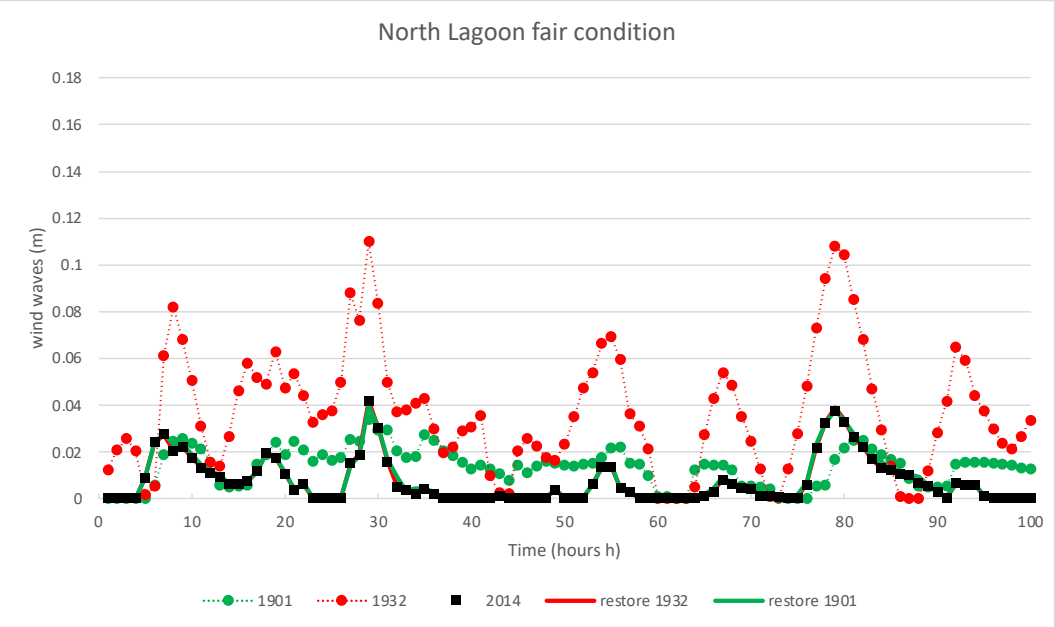

Figure 35: North Lagoon fair weather condition wind-wave height

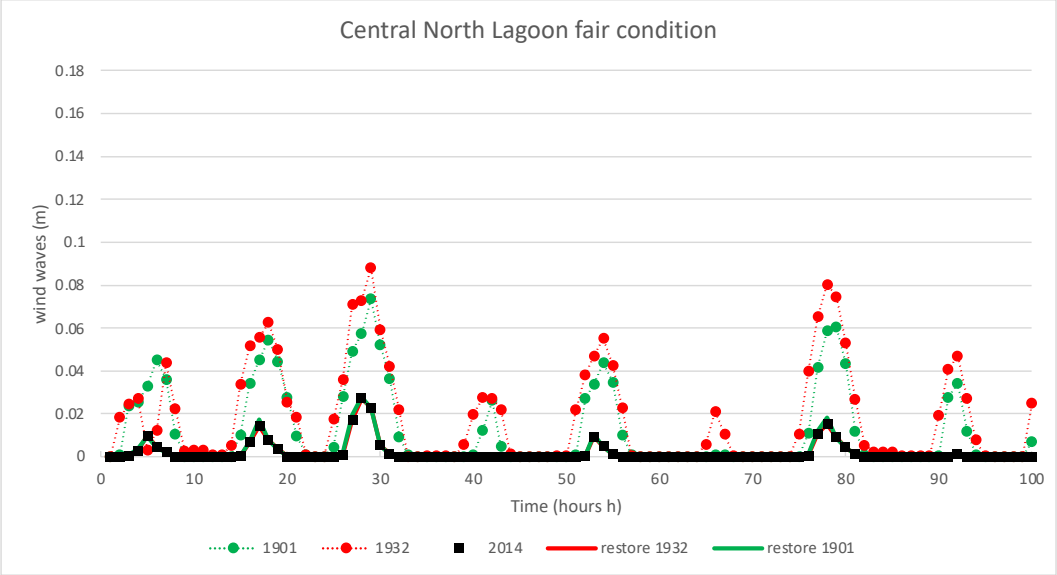

Figure 36: Central North Lagoon fair weather condition wind-wave height

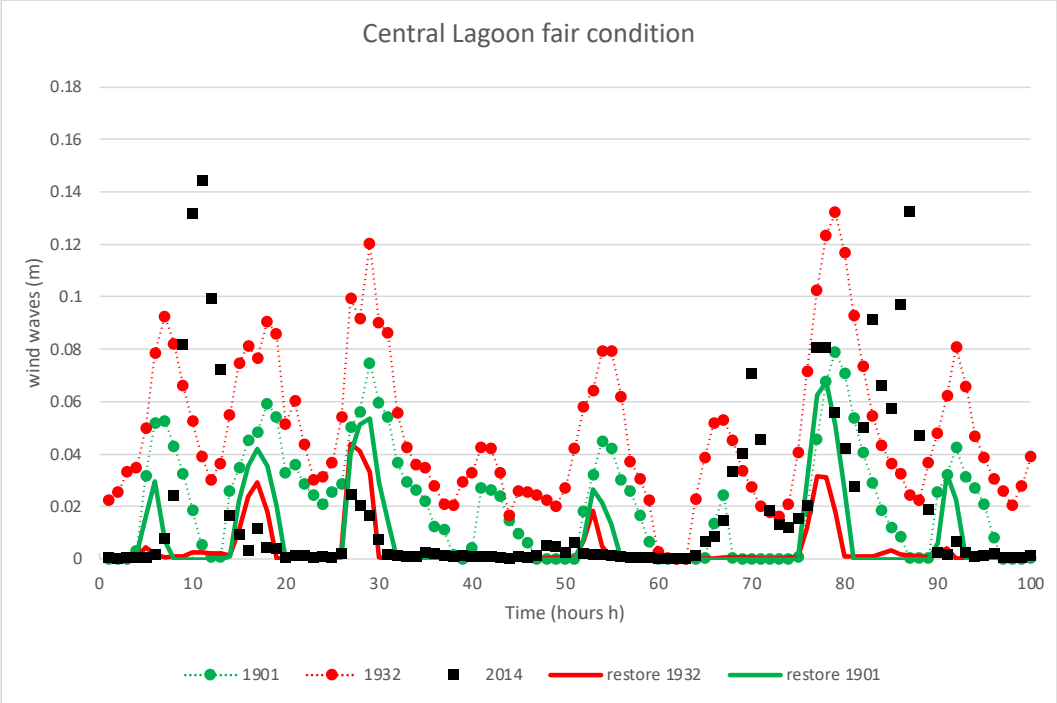

Figure 37: Central Lagoon fair weather condition wind-wave height

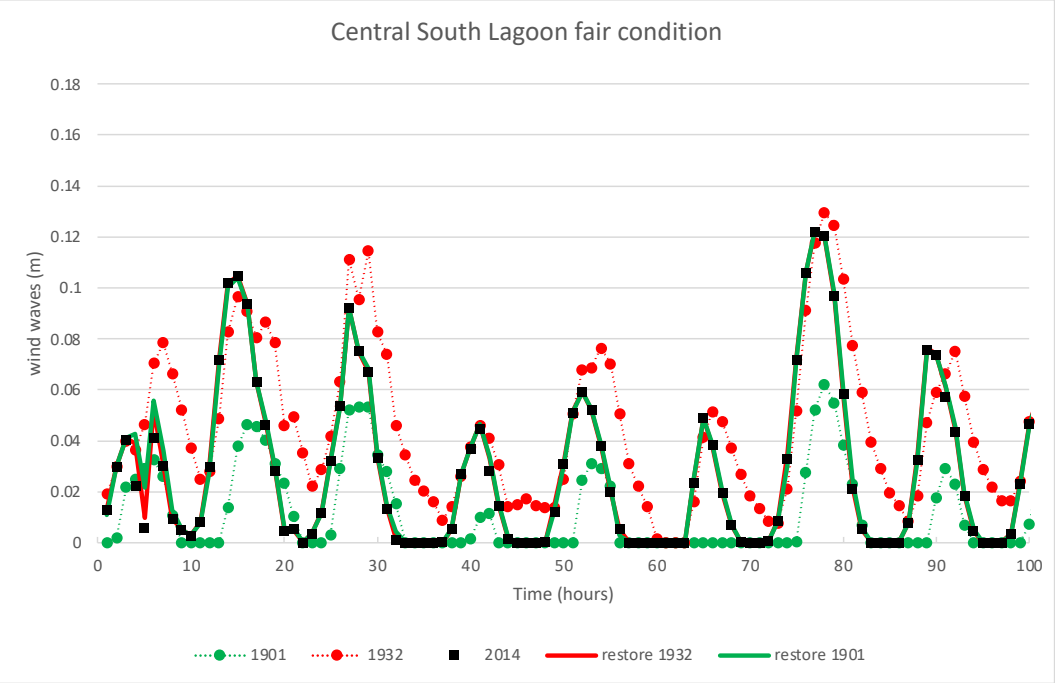

Figure 38: Central South Lagoon fair weather condition wind-wave height

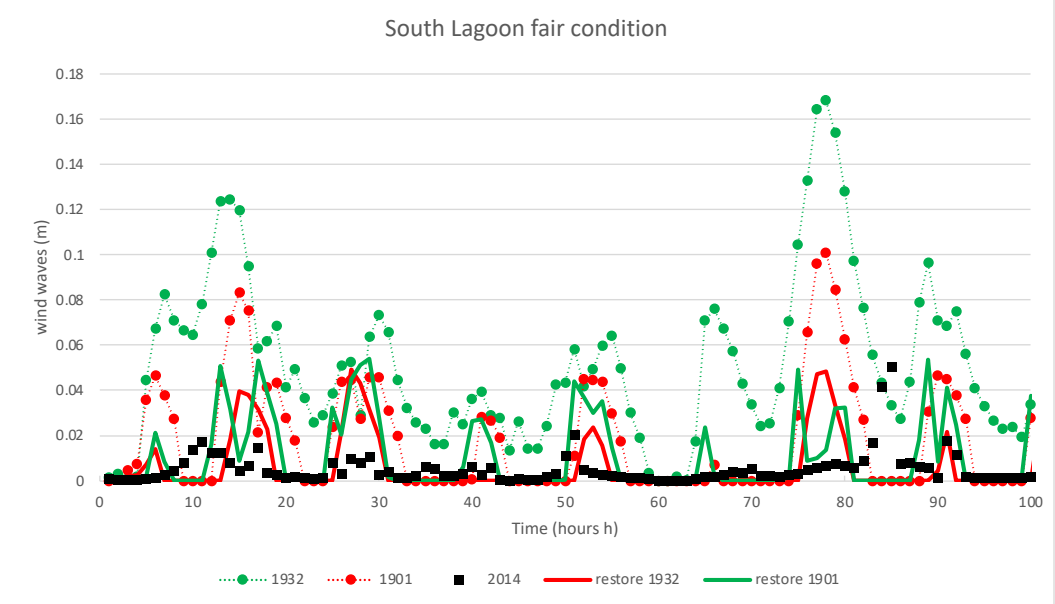

Figure 39: South Lagoon fair weather condition wind-wave height

4.2 Spatio-emporally integrated hydrodynamics

Initially, the focus was on a set of representative points situated on various salt marshes across the lagoon, for the observation of both storm and

fair-weather conditions. In addition to this, a comprehensive analysis was conducted, utilizing both Incidence and QGIS to study the behavior of the lagoon during the entire simulation period. Four keymaps were generated to illustrate the differences between 2014 and 1901/1932, as well as 2014 and the restored configurations (“Restore 1901” and “Restore 1932”), to compare values of water levels and wave heights.

4.2.1 Water levels

When comparing 2014 to the target year, a significant variation in water levels, approximately ±30cm, became evident, signifying notable changes within the lagoon. In contrast, the difference between the 2014 conditions and the restored configurations exhibited a smaller range of approximately ±2.3cm. This underscores once more that the impact of salt marsh restoration is minimal, with only marginal effects observed in specific locations. These locations are quite distant from the city center and important islands of the Lagoon, so there are no discernible benefits in terms of hydrodynamics. Furthermore, this highlights that solely focusing on salt marsh restoration may not be sufficient for comprehensive eco-morphodynamic adjustments; restoring shallow water areas might also be crucial. Tidal flats are a fundamental component that, when combined with salt marshes, mitigate various hydrodynamic phenomena. As observed in the incidence geo file (Fig. 13 and Fig. 14), in the past, the Venice Lagoon was teeming with shallow water areas that, in tandem with salt marshes, enhanced the overall hydrodynamic feedback."

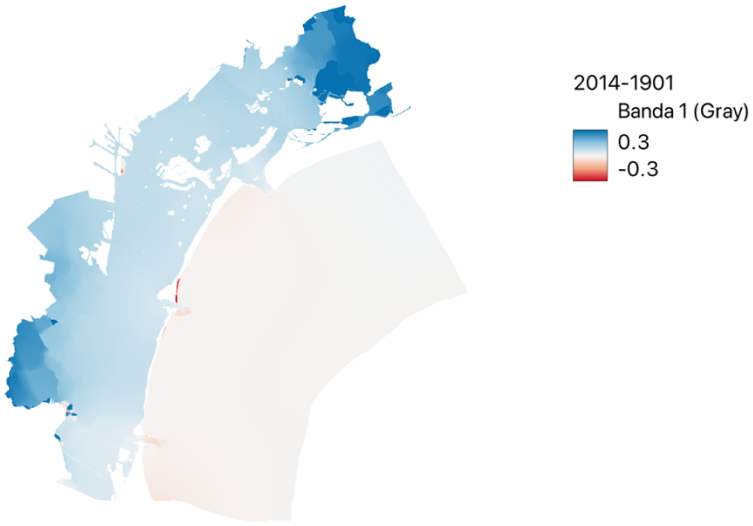

Figure 40: Comparison of water level differences between 2014 and 1901

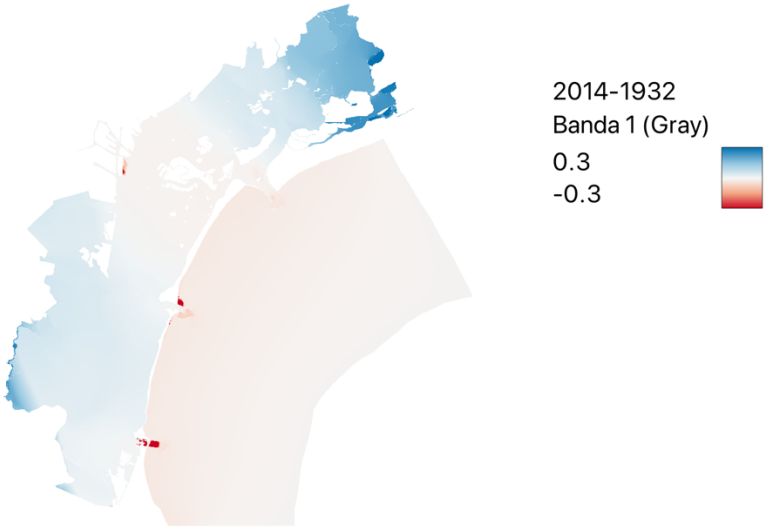

Figure 41: Comparison of water level differences between 2014 and 1932

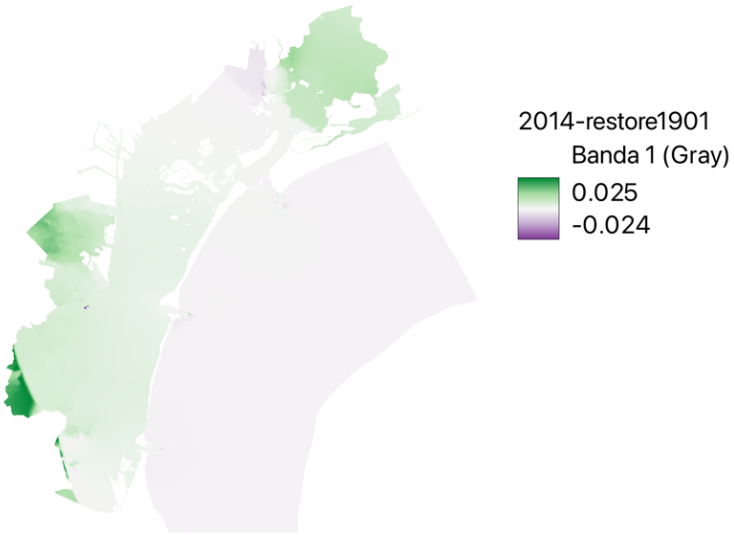

Figure 42: Comparison of water levels between 2014 and "Restore 1901"
I use a different colour scale with all "Restore" configurations.

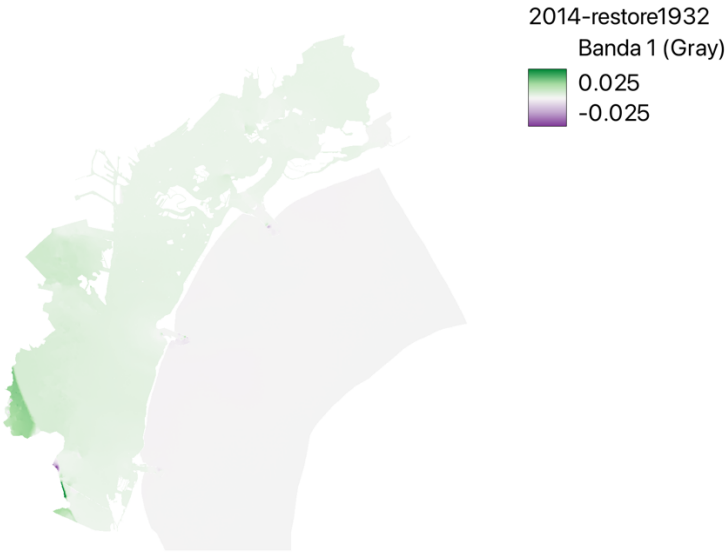

Figure 43: Comparison of water levels between 2014 and "Restore 1932"

4.2.2 Wind-waves heights

In terms of wave heights, the disparities between 2014 and 1901/1932 exhibit higher spatial variability due to the substantial differences between

the configurations. In contrast, the disparities between 2014 and the restored configuration reveal a distinct trend. A clear pattern emerges over the marsh-restored area, indicating an improvement in wind wave height. Marsh restoration appears to yield a modest benefit in this specific area. However, in the majority of the lagoon, denoted by white colors, there are no discernible changes. Similarly, Venice Island remains unaffected. This implies that salt marsh restoration alone cannot directly benefit Venice City. This is because an entire transitional ecosystem, namely shallow water lands, has been eradicated. Consequently, it suggests that solely focusing on salt marsh restoration may not be sufficient. To realize substantial morphodynamic benefits, the restoration of shallow water areas should also be considered.

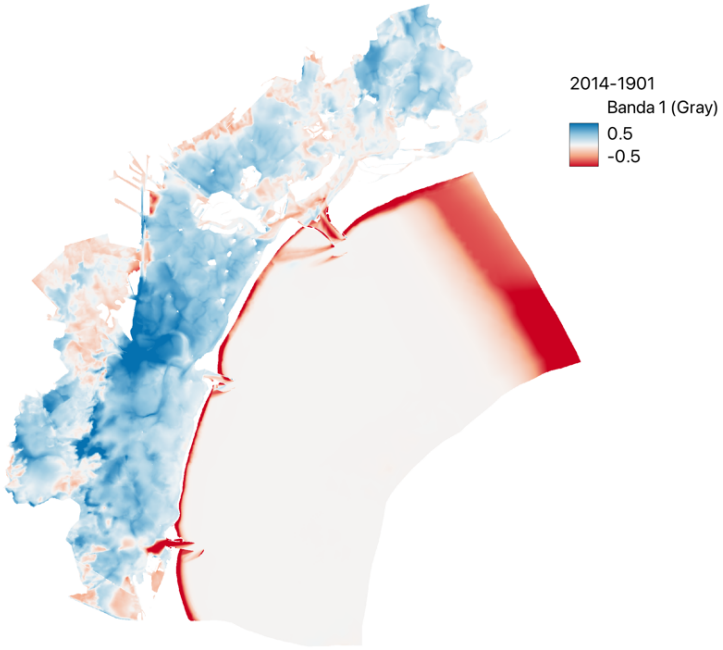

Figure 44: Comparison of wind-wave heights between 2014 and 1901

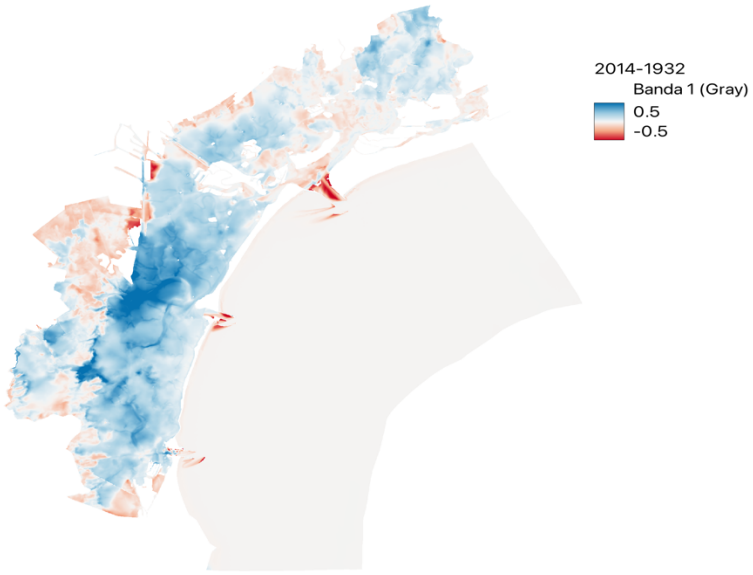

Figure 45: Comparison of wind-wave heights between 2014 and 1932

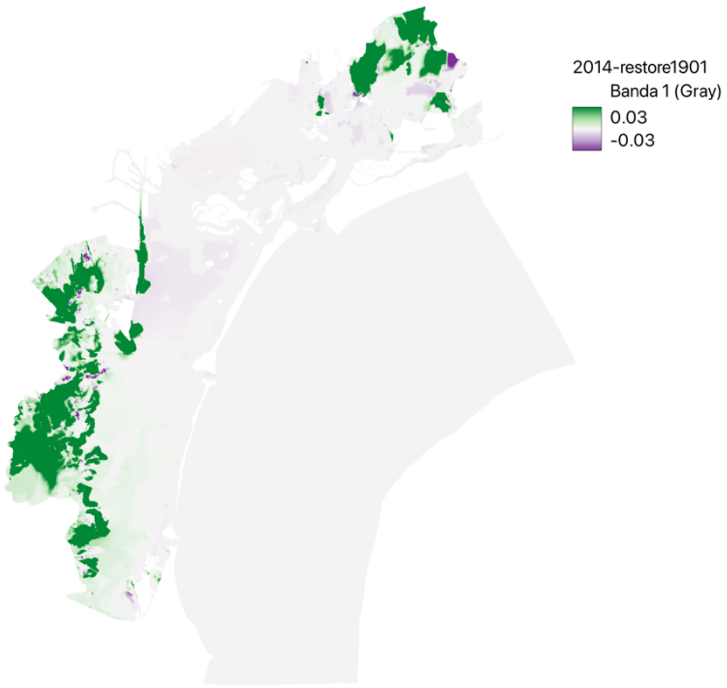

Figure 46: Comparison of wind-wave heights between 2014 and "Restore 1901"

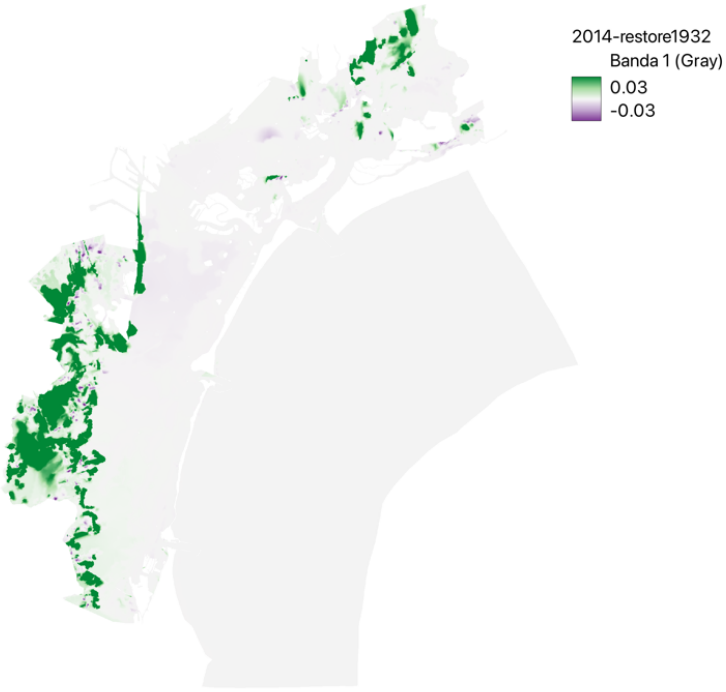

Figure 47: Comparison of wind-wave heights between 2014 and "Restore 1932"

4.2.3 Bed shear stress

Concluding the hydrodynamic analysis, a comprehensive spatial-temporal integrated evaluation was conducted by examining the combined impact of wind waves and water levels to assess shear stress, as performed in the previous chapter. When comparing 1901 and 1932, a significant deviation from the conditions in 2014 was observed. These maps also provided insights into the intricate network of small channels, which have largely vanished due to the absence of shallow water areas. Even in 1932, this network was already in decline.

Shifting the focus to the disparities between 2014 and the restored configuration, the predominant observation was the absence of significant alterations. The majority of the lagoon exhibited white colors, signifying negligible changes. While some alterations were noticeable in the marsh restoration area, they were not particularly substantial. This further emphasizes that the impact of salt marsh restoration on morphodynamics is minimal. It is possible that more noticeable changes might occur if the shallow water areas, characteristic of the lagoon in the early 1900s, were also restored (which is in fact impractical due to the enormous volume of sediment that would be needed).

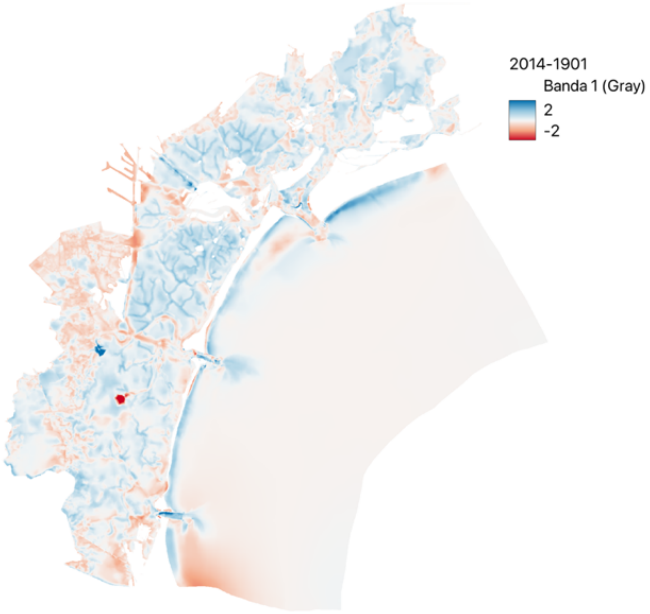

Figure 48: Comparison of bed shear stress between 2014 and 1901

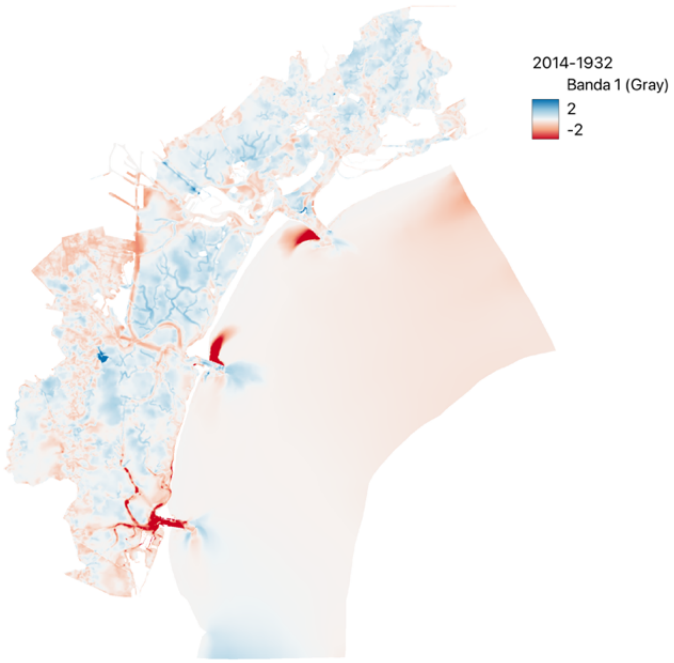

Figure 49: Comparison of bed shear stress between 2014 and 1932

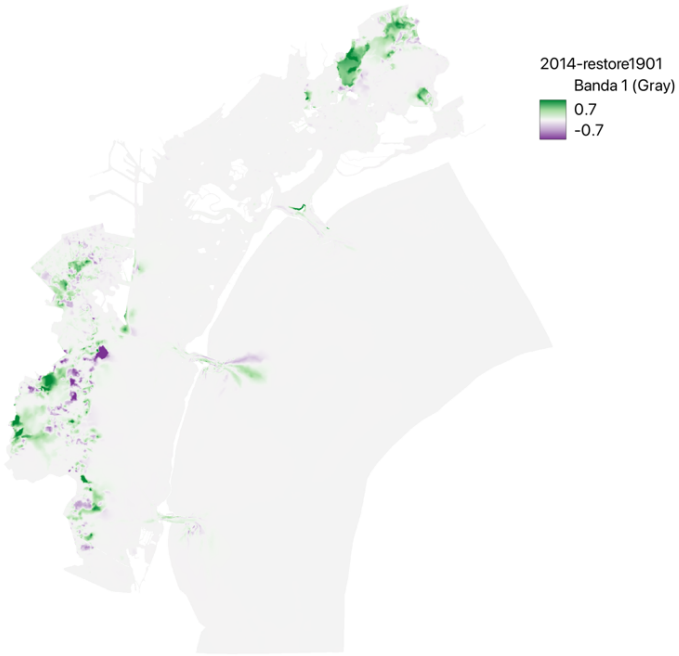

Figure 50: Comparison of bed shear stress between 2014 and "Restore 1901"

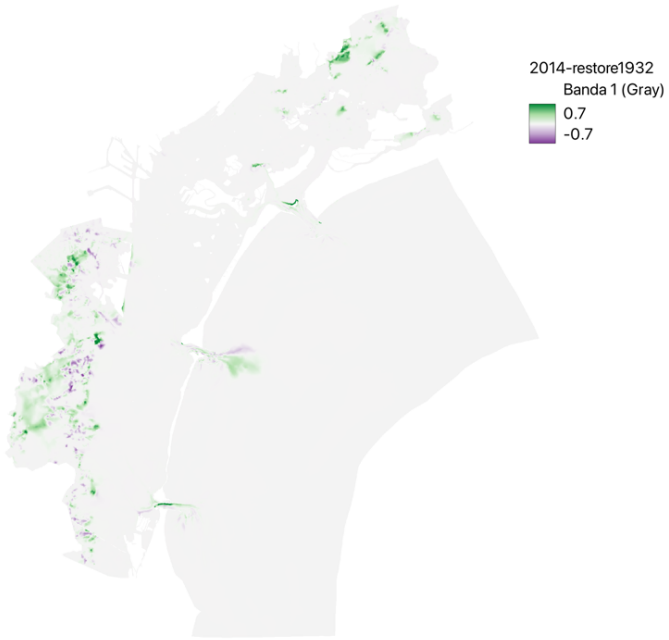

Figure 51: Comparison of bed shear stress between 2014 and "Restore 1932"

4.3 Fluxes at the Lagoon Inlets

To evaluate the broad impact of marsh degradation and restoration at the scale of the entire basin, it is also useful to focus on the fluxes of both water and sediment moving through the lagoon inlets. This is because critical changes in hydrodynamics and sediment transport regimes within the lagoon are going to affect the morphodynamic regime of the inlet. For example, a larger, deeper lagoon might exchange larger volumes of water with the open sea, resulting in increased water flux at the inlet. Additionally, studying sediment flux at the inlet is important because it provides the basis for understanding how much sediment the lagoon is importing from the sea (a beneficial effect, indicating a positive net sediment budget) or exporting to the sea (a negative net sediment budget signifying erosion of the lagoon morphology).

4.3.1 Tidal fluxes

a) Chioggia Inlet

Regarding the inlets, a segmented analysis has been conducted for each one. Chioggia, being the smallest, exhibits the lowest tidal flux, with the possibility of higher values during storm conditions. Notably, storm conditions result in discernible spikes, primarily attributed to the force of the wind. In fair weather, the situation appears to be more uniform. Although slight variations in lagoon conformation exist, it is important to emphasize that the trends for 1932 and 1901 slightly differ from those of 2014 and the restored condition. In the case of both the restored condition and 2014, there is an exact overlap of lines. This strongly suggests that the impact of marsh restoration on hydrodynamics is minimal.

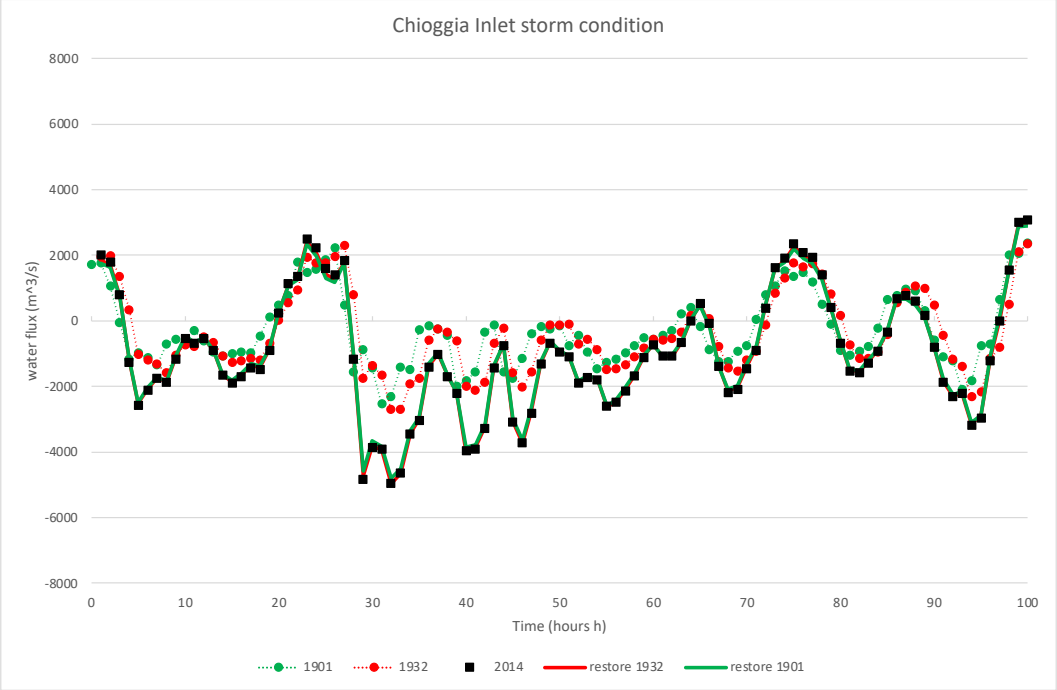

Figure 52: Chioggia Inlet storm condition water flux

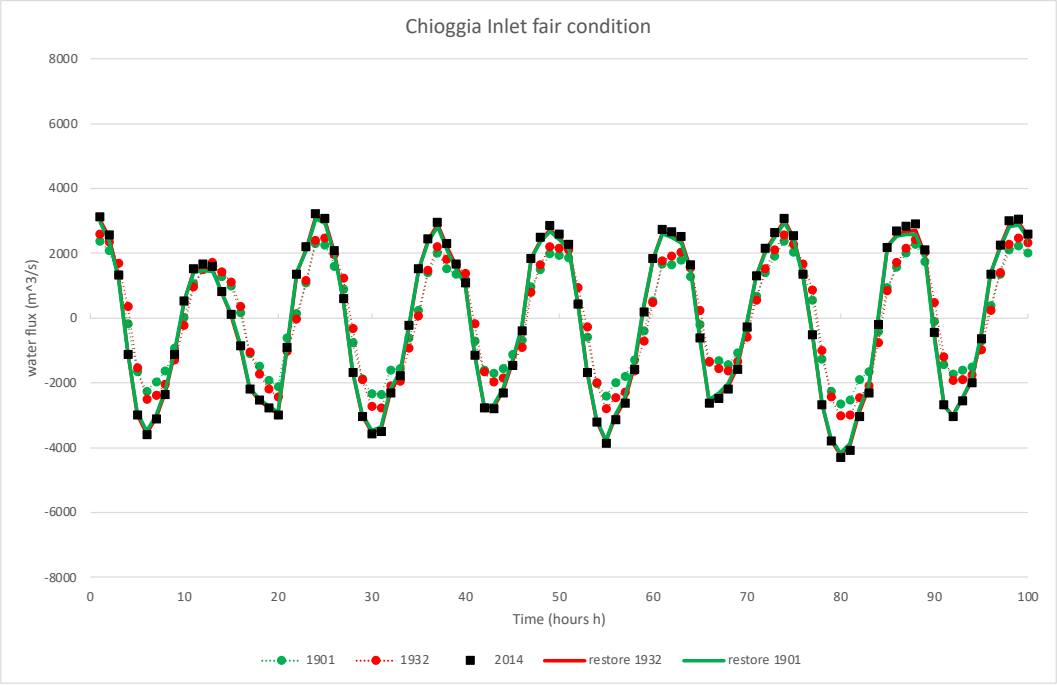

Figure 53: Chioggia Inlet fair weather condition water flux

b) Malamocco Inlet

Malamocco Inlet, which serves Porto Marghera and acts as the intermediary among the inlets, experiences significant traffic. During storm conditions, there is a slight reduction in flux due to southward winds,

resulting in a somewhat irregular pattern. In contrast, fair weather conditions exhibit a more regular pattern, characterized by peaks and troughs following the tidal regime. Similarly, distinctions are not prominent here. The trends of 1901 and 1932 are evidently discernible, while those of 2014 and the restored condition almost perfectly coincide in both scenarios. This reinforces the notion that the impact of marsh restoration remains negligible.

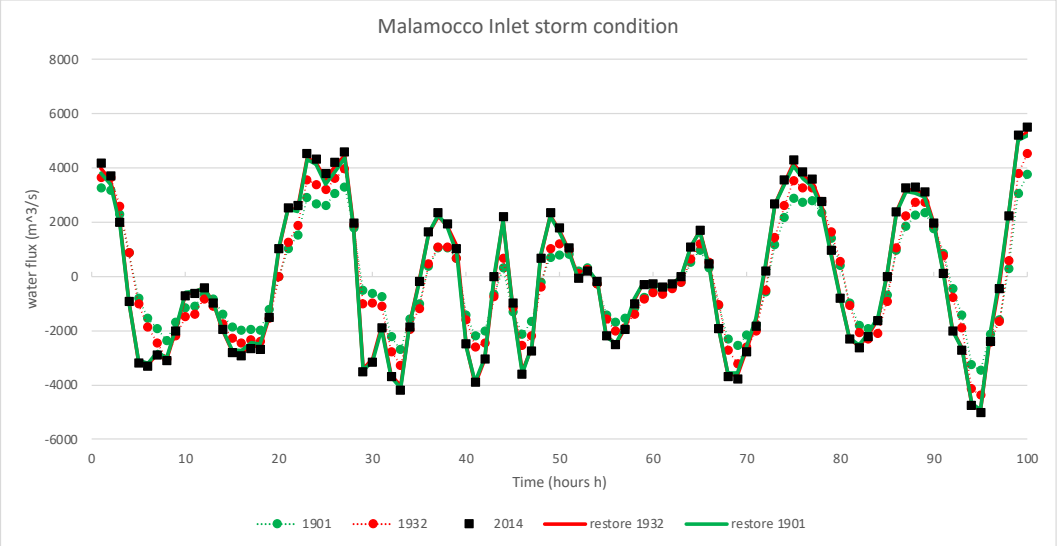

Figure 54: Malamocco Inlet storm condition water flux

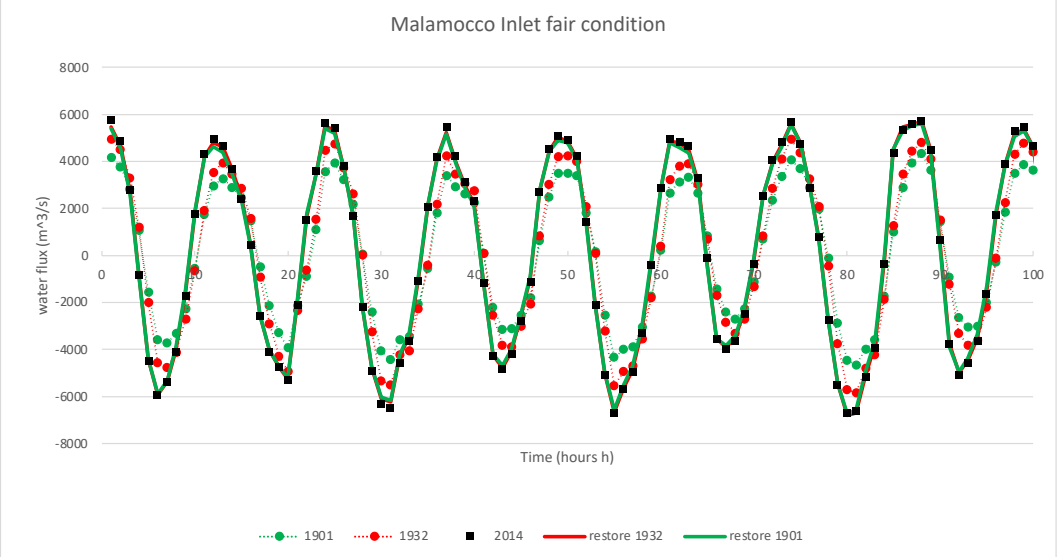

Figure 55: Malamocco Inlet fair weather condition water flux

c) Lido Inlet

The Lido inlet, being the largest and serving Venice city, shares similarities with the other inlets. Its larger size results in slightly less impact from wind conditions. Trends align closely with the other inlets, displaying less regularity in storm conditions and greater definition in fair weather. In terms of conformation, it mirrors the patterns observed in the other inlets. Notably, there are slight distinctions for 1901 and 1932 during storm conditions, while lines for 2014 and the restored condition perfectly overlap. This reinforces the conclusion that the influence of marsh restoration on hydrodynamics is negligible.

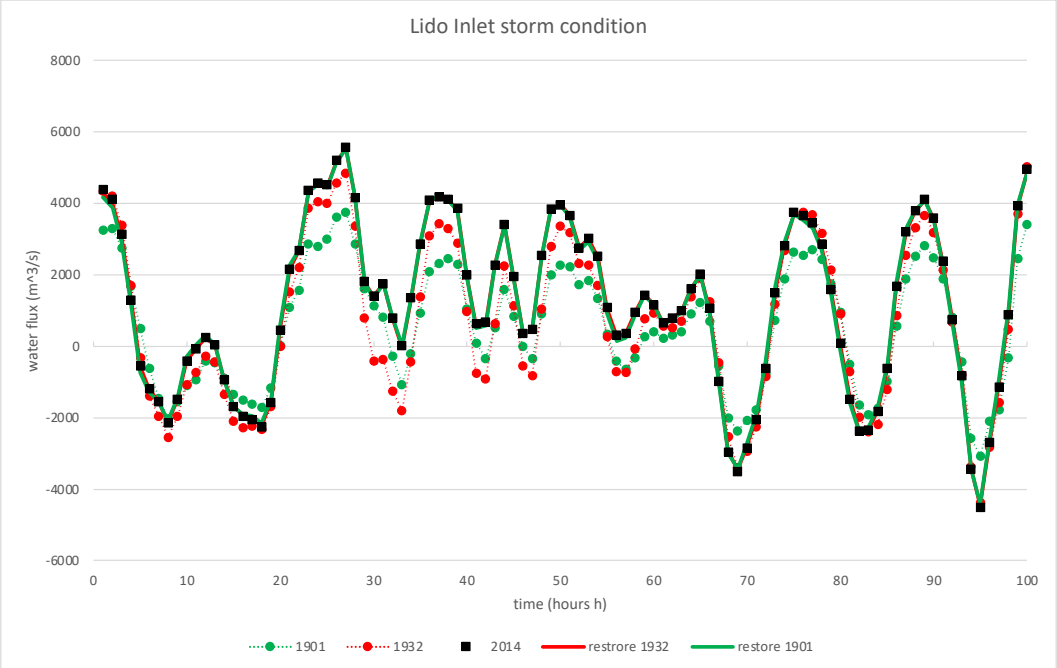

Figure 56: Lido Inlet storm condition water flux

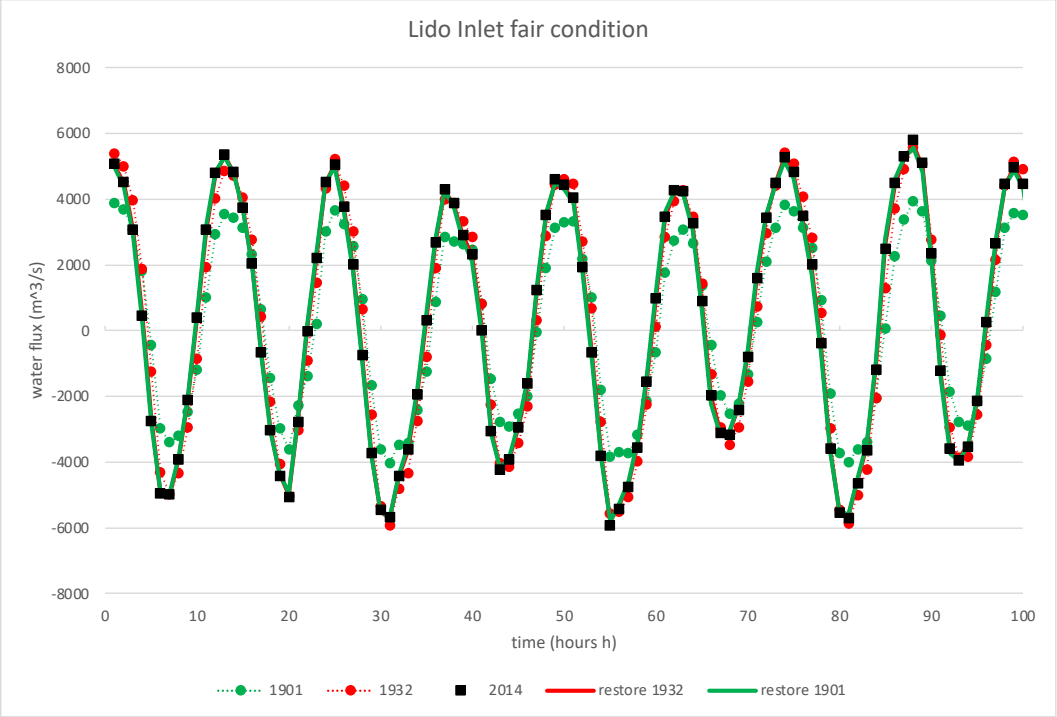

Figure 57: Lido Inlet fair weather condition water flux

4.3.2 Sediment fluxes

a) Chioggia Inlet

Two types of graphs illustrate sediment transport: one depicts the quantity of mud, which represents finer sediment particles, and another represents sand, which consists of coarser, non-cohesive particles. Concerning mud quantity (Qmud), all trends show a significant loss during storm conditions, attributed to the prevailing southward wind. Notably, 1901 and 1932 exhibit slightly less loss compared to 2014 and the restored condition. As mentioned earlier, trends for 2014 and the restored condition once again overlap, reinforcing the notion that the effect of marsh restoration is minimal. Under fair conditions, the situation is slightly more regular, with both influx and outflux observed. Again, trends for 2014 and the restored condition overlap, indicating negligible impact from marsh restoration. As for sand quantity (Qsand), there's a smaller amount of material in comparison. With the exception of 1932, trends are fairly similar. Since Qsand represents finer particles and is of relatively lesser importance for this study, the results are less significant. The conclusion

remains consistent: salt marsh restoration activity has a negligible impact on sediment transport.

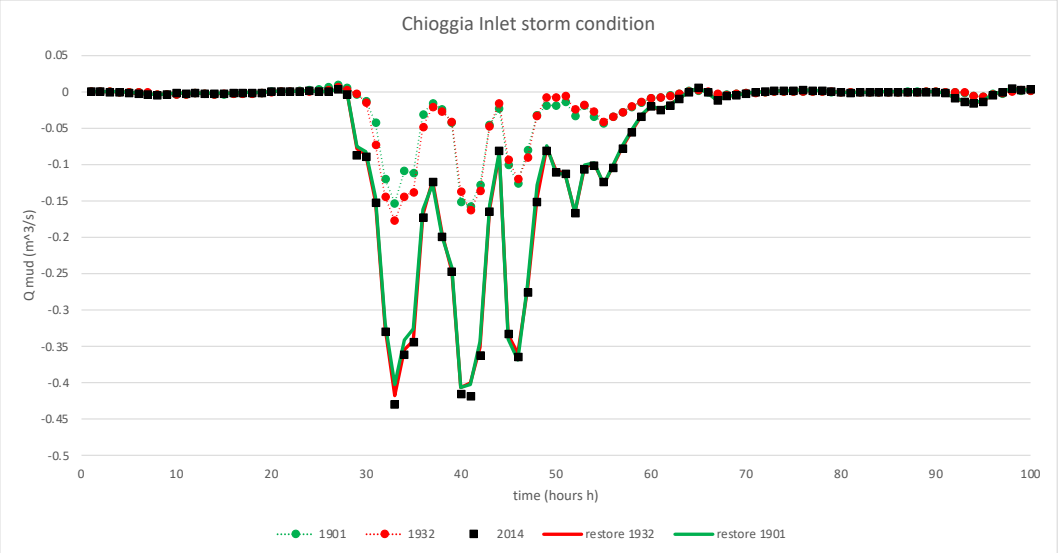

Figure 58: Chioggia Inlet storm condition mud sediment transport

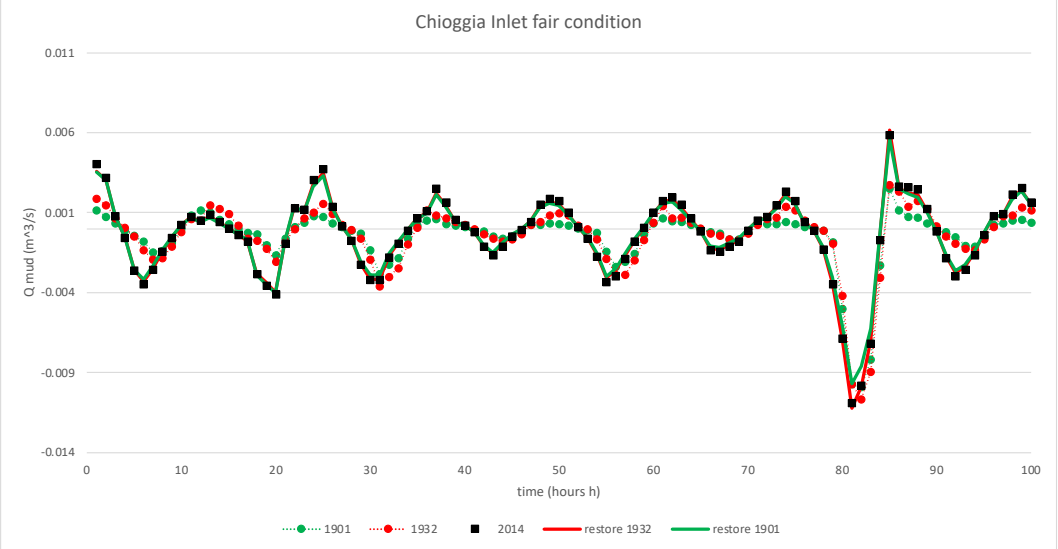

Figure 59: Chioggia Inlet fair weather condition mud sediment transport

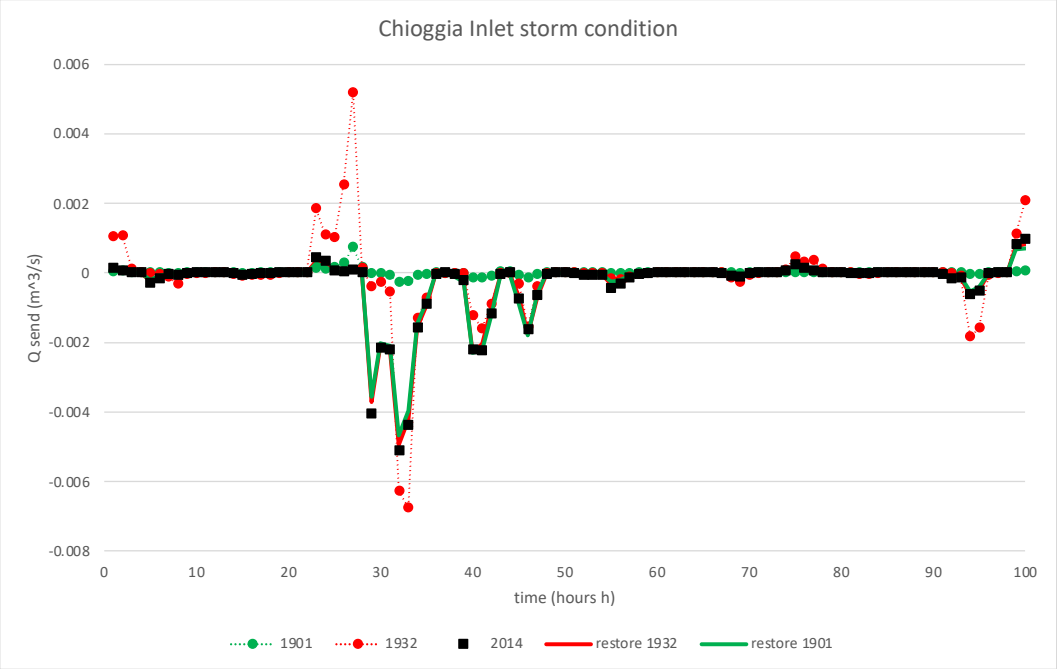

Figure 60: Chioggia Inlet storm condition sand sediment trasport

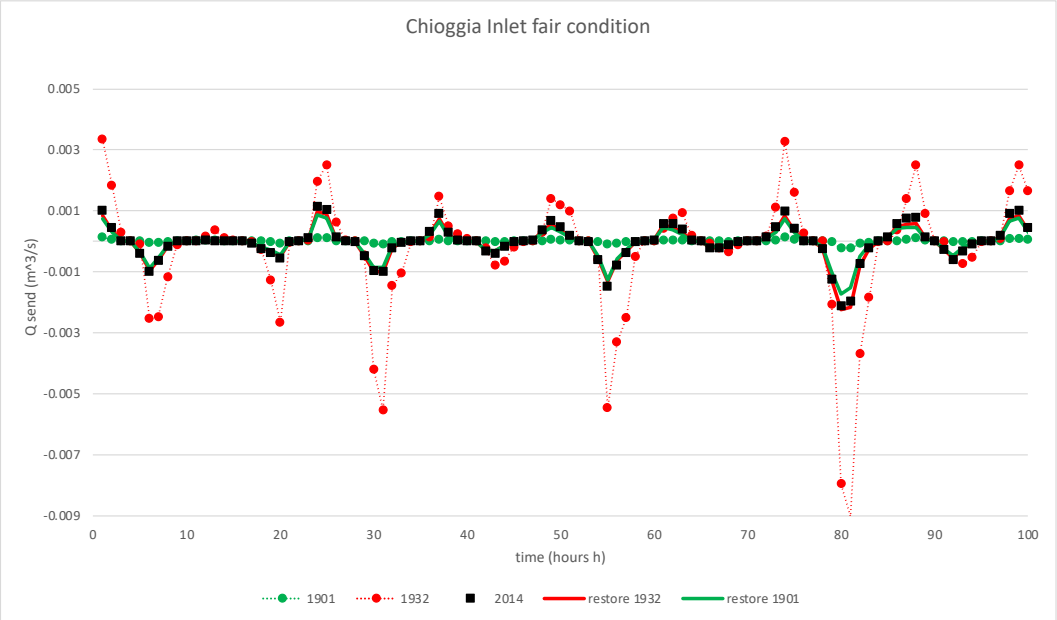

Figure 61: Chioggia Inlet fair weather condition sand sediment trasport

b) Malamocco Inlet

Malamocco experiences relatively less impact from wind, resulting in both materials entering and exiting the lagoon. Concerning Qmud, trends are slightly less consistent in storm conditions compared to fair weather. In

1901 and 1932, the quantity of mud in motion was marginally less than in 2014 and the restored condition. The overlap between the restored condition and 2014 indicates that restoration efforts may not yield significant benefits. Under fair conditions, the situation is somewhat more regular, though there's a notable negative dip at around hour eighty-five. Additionally, the overall quantity of material is less than during storm conditions. Again, the distinctions between the 1901 and 1932 configurations are discernible, while those for 2014 and the restored condition coincide. Regarding Qsand, although the material is scarcer, the trend closely mirrors that of Qmud. Wind's influence remains noteworthy in this part of the lagoon. The conclusion remains the same: salt marsh restoration activity has a negligible impact on sediment transport.

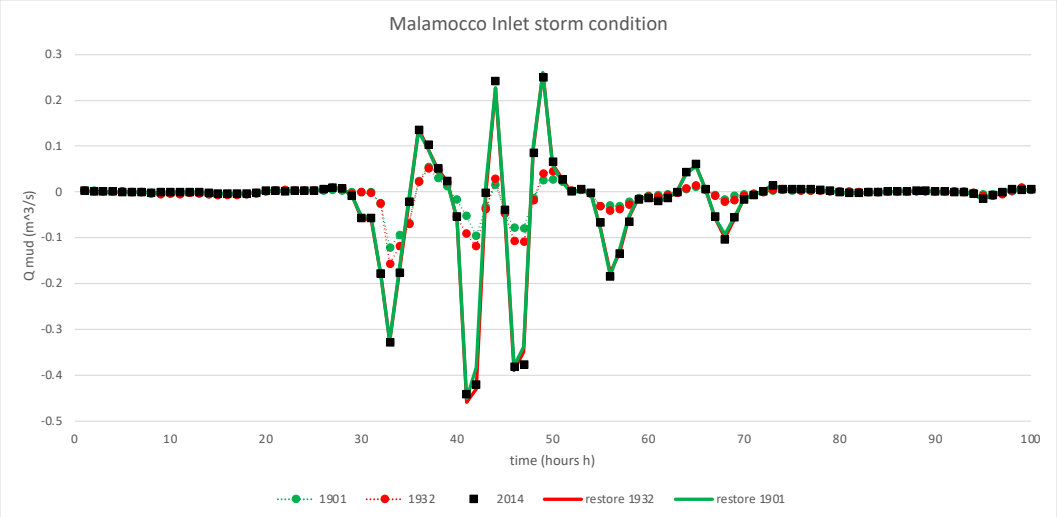

Figure 62: Malamocco Inlet storm condition mud sediment transport

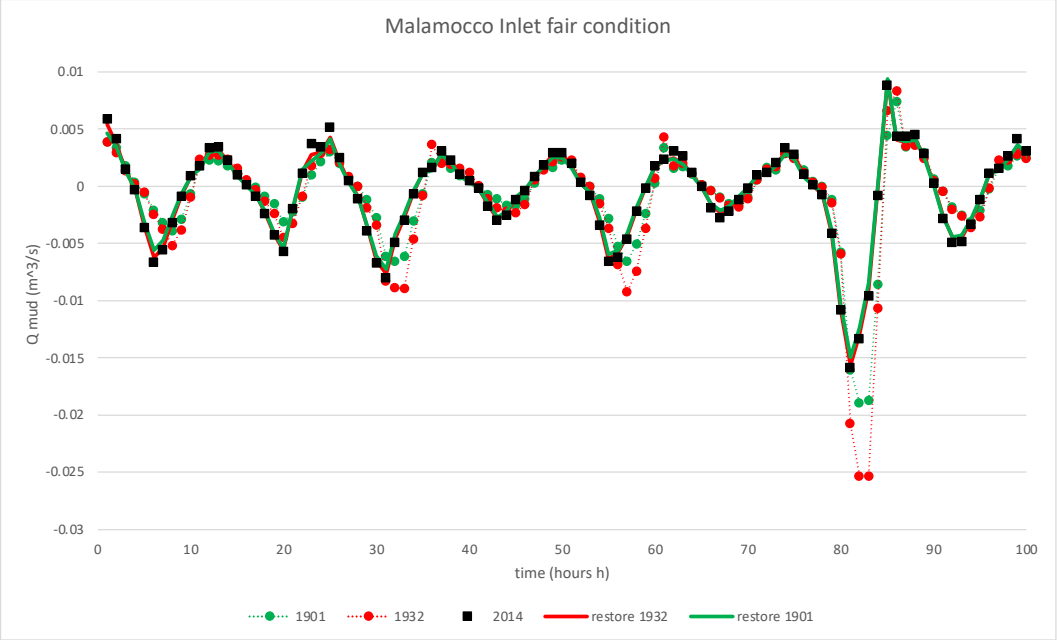

Figure 63: Malamocco Inlet fair weather condition mud sediment transport

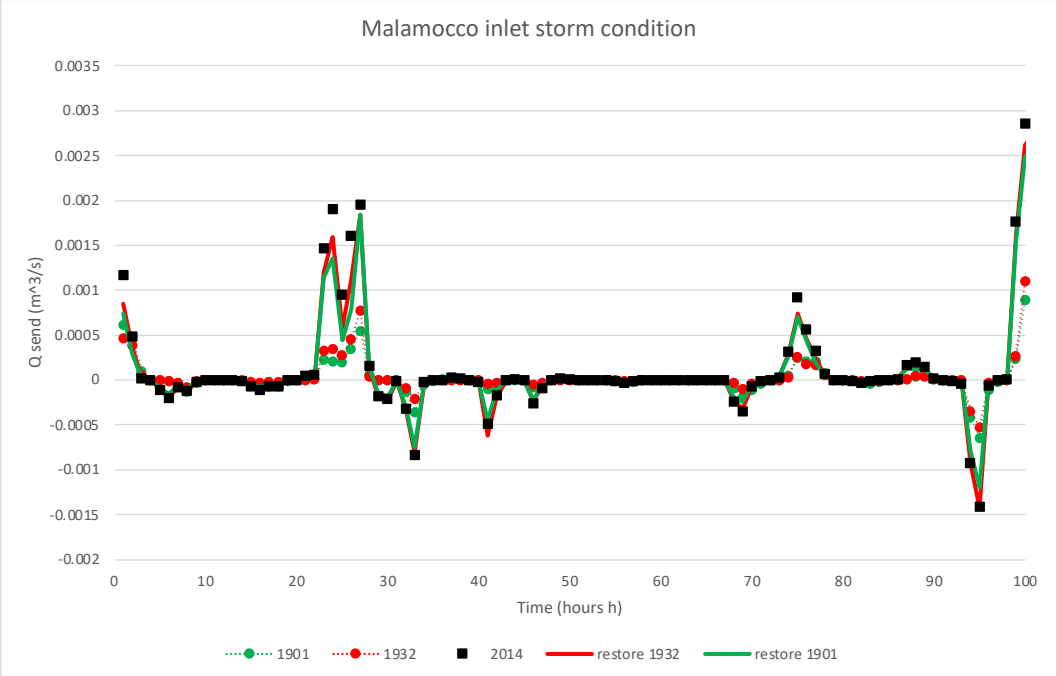

Figure 64: Malamocco Inlet storm condition sand sediment transport

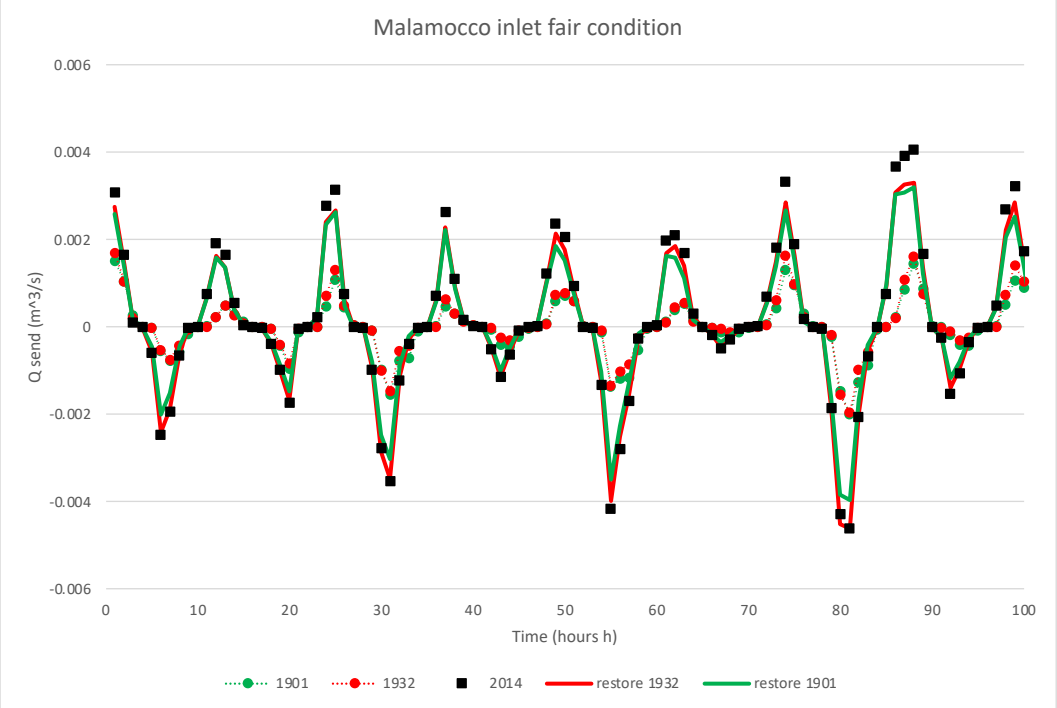

Figure 65: Malamocco Inlet fair weather condition sand sediment transport

c) Lido Inlet

In storm conditions, the Lido Inlet exhibits the smallest quantity of materials, with very few materials entering. This is attributed to the north-to-south wind activity. Notably, around hour thirty-five, it's evident that the trends for 2014 and the restored condition overlap, while those for 1901 and 1932 show some variance. Under fair weather conditions, the situation is slightly different, with a flow of materials in and out. However, once again, the trend remains very similar, with the restored condition closely aligning with the current state. Regarding Qsand, the quantity of material is lower. In storm conditions, there are some dissimilarities, while in fair weather, the trend is more regular. Nevertheless, the overall conclusion remains consistent: the effect of marsh restoration is minimal.

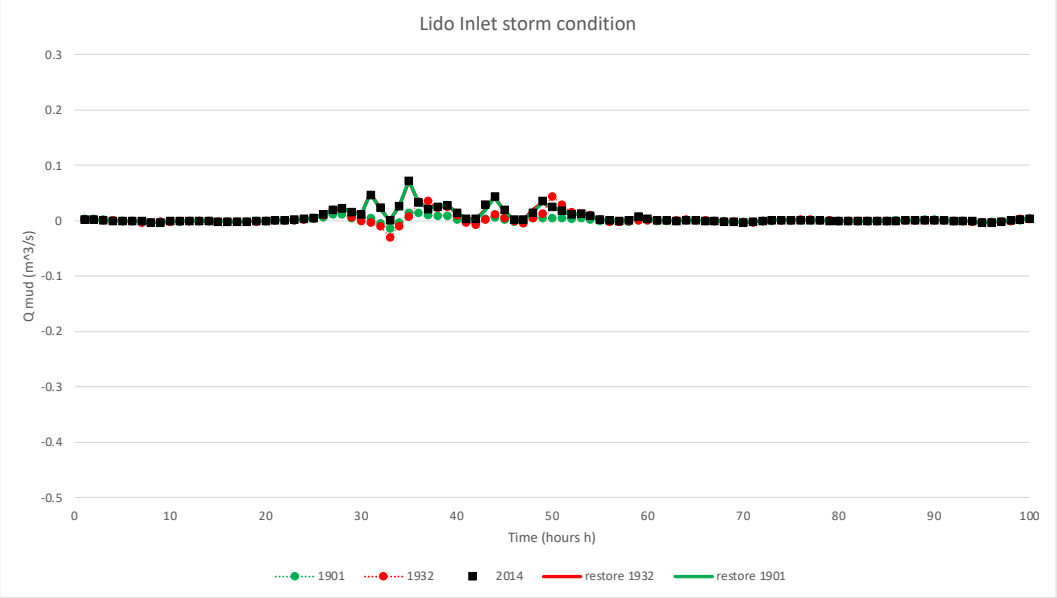

Figure 66: Lido Inlet storm condition mud sediment transport

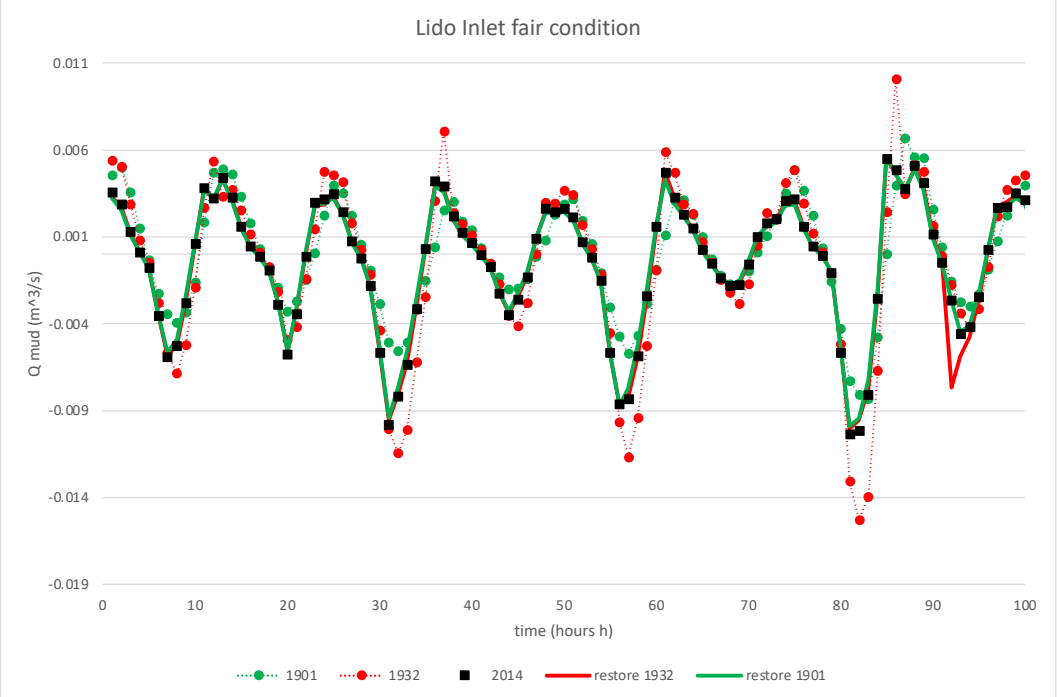

Figure 67: Lido Inlet fair weather condition mud sediment transport

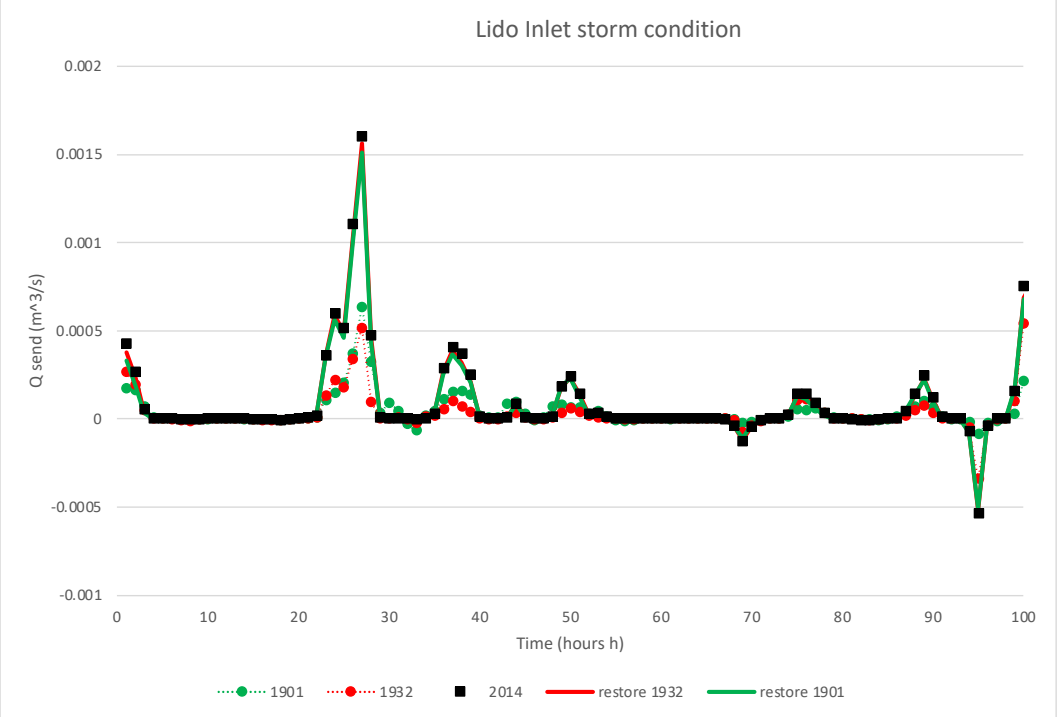

Figure 68: Lido Inlet storm condition sand sediment transport

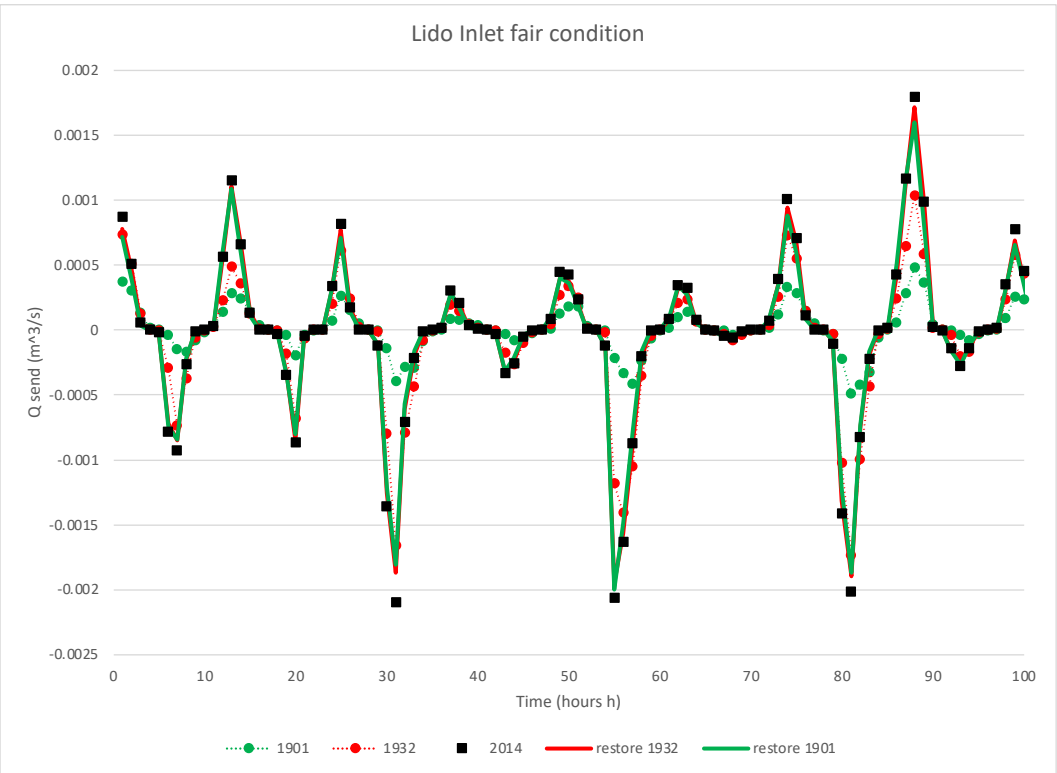

Figure 69: Lido Inlet fair weather condition sand sediment transport

4.1 Patterns of sediment erosion and deposition

4.1.1 Result at the global scale

The comprehensive analysis of bed evolution spanned approximately seven hundred hours at all five designated points, revealing two notable observations. Firstly, a distinct impact was observed during storm events, particularly between hours 100 to 200 and 500 to 600. Secondly, during fair weather conditions, lower accretion was noted compared to storm conditions. Additionally, the south lagoon exhibited higher deposition, primarily attributed to the Bora wind. This trend was consistent in most areas, except for the central north lagoon, where specific analysis points may have contributed to this variation.

Establishing a definitive trend across different configurations proved to be a challenge. While some configurations yielded similar outcomes, with 1901 and 1932 showing consistency, and "Restore 1901," "Restore 1932," and 2014 following a similar pattern, other points exhibited distinct results. In these cases, either the 2014 or restored configuration outperformed the initial condition. These findings emphasize the spatial variability in the effects of marsh restoration, which greatly depends on the morphology and distribution of salt marshes. This underscores the complexity of salt marsh restoration, which, while offering significant ecological benefits, also involves critical morphodynamic considerations that demand careful evaluation.

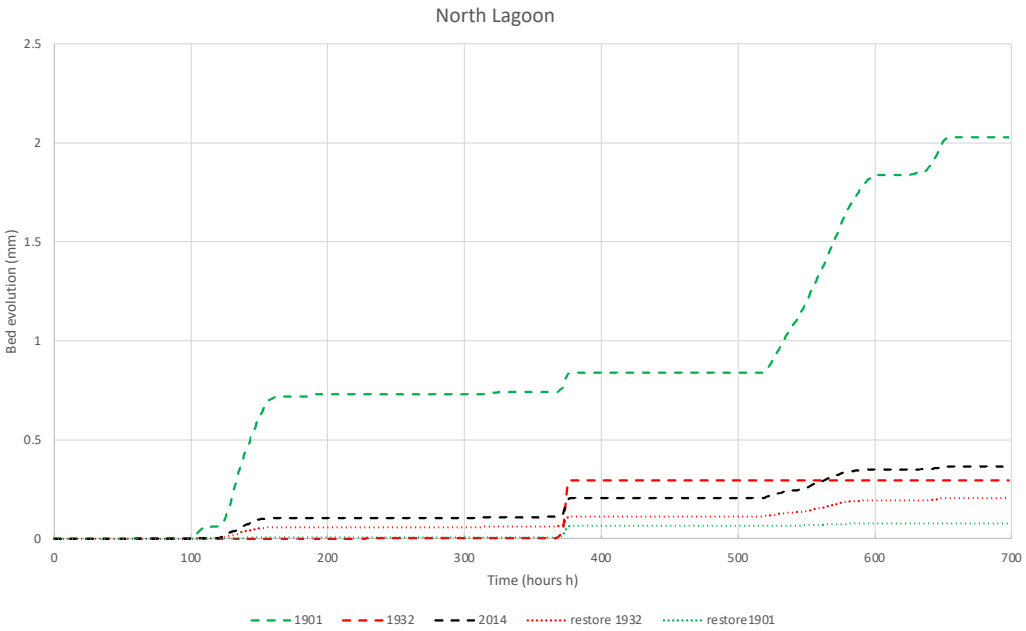

Figure 70: Bed evolution in North Lagoon during all the simulations

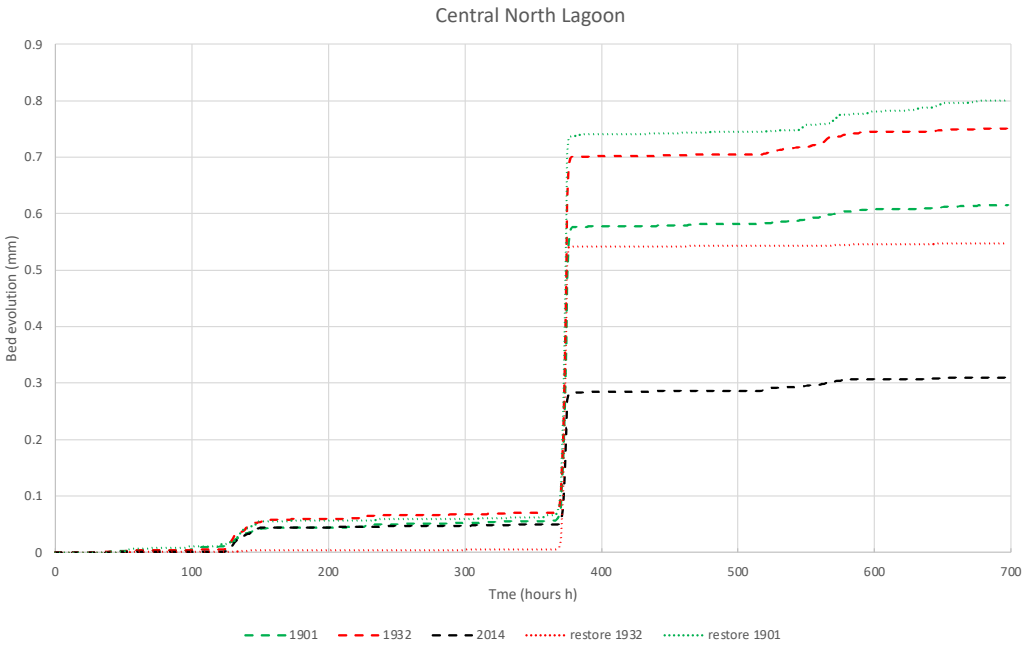

Figure 71: Bed evolution in Central North Lagoon during all the simulations

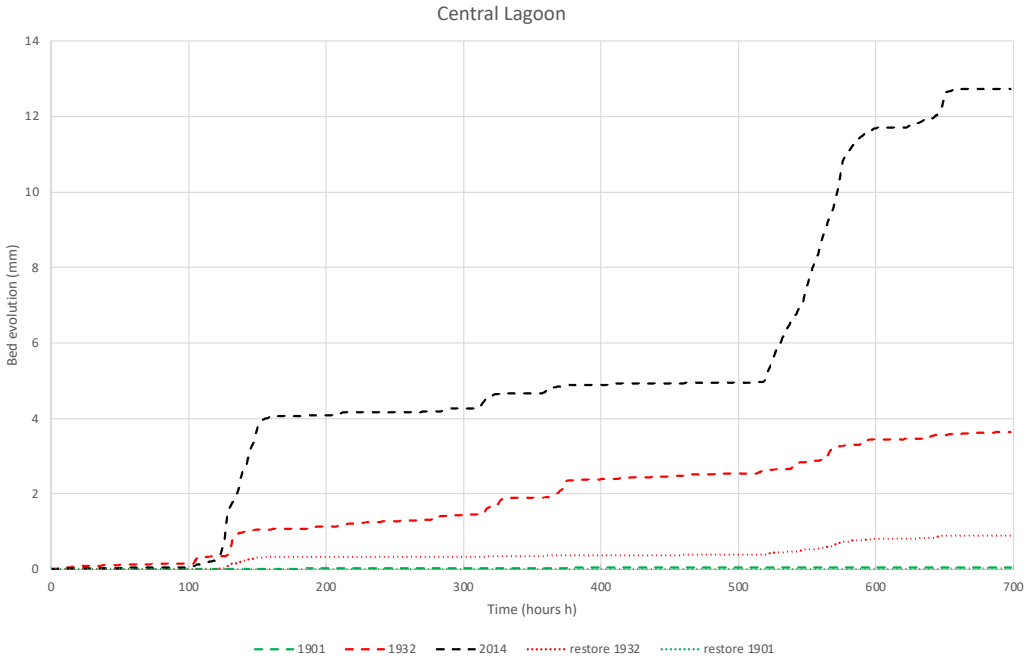

Figure 72: Bed evolution in Central Lagoon during all the simulations

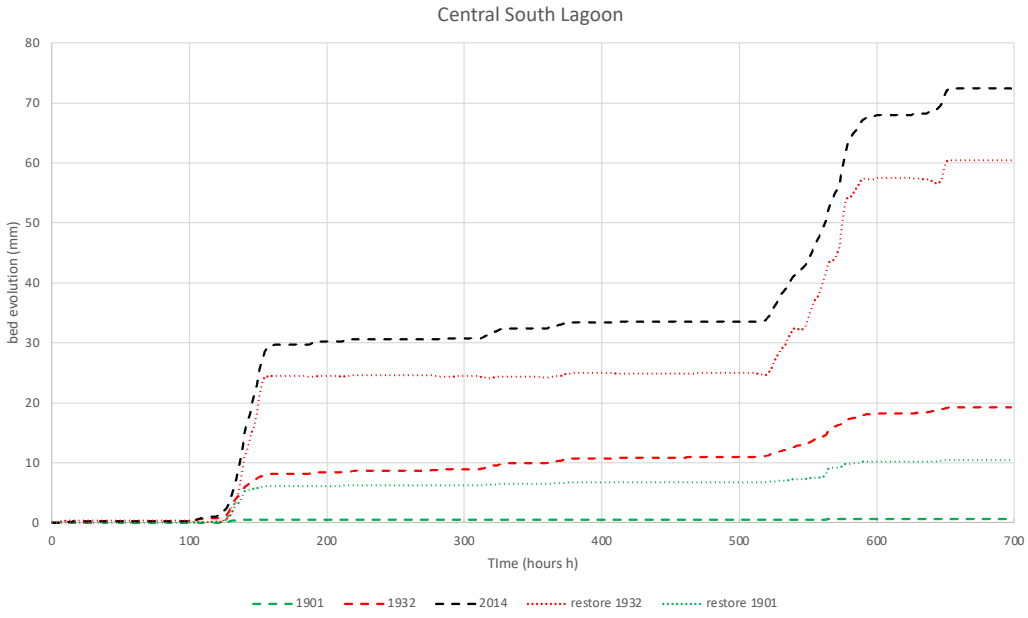

Figure 73: Bed evolution in Central South Lagoon during all the simulations

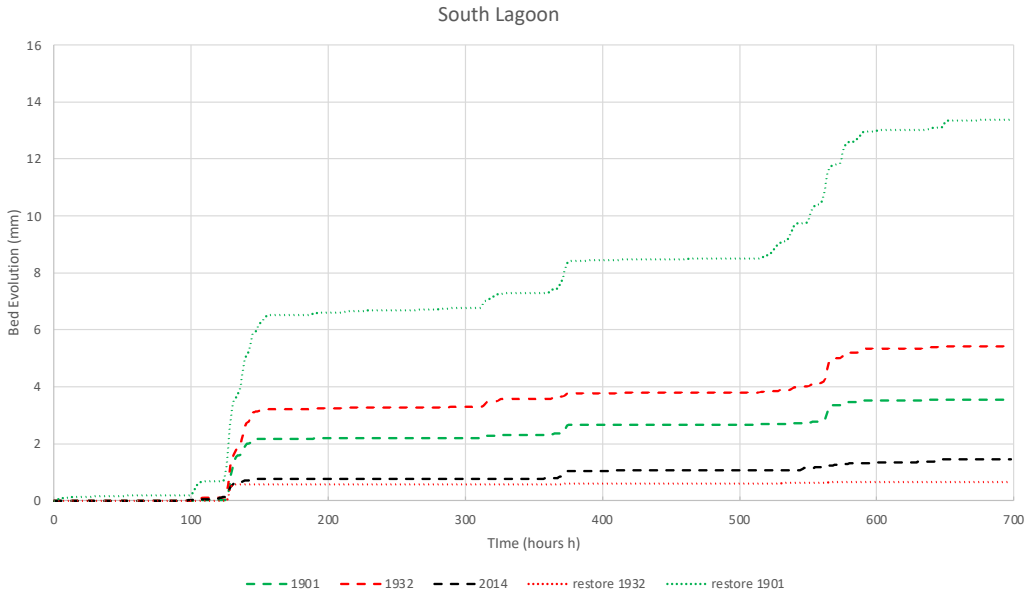

Figure 74: Bed evolution in South Lagoon during all the simulations

4.1.2 Spatially integrative metrics

These results are consistent with the patterns observed in the previous section. Particularly, when comparing 2014 with 1901/1932, notable differences emerge, with 1901 showing more significant disparities. In both the south and north lagoon, the situation appears less favorable in 2014. In the case of the restore configuration, “Restore 1901” follows similar trends to the other integrated findings, with substantial changes, particularly in areas where marsh restoration was carried out. Conversely, Venice city shows no noticeable alterations. Surprisingly, “Restore 1932” displays a more consistent pattern, likely influenced by the specific lagoon configuration and the morphology of the restored marsh. The primary changes primarily affect the south lagoon, driven by the significant influence of wind in this context.

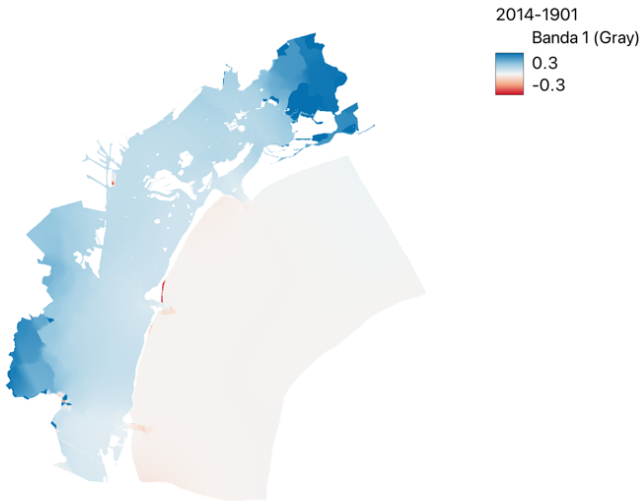

Figure 75: Comparison of sedimentation erosion and deposition between 2014 and 1901

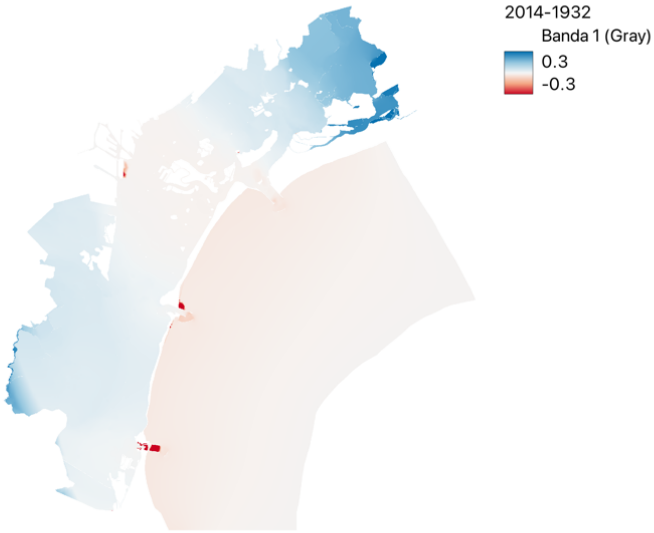

Figure 76 Comparison of sedimentation erosion and deposition between 2014 and 1932

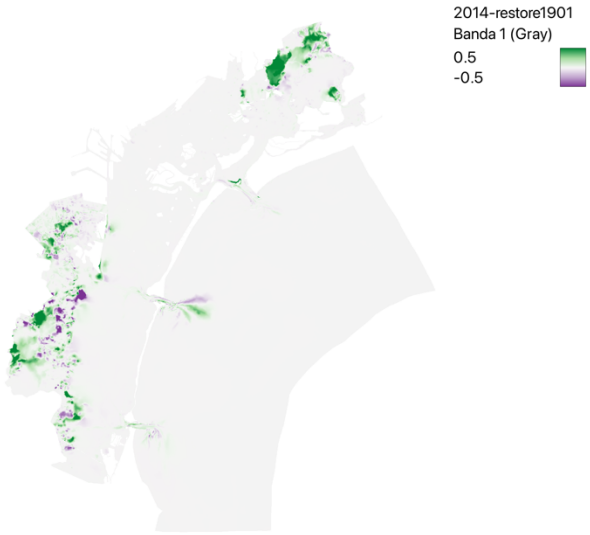

Figure 77: Comparison of sediment, erosion and deposition between 2014 and "Restore 1901"

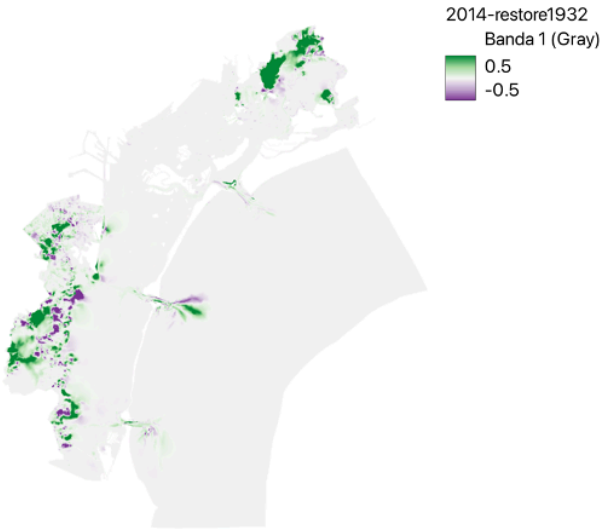

Figure 78: Comparison of sediment, erosion and deposition between 2014 and "Restore 1932"

4.1.3 Sediment budget at the Lagoon scale

The results obtained from the numerical simulations offer insights into the overall sediment budget of the Venice Lagoon, including specific considerations for salt marshes.

In Figure 79, the changes in sediment distribution among different configurations are observed. The total sediment deposition in salt marshes declines from 1901 to 1932. Notably, the 'Restore' configuration exhibits a sediment volume similar to that of 2014, indicating a minimal impact of restoration on sediment dynamics. Other morphological units also experience a significant decline in values. Tidal flats, crucial for Lagoon hydrodynamics, show a decrease in sediment deposition , while channels see an increase due to anthropogenic influences.

A more detailed examination involves three additional graphs. Figure 80 illustrates the decreasing total volume of sediments deposited in salt marshes from 1901 to 2014. Despite a slight growth in deposit for the 'Restore' configuration, none approach the original configuration. This suggests that even with optimistic restoration efforts, the volume deposit would not reach the levels of the initial conditions.

Figure 81 evaluates the total area of marshes in the Lagoon across different years and configurations. The disparity between years and configurations is significant, with reclaimed areas growing over time. The 'Restore' configuration shows a slight increase in area due to the restoration efforts, enlarging the total marsh area. The reduction in tidal flat areas and a more consistent transition from marshes to deep water in recent years highlight the impact of land reclamation.

In Figure 82, the vertical accretion rate is explored. Despite an increase in salt marsh area, the volume remains the same, leading to a decrease in accretion rate. This underscores the challenge of recreating initial conditions even with substantial marsh restoration. It further supports the conclusion that the impact of salt marsh restoration on morphodynamics is minimal."

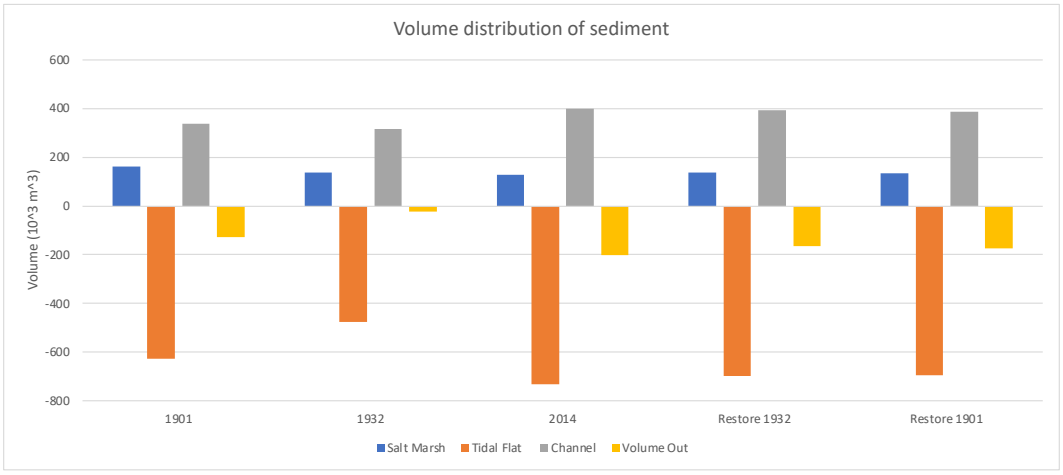

Figure 79: Volume of sediment eroded or deposited differentiated based on different morphological units of the Lagoon (i.e., salt marshes, tidal flats, channels and volume through the inlets)

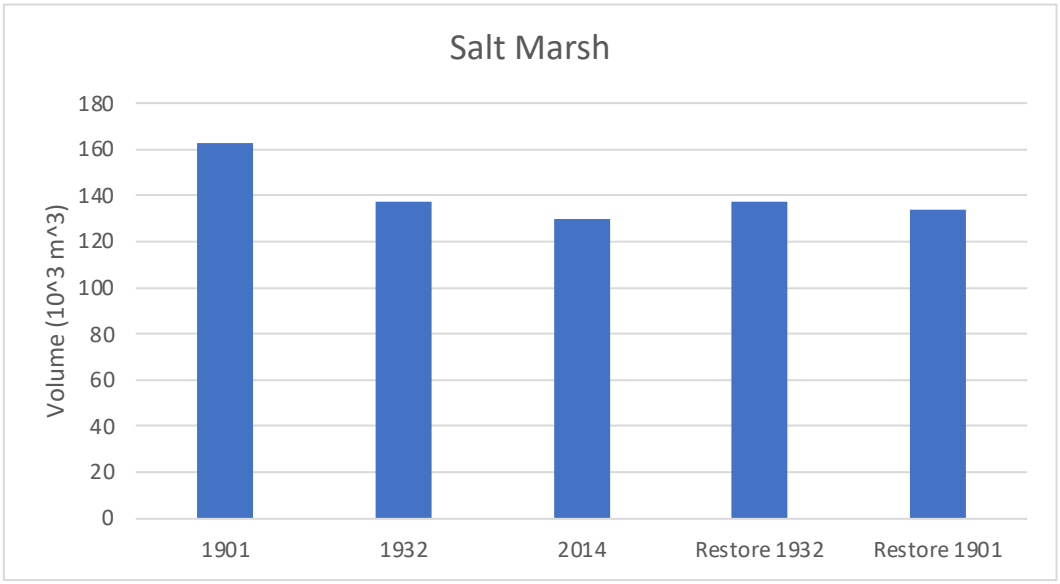

Figure 80: Volume of sediment deposited over salt marshes in the different analyzed configurations of the Venice Lagoon.

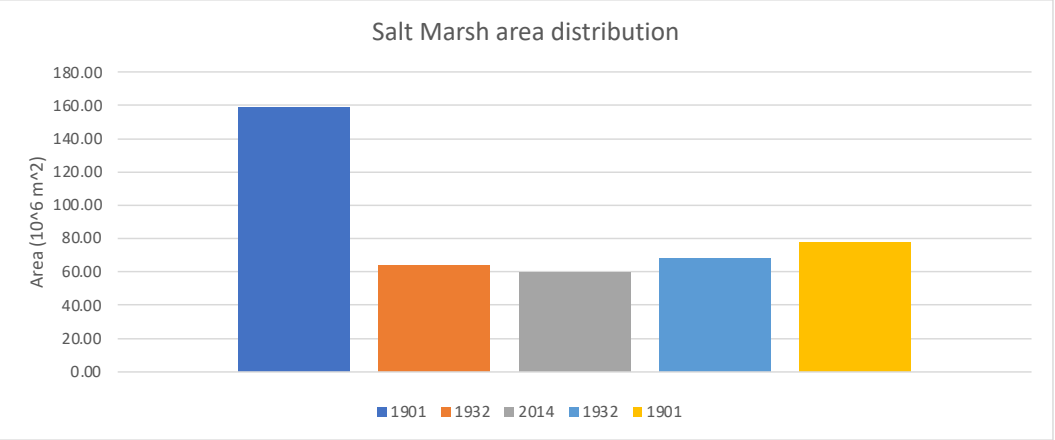

Figure 81: total area of salt marsh marshes in the different analyzed configurations of the Venice Lagoon.

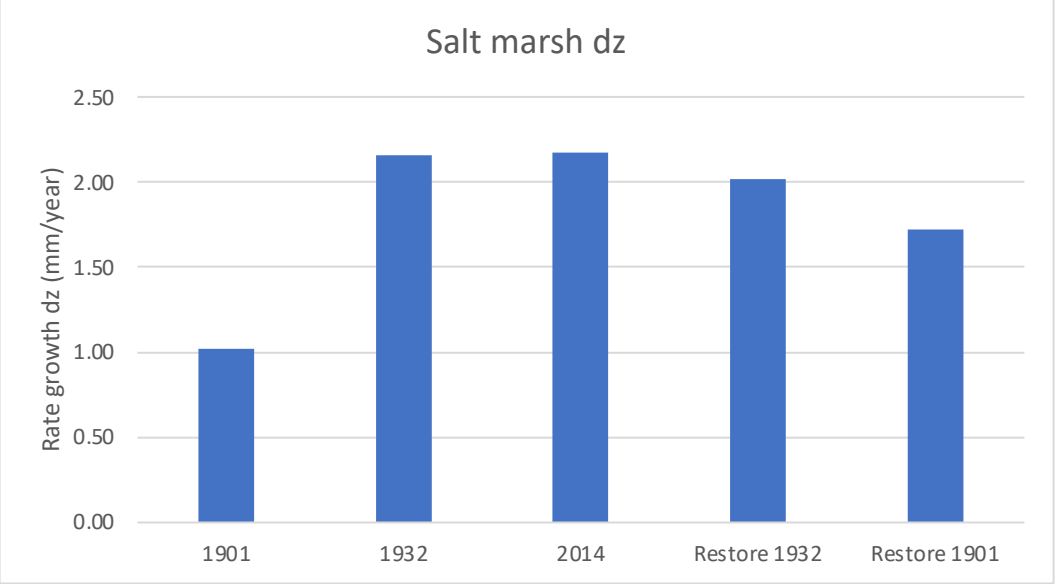

Figure 82: Salt-marsh vertical accretion rate.

5. Observations and conclusions

After conducting an extensive analysis, several key conclusions emerge from this study. The research emphasizes the significance of salt marshes and their interconnected environment, which includes channels and tidal flats, within the delicate ecosystem of the Venice Lagoon. Efforts to model and manipulate this ecosystem have been made, but irreversible changes brought about by land reclamation and channel dredging significantly alter the hydrodynamics.

An image captured, likely near Piazza San Marco and depicting San Giorgio Island in the early 1900s (refer to Fig 83), vividly illustrates the substantial transformations in the lagoon. During low tide events, extensive areas of the lagoon surface become exposed as tidal flats, contributing to the overall system of salt marshes. Salt marshes are not isolated entities but are intricately intertwined with various morphological elements of the lagoon.

The research underscores that while restoring salt marshes has numerous benefits for the broader ecosystem, including ecological advantages, such restoration efforts have relatively minor effects on morphodynamics and hydrodynamics. The findings consistently show that restoring only marshes does not bring about significant changes compared to current conditions.

This highlights the complexity of the subject, emphasizing the need for more in-depth and focused studies for effective restoration campaigns. Restoring salt marshes has a fundamental role for ecosystem benefits but has limited importance for hydrodynamic and sediment dynamics. From the observations presented in this work, restoring salt marshes may not yield significant differences from current conditions. Analyses in this study show a quite similar trend for the 'Restore' configurations and 2014. It is challenging to propose a better way to achieve morphodynamic benefits. The Venice Lagoon has undergone numerous changes over about a century, modifying all morphological units. Restoration efforts should consider other elements of the Lagoon to have a more substantial effect on hydrodynamics and sediment transport.

The collected data and analyses elucidates the inefficiency of salt marsh restoration in providing ecomorphodynamics co-benefits and underscores the delicate ecosystem characterizing the Venice Lagoon.

The decision to study this topic is based on the belief that in marine biology, a consideration of morphodynamics and sediment transport is essential. These elements are fundamental components of the marine environment and, in conjunction with biodiversity, marine conservation, and climate change, provide comprehensive knowledge for a marine biologist.

Figure 83: Venice Lagoon in early 1900 during a low tide event. This image shows a big tidal flat area that characterized the past Lagoon

6. Acknowledgements

Ringrazio il professor Finotello Alvise per avermi insegnato importanti nozioni durante il suo corso; che mi ha accompagnato nella produzione di questo lavoro; e con pazienza ha corretto i miei innumerevoli errori. Lo ringrazio inoltre per avermi fornito tutto il materiale per poter poi avviare il lavoro, portare a termine questo elaborato; e lo ringrazio per avermi prestato il suo computer per poter svolgere le simulazioni.

Ringrazio il professore Tognin Davide che con infinita pazienza mi ha insegnato come usare il software, “Incidenze”, e come “smanettare” con il computer.

Ringrazio la mia famiglia tutta, per avermi dato la possibilità di portare a termine questo percorso e per le occasioni che mi sta dando in tutta la mia vita.

Ringrazio Marta per avermi sopportato e supportato durante questo ultimo anno, durante i miei innumerevoli crolli emotivi.

Ringrazio la ditta “Martini Costruzioni Generali” per avermi permesso di lavorare e dedicare anche il tempo a questo progetto.

7. References

Allen, J. I., Somerfield, P. J., & Gilbert, F. J. (2007). Quantifying uncertainty in high-resolution coupled hydrodynamic-ecosystem models. *Journal of Marine Systems*, *64*(1–4), 3–14. https://doi.org/10.1016/j.jmarsys.2006.02.010

Amos, C. L., Umgiesser, G., Ferrarin, C., Thompson, C. E. L., Whitehouse, R. J. S., Sutherland, T. F., & Bergamasco, A. (2010). The erosion rates of cohesive sediments in Venice lagoon, Italy. *Continental Shelf Research*, *30*(8), 859–870. https://doi.org/10.1016/j.csr.2009.12.001

Barausse, A., Grechi, L., Martinello, N., Musner, T., Smania, D., Zangaglia, A., & Palmeri, L. (2015). An integrated approach to prevent the erosion of salt marshes in the lagoon of Venice. *EQA - International Journal of Environmental Quality*, *18*(1), 43–54. https://doi.org/10.6092/issn.2281-4485/5799

Barbier, E. B., Hacker, S. D. S. D., Kennedy, C., Koch, E. W. E. W., Stier, A. C. A. C., & Silliman, B. R. B. R. (2011). The value of estuarine and coastal ecosystem services. *Ecological Monographs*, *81*(2), 169–193. https://doi.org/10.1890/10-1510.1

Breda, A., Saco, P. M., Sandi, S. G., Saintilan, N., Riccardi, G., & Rodríguez, J. F. (2021). Accretion, retreat and transgression of coastal wetlands experiencing sea-level rise. *Hydrology and Earth System Sciences*, *25*(2), 769–786. https://doi.org/10.5194/hess-25-769-2021

Carbognin, L., Teatini, P., & Tosi, L. (2004). Eustacy and land subsidence in the Venice Lagoon at the beginning of the new millennium. *Journal of Marine Systems*, *51*(1-4 SPEC. ISS.), 345–353. https://doi.org/10.1016/j.jmarsys.2004.05.021

Carniello, L., Defina, A., Fagherazzi, S., & D'Alpaos, L. (2005). A combined wind wave-tidal model for the Venice lagoon, Italy. *Journal of Geophysical Research: Earth Surface*, *110*(4), 1–15. https://doi.org/10.1029/2004JF000232

Carniello, L., Defina, A., & D'Alpaos, L. (2009). Morphological evolution of the Venice lagoon: Evidence from the past and trend for the future. *Journal of Geophysical Research: Earth Surface*, *114*(4), 1–10. https://doi.org/10.1029/2008JF001157

Carniello, L., D'Alpaos, A., & Defina, A. (2011). Modeling wind waves and tidal flows in shallow micro-tidal basins. *Estuarine, Coastal and Shelf Science*, *92*(2), 263–276. https://doi.org/10.1016/j.ecss.2011.01.001

Carniello, L., Defina, A., & D'Alpaos, L. (2012). Modeling sand-mud transport induced by tidal currents and wind waves in shallow microtidal basins: Application to the Venice Lagoon (Italy). *Estuarine, Coastal and Shelf Science*, *102–103*, 105–115. https://doi.org/10.1016/j.ecss.2012.03.016

Carniello, L., Silvestri, S., Marani, M., D'Alpaos, A., Volpe, V., & Defina, A. (2014). Sediment dynamics in shallow tidal basins: In situ observations, satellite retrievals, and numerical modeling in the Venice Lagoon. *Journal of Geophysical Research: Earth Surface*, *119*(4), 802–815. https://doi.org/10.1002/2013JF003015

Costanza, R., D'Arge, R., De Groot, R., Farber, S., Grasso, M., Hannon, B., et al. (1997). The value of the world's ecosystem services and natural capital. *Nature*, *387*(6630), 253–260. https://doi.org/10.1038/387253a0

Cronk, J.K., Fennessy, M. S. (2001). *WETLAND Biology and Ecology*. *America*. Boca Raton, FL: CRC Press.

D'Alpaos, A. (2011). The mutual influence of biotic and abiotic components on the long-term ecomorphodynamic evolution of salt-marsh ecosystems. *Geomorphology*, *126*(3–4), 269–278. https://doi.org/10.1016/j.geomorph.2010.04.027

D'Alpaos, A., & Marani, M. (2016). Reading the signatures of biologic-geomorphic feedbacks in salt-marsh landscapes. *Advances in Water Resources*, *93*, 265–275. https://doi.org/10.1016/j.advwatres.2015.09.004

D'Alpaos, A., Lanzoni, S., Marani, M., & Rinaldo, A. (2009). On the O'Brien-Jarrett-Marchi law. *Rendiconti Lincei*, *20*(3), 225–236. https://doi.org/10.1007/s12210-009-0052-x

D'Alpaos, A., Carniello, L., & Rinaldo, A. (2013). Statistical mechanics of wind wave-induced erosion in shallow tidal basins: Inferences from the Venice Lagoon. *Geophysical Research Letters*, *40*(13), 3402–3407. https://doi.org/10.1002/grl.50666

D'Alpaos, Luigi. (2010). *Fatti e misfatti di idraulica lagunare. La laguna di Venezia dalla diversione dei fiumi alle nuove opere delle bocche di porto*. (L D'Alpaos, Ed.), *Istituto Veneto di Scienze, Lettere e Arti* (Vol. 1999). Venice: Istituto Veneto di Scienze, Lettere ed Arti.

Day, J. W., Britsch, L. D., Hawes, S. R., Shaffer, G. P., Reed, D. J., & Cahoon, D. (2000). Pattern and process of land loss in the Mississippi Delta: A spatial and temporal analysis of wetland habitat change. *Estuaries*, *23*(4), 425–438. https://doi.org/10.2307/1353136

Defina, A. (2000). Two-dimensional shallow flow equations for partially dry areas. *Water Resources Research*, *36*(11), 3251–3264. https://doi.org/10.1029/2000WR900167

DeLaune, R. D., & Pezeshki, S. R. (2003). The role of soil organic carbon in maintaining surface elevation in rapidly subsiding U.S. Gulf of Mexico coastal marshes. *Water, Air, and Soil Pollution: Focus*, *3*(1), 167–179. https://doi.org/10.1023/A:1022136328105

Ferrarin, C., Tomasin, A., Bajo, M., Petrizzo, A., & Umgiesser, G. (2015). Tidal changes in a heavily modified coastal wetland. *Continental Shelf Research*, *101*, 22–33. https://doi.org/10.1016/j.csr.2015.04.002

Finotello, A., Canestrelli, A., Carniello, L., Ghinassi, M., & D'Alpaos, A. (2019). Tidal Flow Asymmetry and Discharge of Lateral Tributaries Drive the Evolution of a Microtidal Meander in the Venice Lagoon (Italy). *Journal of Geophysical Research: Earth Surface*, *124*(12), 3043–3066. https://doi.org/10.1029/2019JF005193

Finotello, A., D'Alpaos, A., Bogoni, M., Ghinassi, M., & Lanzoni, S. (2020). Remotely-sensed planform morphologies reveal fluvial and tidal nature of meandering channels. *Scientific Reports*, *10*(1), 1–13. https://doi.org/10.1038/s41598-019-56992-w

Finotello, A., Capperucci, R. M., Bartholomä, A., D'Alpaos, A., & Ghinassi, M. (2022). Morpho-sedimentary evolution of a microtidal meandering channel driven by 130 years of natural and anthropogenic modifications of the Venice Lagoon (Italy). *Earth Surface Processes and Landforms*, *47*(10), 2580–2596. https://doi.org/10.1002/esp.5396

Fitzgerald, D. M., & Hughes, Z. J. (2019). Marsh processes and their response to climate change and sea-level rise. *Annual Review of Earth and Planetary Sciences*, *47*(1), 481–517. https://doi.org/10.1146/annurev-earth-082517-010255

Gatto, P., & Carbognin, L. (1981). The lagoon of venice: Natural environmental trend and man-induced modification. *Hydrological Sciences Bulletin*, *26*(4), 379–391. https://doi.org/10.1080/02626668109490902

Gedan, K. B., Silliman, B. R., & Bertness, M. D. (2009). Centuries of human-driven change in salt marsh ecosystems. *Annual Review of Marine Science*, *1*, 117–141. https://doi.org/10.1146/annurev.marine.010908.163930

Ghezzo, M., Guerzoni, S., Cucco, A., & Umgiesser, G. (2010). Changes in Venice Lagoon dynamics due to construction of mobile barriers. *Coastal Engineering*, *57*(7), 694–708. https://doi.org/10.1016/j.coastaleng.2010.02.009

Hudson, R., Kenworth, J., & Best, M. (2021). Saltmarsh restoration Handbook.

Jarrett, J. T. (1976). Tidal Prism - Inlet Area Relationships. *J. Waterways and Harbors*, *95*(General Investigation of Tidal Inlets, Report 3), 55.

Leonardi, N., Defne, Z., Ganju, N. K., & Fagherazzi, S. (2016). Salt marsh erosion rates and boundary features in a shallow Bay. *Journal of Geophysical Research: Earth Surface*, *121*(10), 1861–1875. https://doi.org/10.1002/2016JF003975

Lesser, G. R., Roelvink, J. A., van Kester, J. A. T. M., & Stelling, G. S. (2004). Development and validation of a three-dimensional morphological model. *Coastal Engineering*, *51*(8–9), 883–915.

https://doi.org/10.1016/j.coastaleng.2004.07.014

Luternauer, J. L., Atkins, R. J., Moody, A. I., Williams, H. E., & Gibson, J. W. (1995). Salt marshes. *Developments in Sedimentology*, *53*(C), 307–332. https://doi.org/10.1016/S0070-4571(05)80031-7

Marani, M., D'Alpaos, A., Lanzoni, S., & Santalucia, M. (2011). Understanding and predicting wave erosion of marsh edges. *Geophysical Research Letters*, *38*(21), 1–5. https://doi.org/10.1029/2011GL048995

Mariotti, G., & Fagherazzi, S. (2010). A numerical model for the coupled long-term evolution of salt marshes and tidal flats. *Journal of Geophysical Research: Earth Surface*, *115*(1). https://doi.org/10.1029/2009JF001326

Mariotti, G., & Fagherazzi, S. (2013). Wind waves on a mudflat: The influence of fetch and depth on bed shear stresses. *Continental Shelf Research*, *60*, S99——-S110. https://doi.org/10.1016/j.csr.2012.03.001

Matticchio, B., Carniello, L., Canesso, D., Ziggiotto, E., & Cordella, M. (2017). Recent changes in tidal propagation in the Venice Lagoon: effects of changes in the inlet structure. In Luigi D'Alpaos (Ed.), *Commissione di studio sui problemi di Venezia, Volume III: La laguna di Venezia e le nuove opere alle bocche* (Istituto V, pp. 157–183). Venice: Istituto Veneto di Scienze, Lettere ed Arti.

Mehta, A. J., Hayter, E. J., Parker, W. R., Krone, R. B., & Teeter, A. M. (1989). Cohesive Sediment Transport. I: Process Description. *Journal of Hydraulic Engineering*, *115*(8), 1076–1093. https://doi.org/10.1061/(asce)0733-9429(1989)115:8(1076)

Mel, R. A., Viero, D. P., Carniello, L., Defina, A., & D'Alpaos, L. (2021). The first operations of Mo.S.E. system to prevent the flooding of Venice: Insights on the hydrodynamics of a regulated lagoon. *Estuarine, Coastal and Shelf Science*, *261*(August), 107547. https://doi.org/10.1016/j.ecss.2021.107547

Mitsch, W. J., & Gossilink, J. G. (2000). The value of wetlands: Importance of scale and landscape setting. *Ecological Economics*, *35*(1), 25–33. https://doi.org/10.1016/S0921-8009(00)00165-8

Möller, I., Spencer, T., French, J. R., Leggett, D. J., & Dixon, M. (1999). Wave transformation over salt marshes: A field and numerical modelling study from north Norfolk, England. *Estuarine, Coastal and Shelf Science*, *49*(3), 411–426. https://doi.org/10.1006/ecss.1999.0509

Mudd, S. M. (2011). The life and death of salt marshes in response to anthropogenic disturbance of sediment supply. *Geology*, *39*(5), 511–512. https://doi.org/10.1130/focus052011.1

Ratliff, K. M., Braswell, A. E., & Marani, M. (2015). Spatial response of coastal marshes to increased atmospheric CO2. *Proceedings of the National Academy of Sciences of the United States of America*, *112*(51), 15580–15584. https://doi.org/10.1073/pnas.1516286112

van Rijn, L. C. (1984). Sediment Transport. Part I: Bed load transport. *Journal of Hydraulic Engineering*, *110*(10), 1431–1456.

Rogers, K., & Woodrofe, C. D. (2015). Tidal Flats and Salt Marshes. *Coastal Environments and Global Change*, 227–250. https://doi.org/10.1002/9781119117261.ch10

Silvestri, S. (2018). Journal of Geophysical Research : Earth Surface Anthropogenic Modi fi cations Can Signi fi cantly In fl uence the Local Mean Sea Level and Affect the Survival of Salt Marshes in Shallow Tidal Systems, 996–1012. https://doi.org/10.1029/2017JF004503

SMAGORINSKY, J. (1963). General Circulation Experiments With the Primitive Equations. *Monthly Weather Review*, *91*(3), 99–164. https://doi.org/10.1175/1520-0493(1963)091<0099:gcewtp>2.3.co;2

Tagliapietra, D., Baldan, D., Barausse, A., Buosi, A., Curiel, D., Guarneri, I., et al. (2018). Protecting and restoring the salt marshes and seagrasses in the lagoon of Venice. In X. D. Quintana, D. Boix, S. Gascòn, & J. Sala (Eds.), *Management and Restoration of Mediterranean Coastal Lagoons in Europe. Included in the Project "LIFE Pletera (LIFE13 NAT/ES/001001)* (Càtedra d', p. 220). Venice, Italy: Càtedra d'Ecosistemes Litorals Mediterrànis i LIFE Pletera. Retrieved from http://lifepletera.com/wp-

content/uploads/2019/02/Recerca_i_Territori_10_ENG_MdM_web.pdf

Temmerman, S., Bouma, T. J., Govers, G., Wang, Z. B., De Vries, M. B., & Herman, P. M. J. (2005). Impact of vegetation on flow routing and sedimentation patterns: Three-dimensional modeling for a tidal marsh. *Journal of Geophysical Research: Earth Surface*, *110*(4), 1–18. https://doi.org/10.1029/2005JF000301

Tognin, D. (2022). *Natural and anthropogenic drivers of erosional and depositional dynamics in shallow tidal systems* (PhD thesis).

Tognin, D., D'Alpaos, A., Marani, M., & Carniello, L. (2021). Marsh resilience to sea-level rise reduced by storm-surge barriers in the Venice Lagoon. *Nature Geoscience*, *14*(12), 906–911. https://doi.org/10.1038/s41561-021-00853-7

Tognin, D., Finotello, A., D'Alpaos, A., Viero, D. P., Pivato, M., Mel, R. A., et al. (2022). Loss of geomorphic diversity in shallow tidal embayments promoted by storm-surge barriers. *Science Advances*, *8*(13), 1–13. https://doi.org/10.1126/sciadv.abm8446

Tomasin, A. (1974). Recent changes in the tidal regime in Venice. *Rivista Italiana Geofisica*, *23*(5/6), 275–278.

Tommasini, L., Carniello, L., Ghinassi, M., Roner, M., & D'Alpaos, A. (2019). Changes in the wind-wave field and related salt-marsh lateral erosion: inferences from the evolution of the Venice Lagoon in the last four centuries. *Earth Surface Processes and Landforms*. https://doi.org/10.1002/esp.4599

Valle-Levinson, A., Marani, M., Carniello, L., D'Alpaos, A., & Lanzoni, S. (2021). Astronomic link to anomalously high mean sea level in the northern Adriatic Sea. *Estuarine, Coastal and Shelf Science*, *257*(February), 107418. https://doi.org/10.1016/j.ecss.2021.107418

Van Ledden, M., Wang, Z. B., Winterwerp, H., & De Vriend, H. (2004). Sand-mud morphodynamics in a short tidal basin. *Ocean Dynamics*, *54*(3–4), 385–391. https://doi.org/10.1007/s10236-003-0050-y

Viero, D. P., & Defina, A. (2016). Water age, exposure time, and local flushing time in semi-enclosed, tidal basins with negligible freshwater inflow. *Journal of Marine Systems*, *156*, 16–29. https://doi.org/10.1016/j.jmarsys.2015.11.006

Young, I. R., & Verhagen, L. A. (1996). The growth of fetch limited waves in water of finite depth. Part 1. Total energy and peak frequency. *Coastal Engineering*, *29*(1–2), 47–78. https://doi.org/10.1016/S0378-3839(96)00006-3

Zanchettin, D., Bruni, S., Raicich, F., Lionello, P., Adloff, F., Androsov, A., et al. (2021). Sea-level rise in Venice: Historic and future trends (review article). *Natural Hazards and Earth System Sciences*, *21*(8), 2643–2678. https://doi.org/10.5194/nhess-21-2643-2021

Zarzuelo, C., López-Ruiz, A., D'Alpaos, A., Carniello, L., & Ortega-Sánchez, M. (2018). Assessing the morphodynamic response of human-altered tidal embayments. *Geomorphology*, *320*, 127–141. https://doi.org/10.1016/j.geomorph.2018.08.014

Zecchin, M., Baradello, L., Brancolini, G., Donda, F., Rizzetto, F., & Tosi, L. (2008). Sequence stratigraphy based on high-resolution seismic profiles in the late Pleistocene and Holocene deposits of the Venice area. *Marine Geology*, *253*(3–4), 185–198. https://doi.org/10.1016/j.margeo.2008.05.010